

DOE/NASA/0217-1
NASA CR- 168071



(NASA-CR-168071) CREEP-RUPTURE BEHAVIOR OF
6 CANDIDATE STIRLING ENGINE IRON-BASE
SUPERALLOYS IN HIGH PRESSURE HYDROGEN.
VOLUME 1: AIR CREEP-RUPTURE BEHAVIOR Final
Report (IIT Research Inst.) 128 p

#63-22389

Declass
63/25 02651

CREEP-RUPTURE BEHAVIOR OF SIX CANDIDATE STIRLING ENGINE IRON-BASE SUPERALLOYS IN HIGH PRESSURE HYDROGEN

VOLUME 1 - AIR CREEP-RUPTURE BEHAVIOR

S. Bhattacharyya
IIT RESEARCH INSTITUTE
10 West 35th Street
Chicago, Illinois 60616

DECEMBER 1982



Prepared for

NATIONAL AERONAUTICS AND SPACE ADMINISTRATION
Lewis Research Center
Under Contract DEN 3-217

for
U.S. DEPARTMENT OF ENERGY
Office of Transportation Programs

DOE/NASA/0217-1
NASA CR-168071

CREEP-RUPTURE BEHAVIOR OF SIX CANDIDATE
STIRLING ENGINE IRON-BASE SUPERALLOYS
IN HIGH PRESSURE HYDROGEN

VOLUME 1 - AIR CREEP-RUPTURE BEHAVIOR

S. Bhattacharyya
IIT Research Institute
10 W. 35 Street
Chicago, Illinois 60616

December 1982

Prepared for
National Aeronautics and Space Administration
Lewis Research Center
Under Contract DEN 3-217

for
U.S. Department of Energy
Office of Transportation Programs
Under Interagency Agreement
DE-A-101-77CS51040

SUMMARY

The creep-rupture behavior of six candidate Stirling engine iron-base superalloys was determined in air. The test alloys included four wrought alloys (A-286, IN 800H, N-155, and 19-9DL) and two cast alloys (CRM-60 and XF-818). The wrought alloys were used in the form of sheets of 0.89 mm (0.035 in.) average thickness. The cast alloy specimens were investment cast and machined to 6.35 mm (0.250 in.) gage diameter. The creep-rupture specimens were tested to rupture in air at different times up to 3000 h over the temperature range of 650° to 925°C (1200° to 1700°F).

The basic data, namely, rupture life (t_r), minimum creep rate ($\dot{\epsilon}_m$), and time to 1% creep strain ($t_{0.01}$), were statistically analyzed as a function of stress at different temperatures. Also, temperature-compensated analysis was performed to obtain the activation energies for rupture life, time to 1% creep strain, and the minimum creep rate. Microstructural and fracture analyses were also performed. Based on statistical analyses, estimates were made for stress levels at different temperatures to obtain 3500 h t_r and $t_{0.01}$ lives. All the above air data and analyses will be compared with similar data being obtained for these alloys under 15 MPa (2175 psi) hydrogen, to be reported later.

TABLE OF CONTENTS

	<u>Page</u>
SUMMARY.	vi
INTRODUCTION	1
MATERIALS AND EXPERIMENTAL PROCEDURE	1
Test Materials and Analysis.	1
Specimen Design and Preparation.	1
Heat Treatment and Microstructure.	1
Test Equipment	2
Experimental Procedure	3
EXPERIMENTAL RESULTS AND ANALYSES.	4
Basic Data	4
Creep Curves	4
Stress Correlation with Rupture Life, Minimum Creep Rate, and Time to 1% Creep Strain.	4
Rupture Life vs. Stress	5
Time to 1% Creep Strain vs. Stress.	7
Minimum Creep Rate vs. Stress	8
Temperature-Compensated Analysis for Activation Energy and Stress Exponent.	9
Stress Component, n	10
Activation Energy, Q	12
Predicted Stresses for Rupture and 1% Creep in 3500 Hours.	13
Fractography and Microstructural Analysis.	14
Fracture Location and Appearance.	14
Fracture Examination.	14
Cross-Section Examination	16
SUMMARY OF RESULTS	18
REFERENCES	19
APPENDIX A: Complete Air Creep-Rupture Data	75
APPENDIX B: Correlational Analysis of Rupture Life, Time to 1% Creep Strain, and Minimum Creep Rate as a Function of Initial Stress for Six Iron-Base Superalloys Tested in Air at 650° to 925°C.	81
APPENDIX C: Temperature-Compensated Analysis of Rupture Life, Time to 1% Creep Strain, and Minimum Creep Rate as a Function of Initial Stress for Six Iron-Base Superalloys Tested in Air at 650° to 925°C.	85

LIST OF TABLES

<u>Table</u>		<u>Page</u>
1	Nominal Chemical Composition of Iron-Base Superalloys	20
2	Alloy Specifications and Heat Treatment Condition for Test Specimens	21
3	Air Creep-Rupture Test Data for Alloy A-286	22
4	Air Creep-Rupture Test Data for Alloy IN 800H	23
5	Air Creep-Rupture Test Data for Alloy N-155	24
6	Air Creep-Rupture Test Data for Alloy 19-9DL	25
7	Air Creep-Rupture Test Data for Alloy CRM-6D	26
8	Air Creep-Rupture Test Data for Alloy XF-818	27
9	Basic Temperature and Stress Ranges for Direct Correlation of Initial Stress with Rupture Life (t_r), Time to 1% Creep Strain ($t_{0.01}$), and Minimum Creep Rate ($\dot{\epsilon}_m$)	28
10	Temperature-Compensated Analysis Data Subset Conditions for Six Iron-Base Superalloys Tested in Air	29
11	Statistical Data on Temperature-Compensated Analysis of Six Alloys Tested in Air	30
12	Predicted Stress for 3500-Hour Rupture Life in Air	31
13	Predicted Stress to 1% Creep in 3500 Hours in Air	32
14	Fractography and Microstructure Analyses of Specimens Tested in Air	33

LIST OF FIGURES

<u>Figure</u>		<u>Page</u>
1	Creep-rupture specimen design.	34
2	Optical photomicrographs of wrought sheet alloys	35
3	SEM microstructures of as-cast alloys showing interdendritic structure with carbide and boride dispersion	36
4	Creep curves for N-155 tested at 815°C in air.	37
5	Creep curves for CRM-6D tested at 815°C in air	38
6	Stress vs. rupture life of A-286 in air.	39
7	Stress vs. rupture life of IN 800H in air.	40
8	Stress vs. rupture life of N-155 in air.	41
9	Stress vs. rupture life of 19-9DL in air	42
10	Stress vs. rupture life of CRM-6D in air	43
11	Stress vs. rupture life of XF-818 in air	44
12	Stress vs. time to 1% creep strain for A-286 in air.	45
13	Stress vs. time to 1% creep strain for IN 800H in air.	46
14	Stress vs. time to 1% creep strain for N-155 in air.	47
15	Stress vs. time to 1% creep strain for 19-9DL in air	48
16	Stress vs. time to 1% creep strain for CRM-6D in air	49
7	Stress vs. time to 1% creep strain for XF-818 in air	50
18	Stress vs. minimum creep rate of A-286 in air.	51
19	Stress vs. minimum creep rate of IN 800H in air.	52
20	Stress vs. minimum creep rate of N-155 in air.	53
21	Stress vs. minimum creep rate of 19-9DL in air	54
22	Stress vs. minimum creep rate of CRM-6D in air	55
23	Stress vs. minimum creep rate of XF-818 in air	56
24	Temperature-compensated minimum creep rate vs. stress for N-155 tested in air (Case 2B, including Cases 2A and 2C data shown separately).	57

LIST OF FIGURES (cont.)

<u>Figure</u>		<u>P. 3</u>
25	Temperature-compensated minimum creep rate vs. stress for XF-818 tested in air (Case 2B, including Cases 2A and 2C data shown separately).	58
26	Temperature-compensated rupture life vs. stress for N-155 tested in air (Case 2B, including Cases 2A and 2C data shown separately).	59
27	Temperature-compensated time to 1% creep strain vs. stress for N-155 tested in air (Case 2B, including Cases 2A and 2C data shown separately).	60
28	Temperature-compensated rupture life vs. stress for XF-818 tested in air (Case 2B, including Cases 2A and 2C data shown separately).	61
29	Temperature-compensated time to 1% creep strain vs. stress for XF-818 tested in air (Case 2B, including Cases 2A and 2C data shown separately).	62
30	Estimated 3500-hour rupture stress for six alloys tested in air.	63
31	Typical macrofractographs of wrought specimens creep-rupture tested in air.	64
32	Typical macro- and microfractographs of the 19-9DL specimen creep-rupture tested at 870°C and 41 MPa	66
33	Typical macrofractographs of the cast specimens creep-rupture tested in air.	67
34	Typical macrofractographs of XF-818 specimen creep-rupture tested at 815°C and 138 MPa.	69
35	Typical optical and SEM photomicrographs of cross-sections from 19-9DL specimen creep-rupture tested in air	70
36	Typical optical and SEM photomicrographs of cross-sections from A-286 specimen creep-rupture tested in air, 815°C, 55 MPa .	71
37	Typical optical and SEM photomicrographs of cross-sections from N-155 specimen creep-rupture tested in air, 870°C, 47 MPa .	72
38	Optical photomicrographs of cross-sections from IN 800H and XF-818 specimens creep-rupture tested in air	73
39	Typical optical and SEM photomicrographs of cross-sections of CRM-6D specimens creep-rupture tested in air	74

INTRODUCTION

The Stirling cycle engine for automotive application, currently under development by the Department of Energy, employs high-pressure hydrogen as the working fluid. The long-term effects of high-pressure hydrogen at high temperature on the physical and mechanical properties of high-temperature alloys are unknown. The most critical component in the engine is the heater head which consists of the cylinders, tubings, and regenerators. Candidate alloys for these applications must not only meet all the property requirements in air as well as in high-pressure hydrogen but must also be of low cost to be compatible with automotive application. With these considerations in mind, six iron-base superalloys were selected for creep-rupture property evaluation over the temperature range of 650°-925°C in air as well as in 15 MPa (2175 psi) H₂. This report analyzes in detail the data obtained in air. In a later report, the H₂ creep-rupture data will be presented and the effect of H₂ environment on air creep-rupture properties of these six alloys will be analyzed.

MATERIALS AND EXPERIMENTAL PROCEDURES

Test Materials and Analysis

Six iron-base alloys--A-286, Incoloy 800H, N-155, 19-9DL, CRM-6D, and XF-818--were evaluated for creep-rupture properties in air. The chemical analyses and specifications are given in Tables 1 and 2.

Of these six alloys, CRM-6D and XF-818 are cast alloys and the other four are sheet alloys in the thickness range of 0.79 to 0.99 mm (0.031 to 0.039 in.)--comparable to the wall thickness of the tubes used in the Stirling engine. The threaded investment cast CRM-6D and XF-818 specimens were made by Climax Molybdenum Company of Ann Arbor, Michigan; the wrought sheet alloys were purchased from commercial suppliers meeting the AMS specifications.

Specimen Design and Preparation

The specimen drawings and dimensions are shown on Fig. 1. They conform to ASTM E-8. All specimen surfaces were finished to 0.8 μm (32 $\mu\text{in.}$) rms or better.

All investment cast specimens were radiographed, and those with no detectable flaws were selected for testing.

Heat Treatment and Microstructure

The recommended heat treatments are given in Table 2. All specimens were heat-treated in helium environment to prevent surface deterioration. Final surface finishing was done after the heat treatment. The heat-treated hardnesses of the wrought alloys were as follows:

<u>Alloy</u>	<u>Hardness, Rockwell A Scale</u>	
	<u>Average</u>	<u>Range</u>
A-286	51.9	48.6-53.6
IN 800H	40.0	37.4-42.5
N-155	51.5	51.2-51.9
19-9DL	50.5	50.0-50.9

The two cast alloys CRM-6D and XF-818 had the following average hardnesses:

CRM-6D	HRA 62.4*
XF-818	HRA 59.8*

*Converted from HRC

A microstructural analysis of the four wrought alloys and the two cast alloys was made. All the wrought alloys had single-phase austenitic structures with fine inclusions indicating the rolling direction as shown in Fig. 2a to d. In the wrought alloys, the average grain diameter was estimated from optical photomicrographs at a magnification of 100X using the random line intercept method. Between 200 and 250 grains were measured in each alloy including two representative areas. The estimated grain sizes are given below:

<u>Alloy</u>	<u>Average Grain Diameter, μm</u>
A-286	108
IN 800H	64
N-155	42
19-9DL	33

The microstructures of the two cast alloys, CRM-6D and XF-818, are shown in Fig. 3. Figure 3a shows the dendritic cast structure of the CRM-6D alloy, and Fig. 3b reveals the details of the carbide structure of the high carbon-high chromium chemistry. In Fig. 3c, the dendritic cast structure of XF-818 is revealed. The lamellar M_3B_2 structure of this high-boron alloy is seen in Fig. 3d.

Test Equipment

Tests were conducted at the IITRI laboratory as well as at the Joliet Metallurgical Laboratory (JML), Joliet, Illinois. JML is a certified laboratory and conducted over 80% of the tests. At both IITRI and JML, tests were conducted conforming to ASTM E139.

At JML, extension was measured with two dial micrometers reading to 1.27 μm (50 $\mu\text{in.}$), and the results were averaged. At IITRI, a sensitive capacitance-type displacement transducer extensometer was used, with a signal conditioner to obtain millivolt outputs where 1 mV = 0.50 μm (20 $\mu\text{in.}$).

A three-zone furnace with a 76 mm (3 in.) ID Alundum tube was controlled by a Barber-Colman Model 560 temperature controller. Two chromel-alumel thermocouples were tied to the end of the gage length, and the maximum temperature difference was limited to 2°C.

Deadweight loading with a lever ratio of up to 20:1 was used to obtain the initial stress. The accuracy of the lever ratio was carefully checked by means of a 22.2 kN (5000 lbf) proving ring. Excellent specimen alignment was obtained using universal joints at both the top and bottom ends of the pull rods.

All extension and temperature data were recorded periodically at 2 to 4 h intervals on printed tapes, and later on magnetic disks. On failure, a switch automatically tripped off the timer and furnace circuits.

Experimental Procedure

Specimen dimensions were measured to $\pm 25.4 \mu\text{m}$, and the cross-sectional areas were calculated to three significant digits. Both the sheet and round specimens had a length/width (dia) ratio of 4, and the reduced section length was 31.8 mm. Extensometers were attached to the specimen shoulders. The fractured specimens were fitted together, and the distance separating the extensometer positions were measured to obtain the total extension. To calculate elongation (as percent), the divisor was taken as the adjusted length of the reduced section as defined in ASTM E139.

Full loading (IITRI) as well as incremental loading (JML) was used, and extension due to loading was noted. Dial micrometer (JML) and capacitance transducer extensometer (IITRI) readings were set to zero immediately after loading so that all subsequent extensions reflected the creep extension of the specimen. All the reported creep curves thus originate at the zero values of creep strain and time axes.

In several early tests at JML, tests were discontinued without failure or loaded to a higher stress to fracture because of test times exceeding the expected values due to low stress level selection. While no definite rupture life data were obtained in these tests, other valuable information on minimum creep rate and time to obtain specific creep strains was documented and used in the analysis.

EXPERIMENTAL RESULTS AND ANALYSES

Basic Data

The complete set of air creep-rupture data is given in Appendix A. The data can be broadly grouped into two categories, namely, independent (controlled) and dependent (derived). The independent category covers the data from cols. (1) to (4) of Appendix A, i.e., environment - air; alloy type - any one of the six alloys; temperature - any one of the six temperatures, 650 to 925°C; and applied initial stress spread over a wide range, 17 to 483 MPa (2.5 to 70 ksi).

The values in cols. 5 to 11 are the observed data, i.e., rupture life (t_r), minimum creep rate ($\dot{\epsilon}_m$), total elongation (%), duration of secondary creep (t_{sc}), time to reach 1% creep strain ($t_{0.01}$), time to reach tertiary creep stage (t_{ter}), and effective life ($t_r - t_{ter}$). Of these, t_r , $\dot{\epsilon}_m$, and $t_{0.01}$ were statistically analyzed as a function of stress (σ).

Creep Curves

The creep-strain vs. time plots for the six alloys were obtained at the various temperatures. Two typical creep curves at 815°C, one for wrought alloy N-155 and the other for cast alloy CRM-6D, are shown in Figs. 4 and 5, respectively.

In both Figs. 4 and 5, the creep curves show the three stages of creep--primary, secondary, and tertiary--leading to rupture. The extent of the secondary creep range and the onset of tertiary creep as well as the duration of tertiary creep stage leading to fracture depend on alloy structure and stress levels. In the cast alloy CRM-6D, the tertiary stage is considerably shorter than that in the wrought alloy N-155, and the total strain is also much less.

Stress Correlation with Rupture Life, Minimum Creep Rate, and Time to 1% Creep Strain

After assessing all the data in Appendix A with the help of initial analysis, the data points which obviously fell out of range or were otherwise considered faulty and inadmissible were deleted from further analysis. In addition, the overall temperatures and stress ranges of tests which cover diverse creep mechanisms leading on to creep-rupture were broadly grouped according to the predominant mechanism models, and the data were analyzed in smaller subsets as dictated by these groupings. This procedure, with some iteration, resulted in excellent correlation between stress and temperature, on the one hand, and the observed parameters, e.g., rupture life (t_r), minimum creep rate ($\dot{\epsilon}_m$), and time to 1% strain ($t_{0.01}$), on the other hand. All the data thus selected for analysis are given in Tables 3 to 8 for the six superalloys.

In all three correlational analyses, the following simple power relationship was assumed:

$$Y = k\sigma^n$$

$$\text{or, } \ln Y = \ln k + n \ln \sigma$$

where Y is either t_r , ϵ_m , or $t_{0.01}$, σ is the initial stress, k and n are constants to be evaluated. The slope n is, however, assumed constant within certain temperature and stress ranges which depended on the alloy strength and structure, wrought vs. cast. Table 9 summarizes the ranges of temperature and stress levels over which this constancy was assumed and the key temperatures which were used to determine the slope, n. The basis for this is related to the different creep mechanisms assumed to be operative under diverse temperature and stress levels related to alloy structure and strength properties, and may be summarized as follows:

1. In the intermediate stress range and extending over practically all the six temperatures, but more definitely over 705° to 870°C, one creep mechanism is assumed to be predominantly operative--a dislocation-climb model.
2. At the higher two temperatures of 870° and 925°C and depending on the stress level, a diffusional mode of creep was assumed.
3. At the two lowest temperatures of 705° and 650°C, a dislocation-glide model similar to and approaching a tensile-type failure was assumed with some consideration given to the stress level in relation to the inherent strength of the alloy and the nature of the product, wrought vs. cast.

A temperature-compensated analysis based on the Orowan-Sherby-Dorn method is given in the next section.

Rupture Life vs. Stress

The rupture life data at each temperature were correlated with stress using the simple power relationship mentioned earlier. Regression analysis was used to obtain the constants, and all the basic statistical information is given in Appendix B. A typical example for N-155 at 760°C shows the following correlation:

$$\ln t_r = 38.96 - 6.712 \ln \sigma$$

with a correlation coefficient of $R^2 = 0.998$ and a 90% confidence range of 0.4252. Based on the above equation and the 90% range value, the estimated mean initial stress for 3500 h rupture life was calculated to be 98.3 MPa with low and high values of 92.3 and 108 MPa at the 90% confidence level.

Based on these correlations, the data were fitted graphically to obtain rupture life vs. stress relationships shown in Figs. 6 to 11 for the six alloys. In all the figures, the regression lines were fitted to the data analyzed. The remaining data at the higher and lower temperature levels are also plotted on these figures. At these temperatures, the data were too few to obtain the slopes which differ from the slopes of the fitted lines indicating a different model of creep at these extreme temperature ranges.

The slopes (n) and R² values for the six alloys were as follows:

<u>Alloy</u>	<u>n</u>	<u>R²</u>
A-286	-4.695	0.931 to 0.995
IN 800H	-5.945	0.985 to 1.000
N-155	-6.712	0.966 to 0.996
19-9DL	-6.548	0.960 to 0.999
CRM-6D	-12.29	0.908 to 0.998
XF-818	-15.34 ^a -7.657 ^b	0.971 0.993 to 1.000

^aFor temperatures 650° and 705°C.

^bFor temperatures 760°, 815°, and 870°C.

The four wrought alloys have, in general, similar and less negative slopes than the two cast alloys. Alloy A-286, however, differs in slope value from the other three wrought alloys, IN 800H, N-155, and 19-9DL. The mean slope of these three alloys is approximately -6.4, which differs less than 10% from the individual slopes of these three alloys but differs by more than 30% from that of A-286.

CRM-6D had a very high slope of -12.3, almost twice as large as that of the wrought alloys, indicating that its rupture life is far more sensitive to small stress fluctuations than that for the wrought alloys. The cast alloy XF-818 at the higher temperature range (760° to 815°C) has a slope significantly smaller than that of CRM-6D and only 20% more than that of the mean slope of the three wrought alloys mentioned above. This indicates that the rupture life of XF-818 will not be affected as seriously as that of CRM-6D at these temperatures due to small fluctuations of stress. On the other hand, at the low temperature ranges of 650° and 705°C, the XF-818 slope of -15.34 is the highest observed in this study and indicates a drastic potential loss in rupture life at these temperatures with a small increase in operating stress. More data at the lower temperatures in tests for long rupture lives will be desirable to more fully substantiate this behavior.

ORIGINAL PAGE IS
OF POOR QUALITY

Time to 1% Creep Strain vs. Stress

Regression analysis data correlating $\ln \sigma$ vs. $\ln t_{0.01}$ are given in Appendix B. A typical example for N-155 at 760°C shows the following correlation:

$$\ln t_p = 36.91 - 7.012 \ln \sigma$$

with a correlation coefficient of $R^2 = 0.992$ and a 90% confidence range of 0.6290. Based on the above equation and the 90% range value, the estimated mean initial stress to obtain 1% creep strain in 3500 h was calculated as 60.3 MPa, with 55.2 and 66.0 MPa as the low and high 90% confidence limits.

Based on these correlations, the data were fitted graphically to obtain time to 1% creep strain vs. stress relationships as shown in Figs. 12-17 for the six alloys. All the $t_{0.01}$ data are plotted on these figures though the regression lines were fitted to those analyzed. At higher and lower temperatures more data are needed to obtain the line slopes and the stress levels where the slopes deviate from each other.

The slopes (n) and R^2 values for the six alloys were as follows:

<u>Alloy</u>	<u>n</u>	<u>R²</u>
A-286	-4.251	0.955 to 0.998
IN 800H	-4.795 ^a -10.18 ^b	0.923 to 1.000 0.844 to 1.000
N-155	-7.012	0.987 to 1.000
19-9DL	-5.919	0.971 to 0.997
CRM-6D	-9.935	0.961 to 0.989
XF-818	-6.839 ^c -15.25 ^d	0.990 to 1.000 0.890

^aFor temperatures 870° to 925°C.

^bFor temperatures 650° to 815°C.

^cFor temperatures 760° to 870°C.

^dFor temperatures 650° to 705°C.

There is a significant range in the slopes of the wrought alloys from 4.25 to -7.01 with IN 800H showing an even higher slope of -10.2 at the lower temperature levels where the R^2 values were low. CRM-6D has a high slope of -9.94, and XF-818 has an even higher slope of -15.3 at the two lowest temperatures; the higher temperature slope of -6.84 is similar to those of N-155 and 19-9DL. These slopes indicate how significantly the stress to 1% creep strain is affected with a change in stress, and the larger negative numbers indicated the possibility of sharper reductions with increasing stress in CRM-6D, and in XF-818 and IN 800H, at the lower temperature ranges. On the other hand, A-286 and IN 800H, at the higher temperatures will not be that significantly affected by a change in stress as compared to the others.

Minimum Creep Rate vs. Stress

Stress correlation with minimum creep rate at each temperature was carried out in a manner similar to that for t_r and $t_{0.01}$ using a simple power relationship. A temperature-compensated analysis is given in the next section. Linear regression analysis was used to obtain the basic statistical information as shown in Table B-3, Appendix B. A typical example for N-155 at 760°C is as follows:

$$\ln \dot{\epsilon}_m = 50.07 + 6.842 \ln \sigma$$

with a correlation coefficient or $R^2 = 0.953$ and a 90% confidence range of 1.487. Based on these correlations, the $\dot{\epsilon}_m$ data were fitted graphically to obtain minimum creep rate vs. stress relationships shown in Figs. 18 to 23 for the six alloys. While the regression lines were fitted to the analyzed data, the additional data are also plotted for reference, and only with more data in these low and high temperature ranges will it be possible to obtain adequate correlation.

The slopes (n) and R^2 values for the six alloys were as follows:

<u>Alloy</u>	<u>n</u>	<u>R²</u>
A-286	3.467 ^a 10.14 ^b	0.981 to 0.994 0.850 to 0.985
IN 800H	6.637	0.948 to 0.997
N-155	6.842	0.958 to 0.997
19-9DL	6.353	0.976 to 1.000
CRM-6D	11.26	0.925 to 0.997
XF-818	7.350 ^c 12.49 ^d	0.987 to 0.996 0.988

^aFor temperatures 815° to 925°C.

^bFor temperatures 650° to 760°C.

^cFor temperatures 760° to 925°C.

^dFor temperatures 650° to 705°C.

Excepting A-286, the other three wrought alloys have very similar slopes, an average of 6.61. A-286 showed two distinct slopes, a very low value of 3.47 at the higher temperatures, and a slope three times larger at the lower temperature ranges. A similar behavior is seen in the cast alloy XF-818 though the slopes at both the higher and lower temperatures were higher than those for A-286. CRM-6D showed a high slope, about twice that of the wrought alloy average slope of 6.61. In other words, CRM-6D minimum creep rate will increase at a much faster rate with stress than that for the wrought alloys.

An n value of about 7 is noted in the three wrought alloys IN 800H, N-155, and 19-9DL and in XF-818 between 760° and 925°C. A higher value of about 11 is noted in CRM-65, XF-818, and A-286 (low temperatures only).

Many semiempirical $\dot{\epsilon}$ vs. σ relationships have been developed, and an equation with $n = 7.5$ has been related to dislocation climb (lattice diffusion control).⁴ An n value of 9.5 has been related to dislocation climb (core diffusion control).⁴ Higher n values up to 40 have been reported in many alloys. The value of $n = 7$ observed in these tests appears to indicate that the assumption of dislocation climb/glide mechanisms made earlier is basically valid.

In A-286, at the higher temperatures of 815° to 925°C, the slope is smaller with an n value of 3.47. A value of $n = 3$ is considered representative of viscous glide behavior.⁴ Alloy A-286 was aged at 720°C, and it is expected that any age-hardening effect present in the structure will be lost in the 815° to 925°C test range. Thus, the material will behave as an over-aged alloy with no appreciable dispersed phases such as carbides and borides, because C was only 0.05% and B, 0.003%. It is not altogether surprising, therefore, that A-286 at this high temperature gave a lower value of $n = 3.47$.

Because of lack of adequate data, the n value of the lower temperature/higher stress range cannot be properly evaluated. But the observed tendency of increasing n at lower temperature and higher stresses is consistent with reported literature data. Thus, with the exception of A-286, in the other alloys the stress dependence of minimum creep rate is exceptionally large, about 2 to 3 times the value at the higher temperature/lower stress ranges.

Temperature-Compensated Analysis for Activation Energy and Stress Exponent

Of the many different methods⁽⁵⁻¹⁰⁾ of analysis of creep-rupture parameters taking into consideration both stress and temperature in a combined form, the Drowan-Sherby-Dorn (OSD) method was selected for analyzing the data and obtaining the activation energies for the creep-rupture parameters:

$$Y = \ln k + n \ln \sigma + Q/RT \quad (1)$$

where $Y = \ln \dot{\epsilon}_m, \ln t_r$ or $\ln t_{0.01}$,

Q = the activation energy

σ = the initial stress

T = the test temperature, K

R = the universal gas constant, 8.314 J/K mol

$\ln k$ and n are constants to be determined.

Equation 1 can be rearranged in the following manner:

$$(Y - Q/RT) = \ln k + n \ln \sigma \quad (2)$$

With this rearrangement, a linear regression analysis of $(\dot{\epsilon} - Q/RT)$ vs. $\ln \sigma$ will determine Q , the activation energy, and the slope of the fitted line, n , which is the stress slope based on the power relationship.

In order to perform this analysis, the prior direct correlational analysis was made use of to classify the data into suitable subsets, as given in Table 10. All the data were divided into 3 cases (2A, 2B, and 2C) where Case 2B contains the largest set of data, while Cases 2A and 2C are limited in data, and fall in the extreme ranges of temperatures and/or stresses, occasionally overlapping Case 2B data. Case 2B data were analyzed statistically and graphically plotted using Equation 2, and data from Cases 2A and 2C were plotted on the figures to show the extent of deviation at the higher temperatures and stress levels.

For XF-818, two additional cases for $\dot{\epsilon}_m$ were also analyzed containing a larger collection of data and these were

Case 2D: $\dot{\epsilon}_m > 1.0 \text{ E-}09 \text{ s}^{-1}$ (23 data)

Case 2E: $\dot{\epsilon}_m < 3.0 \text{ E-}06 \text{ s}^{-1}$ (21 data)

with the bulk of the data common in both cases. The reason for considering Case 2D was that creep rate measurements less than or equal to $1.0 \text{ E-}09 \text{ s}^{-1}$ would have uncertainties associated with them unless tests were conducted over very long periods of time. Case 2E was considered because $\dot{\epsilon}_m$ greater than or equal to $3.0 \text{ E-}06 \text{ s}^{-1}$ approached overload/tensile type failure associated with very high stresses and very short rupture lives of a few hours.

Stress Exponent, n

All the basic analytical statistical parameters for Case 2B only are given in Table 11. Based on these analyses, graphical correlations of the data are shown in Figs. C-1 to C-36, in Appendix C. For two selected alloys, N-155 and XF-818, the associated graphical correlations for minimum creep rate are shown in Figs. 24 and 25, respectively.

For the three different cases, the creep rate equations for N-155 may be written as follows:

$$\text{Case 2A } \ln \dot{\epsilon}_m = 15.9 + 7.36 \ln \sigma - 593/RT \quad (3)$$

$$\text{Case 2B } \ln \dot{\epsilon}_m = 8.85 + 7.39 \ln \sigma - 527/RT \quad (4)$$

$$\text{Case 2C } \ln \dot{\epsilon}_m = -9.19 + 8.80 \ln \sigma - 439/RT \quad (5)$$

The stress slopes are 7.36, 7.39, and 8.80 for the three different subsets of all the N-155 data and compare well with the slope of 6.84 obtained earlier assuming a common creep mechanism in the intermediate stress range which covers the bulk of the data and corresponds to Case 2B of this analysis.

ORIGINAL PAGE IS
OF POOR QUALITY

For XF-818, the five different cases may be written as:

$$\text{Case 2A } \ln \epsilon_m = 12.8 + 6.44 \ln \sigma - 554/RT \quad (6)$$

$$\text{Case 2B } \ln \epsilon_m = 6.85 + 7.47 \ln \sigma - 545/RT \quad (7)$$

$$\text{Case 2C } \ln \epsilon_m = -32.7 + 12.6 \ln \sigma - 458/RT \quad (8)$$

$$\text{Case 2D } \ln \epsilon_m = 0.700 + 6.92 \ln \sigma - 461/RT \quad (9)$$

$$\text{Case 2E } \ln \epsilon_m = 0.524 + 6.83 \ln \sigma - 456/RT \quad (10)$$

Except for Case 2C (for $\sigma > 300$ MPa, at 650° and 705°C), the average slope is 6.92 and compares well with the simpler earlier analysis which gave a value of 7.35. The higher value of 12.6 for case 2C is also similar to the earlier value of 12.5 for similar subset conditions.

The extreme temperature and stress level data (Cases 2A and 2C) are plotted on Figs. 24 and 25 (based in Equations 4 and 7, respectively) to indicate the trend in correlation at these extreme levels.

The analytical data for temperature-compensated analysis for t_r and $t_{0.01}$ (Case 2B) are also given in Table 11. Graphical correlations of rupture life and time to 1% creep strain data for N-155 and XF-818 for Case 2B are given in Figs. 26 to 29, where the data for Cases 2A and 2C are plotted to indicate the trend at the extreme temperature and stress levels.

For alloy N-155, the analytical relationships for t_r and $t_{0.01}$ (for Case 2B) are as follows:

$$\begin{array}{l} \text{N-155} \\ \ln t_r = -13.9 - 6.28 \ln \sigma + 435/RT \end{array} \quad (11)$$

$$\ln t_{0.01} = -17.4 - 7.04 \ln \sigma + 467/RT \quad (12)$$

The stress slopes of -6.28 and -7.04 compare well with the stress slopes of -6.71 and -7.01 obtained earlier.

For alloy XF-818, the analytical relationships for t_r and $t_{0.01}$ (for Case 2B) are as follows:

$$\begin{array}{l} \text{XF-818} \\ \ln t_r = -13.2 - 7.52 \ln \sigma + 505/RT \end{array} \quad (13)$$

$$\ln t_{0.01} = -20.8 - 6.86 \ln \sigma + 522/RT \quad (14)$$

Again, the stress slopes of -7.52 and -6.86 compare very well with the stress slopes of -7.66 and -6.84 obtained earlier.

For Case 2C in XF-818, which deals with the lowest temperatures (and very high stresses), the stress slopes observed in the temperature-compensated analysis were -13.2 and -14.8 for t_r and $t_{0.01}$, respectively; the corresponding values obtained earlier were -15.3 for both t_r and $t_{0.01}$, and also indicate good correlation with the above data.

ORIGINAL PAGE IS
OF POOR QUALITY

Activation Energy, Q

The activation energies determined from this analysis are also summarized in Table 11. Out of 170 data, about 110 data (Case 2B) essentially fall under a single creep mode at intermediate stress and temperature levels. Thus, the Q values of Case 2B (Table 11) represent better correlation with a higher R² and a narrower 90% confidence limit on the estimated Q values. The activation energies for the different creep parameters ranged as follows:

	<u>Q, kJ/mole</u>	
	<u>Lowest</u>	<u>Highest</u>
Minimum creep rate	384 (IN 800H)	613 (A-286)
Rupture life	406 (IN 800H)	544 (A-286)

The much higher Q for $\dot{\epsilon}_m$ in A-286 merely reflects the observed large separation in the 760°-870°C^m range in the $\dot{\epsilon}_m$ vs. σ curves (Fig. 18). Similarly, the low Q for $\dot{\epsilon}_m$ in IN 800H indicates the much closer spacing observed in $\dot{\epsilon}_m$ vs. σ curves (Fig. 19) in the 815°-925°C range. A similar explanation may be noted for the high and low Q values of t_r for A-286 and IN 800H, respectively (Figs. 12 and 13).

With the exceptions of A-286 and IN 800H, the activation energies for $\dot{\epsilon}_m$ of the four other alloys were very similar:

<u>Alloy</u>	<u>Q for $\dot{\epsilon}_m$, kJ/mole^m</u>
N-155	527
19-9DL	573
CRM-6D	551
XF-818	545

The average Q of these four alloys is 549 kJ/mole, differing by less than 5% from the individual Q values.

Similarly, the activation energies for t_r for these four alloys were:

<u>Alloy</u>	<u>Q for t_r, kJ/mole</u>
N-155	435
19-9DL	461
CRM-6D	461
XF-818	505

Again, the average Q of these four alloys is 466 kJ/mole and close to the individual values.

The activation energy for time to rupture is less than that governing the creep phenomenon. Similar observations may be noted from Q values determined in other studies.² The difference in these two Q values may be related to the additional considerations of primary and tertiary creep stages in the case of

rupture when compared strictly to the secondary creep phenomenon in the case of minimum creep rate.

The activation energy for time to 1% creep strain ($t_{0.01}$) has a fairly narrow range (Case 2B) between the six alloys with an average of 511 kJ/mole and a range of 467 to 559 kJ/mole. As expected, the average Q for stress to 1% creep strain is higher than that for t_r and less than $\dot{\epsilon}_m$, because the average Q for $t_{0.01}$ is only affected by the primary creep conditions preceding its reaching the 1% creep strain while in the secondary creep mode.

The 90% confidence limits vary between alloys and between the three different parameters and are also significantly affected by the amount of data available. For Case 2B analyses, with between 12 and 28 data points for each of the three parameters, the 90% confidence limits are usually well within $\pm 10\%$ of the estimated mean Q values for $\dot{\epsilon}_m$ and t_r , and occasionally somewhat more for $t_{0.01}$ analysis. The major deviations were noted in A-286 and IN 800H and the least in the two cast alloys, CRM-6D and XF-818.

Predicted Stresses for Rupture and 1% Creep in 3500 Hours

Based on the temperature-compensated analytical regression data given in Table 11, stresses for 3500-h rupture lives were estimated and are given in Table 12. Along with these data, the 3500-h rupture life stresses estimated from linear regression at individual temperatures (including 90% confidence levels) are also tabulated. In practically all cases, the two estimated mean stresses are within $\pm 10\%$ of their mean values indicating the reliability of the data and the predictive analytical techniques used to determine the estimated stresses.

The 3500-h estimated rupture stresses based on temperature-compensated analysis were fitted with regression lines as a function of inverse absolute temperatures, as shown in Fig. 30. The MOD 1 and Reference Engine operation temperatures of 770° and 870°C,¹ respectively, are shown as vertical lines on Fig. 30. At the Mod 1 Engine temperature, IN 800H, A-286, and 19-9DL are considered inadequate to meet the requirements of the engine operating stress level.² The two cast alloys, CRM-6D and XF-818, as well as the wrought alloy, N-155, have adequate strength for MOD 1 engine service. At the higher operating temperature of 870°C for the Reference Engine, alloy A-286 strength is quite inadequate and IN 800H and 19-9DL become marginal at the design stress level of 28 MPa.³ Wrought alloy N-155 retained the best strength properties, whereas cast alloy CRM-6D remained twice as strong as N-155 at 870°C.

Table 13 summarizes the predicted stresses to 1% creep strain in 3500 h based on temperature-compensated analysis. Along with these data, estimated stress levels to 1% creep strain in 3500 h based on regression analysis at individual temperatures are also tabulated with their 90% confidence levels. The differences between these two estimates are well within $\pm 10\%$ of the mean estimated values, except for alloys A-286 and IN 300H.

Fractography and Microstructural Analysis

Fracture Location and Appearance

All the specimen fractures were carefully examined and fracture locations identified. In the two cast alloys, with one exception, all the fractures were located well within the reduced parallel section. In the wrought alloys, A-286 had 8 specimens where the fractures were located beyond the parallel section, though in all cases very close to the end of the section. Five or six specimens showed similar fracture locations in IN 800H, N-155, and 19-9DL.

In general, at the lower temperatures multiple fine cracking near the fracture region was minimal. Light to heavy multiple cracking appeared at 760°C and higher.

Only small degrees of localized area reduction were noted with most wrought specimens, indicating uniform extension. In the cast alloys, a similar pattern was also observed with a strong effect of stress level and time to rupture affecting the degree of necking. At the higher temperatures of 870° and 925°C, XF-818 specimens showed more necking than CRM-6D specimens with reduction in area as high as 48%.

A number of ruptured specimens from different creep tests were selected for the metallurgical examination of creep fractures (Table 14). Since creep fracture may be associated with significant microstructural changes, some of the creep fracture specimens (Table 14) were polished in their longitudinal cross-section to examine the microstructure extending from undeformed areas to the fracture edge. Results of this study are presented below with some typical illustrations.

Fracture Examination

Fracture analysis was performed on a selected number of creep-rupture specimens of various alloys tested in air. This study reveals the modes and mechanisms of failure in each case and their relation to alloy composition, fabrication mode (wrought or cast), stress, and test temperatures. Typical fracture surfaces from wrought and cast alloys are shown in Figs. 31 to 34.

19-9DL. Macroexamination at low magnifications showed rough and granular fractures, light to dark gray in appearance. The lower temperature fractures were more rugged and rough. These fractures seemed to have originated at multiple locations at surface and edge cracks, and the overload (final rupture) region was usually located near the middle of the specimen width. Microfractographic examination revealed that the main fracture mechanism was dimple rupture. These fractures were normally more oxidized in the initiation and propagation zones than in the overload region. The extent of oxidation increased with increasing test temperatures. Figure 32 clearly illustrates this fact for the case of the 19-9DL specimen tested at 870°C. Figure 32 shows typical macro- and microfractographs from the 19-9DL alloy creep-rupture specimen exposed at 870°C and 41 MPa stress level. Figure 32a shows macrofractographic views (A and B) of the mating fractured surfaces. In general, the fracture surfaces appeared very rough and heavily oxidized due to exposure to air at this high temperature (870°C). Figure 32b is a side view of the

fracture surface in Fig. 32a (B). Many surface cracks are visible. This fracture also started at multiple locations at the outer surface. The separation of the fractured surfaces seemed to have progressed from the left end of the specimen to the right, because the fracture appeared increasingly rougher toward the right due to overload. Figure 32c presents a typical microfractograph from the center of the specimen on surface B (Fig. 32a). Again, dimple rupture is the main mode of fracture. Figure 32c also shows a thick granular oxide layer covering nearly the entire area.

A-286. All the three fractures examined for this alloy (Table 14) showed very rough and granular fractures at low magnifications (Fig. 31c). For the specimens tested at 705° and 815°C, the main fracture mode was decohesive rupture. At 870°C, the fracture showed mixed modes ranging from intergranular fracture in the initiation zone to fracture by dimple-rupture mode in the overload zone. The degree of oxidation increased with increasing test temperature. All the fractures examined had originated at multiple sites from surface cracks.

N-155. Figures 31d and e show typical low-magnification views of fracture surfaces for this alloy. Fractures from this alloy exhibited varying degrees of roughness and colors ranging from yellowish brown to deep blue. The bluish area tended to be more oxidized. In the 650°C specimen, a rough intergranular fracture showing fine dimple covered facets was observed. In the 760°C, 165 MPa specimen, the fracture appeared rough near both ends and relatively smoother, dull gray and oxidized in the middle region. At 815° and 870°C, fractures had a rough, fine granular appearance and were considerably oxidized. The 925°C fracture was very rugged. Its one end and middle regions were heavily oxidized, and the less oxidized other end showed large dimples surrounded by a high density of smaller dimples (overload region). All these specimens showed abundant surface cracks (Figs. 31d and e) which probably acted as multiple initiation sites.

IN 800H. In the specimen tested at 650°C and 207 MPa, the fracture was very rough and uneven. It had originated at multiple locations near one end and progressed by dimple-rupture mechanism. For the 760°C specimen tested at 124 MPa, the fracture showed sharp ridges with shiny slopes showing fine granular fracture. For the 760°C specimen tested at 70 MPa, the fracture was rough and had propagated from the ends toward the middle at sharp angles (Fig. 31f). Figure 31g shows a view of the fracture in the specimen tested at 815°C and 45 MPa. This fracture showed a coarse granular topography and extensive surface cracking. At 925°C and 48 MPa, the fracture was very rugged and showed very prominent edge cracks. All the above fractures showed varying degrees of oxidation, and the heavy oxidation in the 925°C specimen had completely masked the finer fracture features.

XF-818. Six specimens were examined from this alloy (Table 14). The fracture features observed were very similar--rough and jagged textures consisting of smooth facets intermixed with rugged areas. All the specimens showed varying degrees of surface cracking. These fractures originated at multiple locations at surface cracks and progressed along smooth facets by ductile fracture of dendrites. Figures 33a and b are macroscopic views of fracture surfaces in two XF-818 specimens. The dendritic texture on smooth facets is obvious. High-temperature fractures showed more oxidation. Figure 34 shows two halves of the fracture for the specimen tested at 815°C and 138

MPa. This fracture apparently initiated at the edge of the specimen (areas a and b of Fig. 34a) where the fracture was relatively smoother and fine textured. The entire fracture displayed a jagged topography, and the areas c and d (Fig. 34a) were rough in appearance. The final separation occurred near the center of the specimen. Many surface cracks which could act as initiation sites were observed. In the initiation regions (areas a and b, Fig. 34a), the primary mode of fracture was dimple rupture, exhibiting a layer of fractured dendrites. The entire fracture surface was oxidized, especially areas c and d (Fig. 34a) where oxidation masked the entire fracture area. Heavy oxidation was observed in the area at the center of the specimen where the final separation seemed to have occurred.

CRM-6D. Five specimens were analyzed for this alloy (Table 14). The general fracture features observed were quite similar to those for the XF-818 fractures discussed earlier. At low magnifications, fractures appeared rough and rugged, displaying smooth facets of various sizes intermixed with rough and rugged areas. Surface cracks were observed invariably, especially close to the fracture, indicating multiple initiation sites. Figures 33c and d show fractures from two CRM-6D specimens. Microfractographic examination generally showed ductile dimple rupture of fine and coarse columnar dendrites in the smoother areas. Rougher areas showed either a coarse columnar fracture or ductile tearing with banded dimples in some cases. Overload regions were normally less oxidized than the initiation and propagation regions.

Cross-Section Examination

Mating halves of some of the fracture specimens listed in Table 14 were metallurgically polished in their longitudinal cross-section direction approximately halfway through the specimen thickness. In order to preserve the integrity of the fracture edge and surface oxides, these specimens were nickel-plated before polishing. After polishing, all the specimens were electrolytically etched with 10% oxalic acid to reveal various constituents and their microstructures. They were examined under optical microscope and SEM. In most cases creep rupture failure was found to be a result of intergranular cracking propagating from the surface or from within the matrix. These cracks usually originated at grain boundary regions.

19-9DL. Figure 35a is a low-magnification optical photomicrograph of the cross-section from the 870°C, 29 MPa specimen (Table 14). It shows numerous intergranular cracks near the fracture edge and extending back into the test piece cross-section. The microstructure of the 815°C, 59 MPa specimen appeared to be similar to the 870°C, 29 MPa specimen. At higher magnifications, both these cross-sections showed larger angular grain boundary (gb) carbides and fine matrix carbides, with gb carbide size being somewhat smaller for the 870°C specimen. The gb phases close to the fracture edge appeared to be continuous as opposed to those in the matrix. Figure 35b shows a 200X SEM view of the area near the fracture edge in the 815°C, 59 MPa specimen. On the right-hand side, intergranular cracks appear dark. The magnified view of the area inside the inset is shown on the left (Fig. 35b). Continuity of the gb phases is to be noted. As a result of this continuity, even the matrix intergranular cracks had developed considerable amounts of oxides.

A-286. Only the cross-section from the 815°C, 55 MPa specimen was examined for this alloy. At low magnification (Fig. 36a), this specimen showed mostly smaller intergranular cracks near the fracture edge, but such cracks were not observed to extend backwards from the edge. Both large and small side-edge cracks were observed over the entire length of the cross-section. The microstructure consisted of large gb and matrix platelet precipitates and an overaged matrix containing a high density of needle-shaped eta phase (Ni_3Ti) precipitates. Figure 36b shows a view of the gb and matrix precipitates in the 815°C, 55 MPa specimen (Table 14).

N-155. The 815°C, 63 MPa and 870°C, 47 MPa specimens both showed profuse intergranular cracking, especially near the fracture edge. Grain boundary and matrix secondary carbides (M_6C or M_{23}C_6) were observed both near and away from the fracture edge. The gb precipitates exhibited continuity and were probably responsible for initiating the intergranular cracking in these specimens. Figures 37a and b show the fracture edge and gb carbides in the 870°C, 47 MPa specimen with abundant intergranular cracks on side edges.

IN 800H. Cross-sections from the 760°C, 70 MPa and 815°C, 45 MPa specimens were examined for this alloy. The 760°C specimen showed an intergranular fracture. Not many cracks were observed near the fracture edge because of less material from this area in cross-section preparation. The gb near the fracture edge showed continuous precipitates. Away from the fracture edge, the gb appeared narrower. Some side-edge cracks were also observed near the fracture zone.

The 815°C specimen had fractures in two different areas and showed numerous intergranular cracks, both near and away from the fracture zones. Many side-edge cracks, some penetrating deep into the specimen, were observed throughout the length of the specimen. Figure 38a shows a low-magnification view of the cross-section from the 815°C specimen. Continuous gb precipitates were observed in the vicinity of intergranular cracks.

XF-818. The fracture in the 815°C, 103 MPa specimen had occurred by an interdendritic mode. No difference in dendrite size was noted between the fracture edge and the matrix. A few side-edge cracks were present. These cracks, too, had progressed along interdendritic paths. Interdendritic precipitates consisted of a lamellar phase plus some blocky precipitates. The lamellar phase appeared somewhat more outlined near the fracture edge. In addition, a finer matrix precipitate was also observed.

In the 760°C, 193 MPa specimen, most of the dendrites close to the fracture edge were oriented perpendicular to the fracture edge. The fracture had followed an interdendritic path. The interdendritic precipitate areas in this specimen were thicker than in the 815°C specimen and consisted of a major lamellar phase with some blocky particles. Close to the fracture edge, blocky particles were generally absent and the lamellar phase appeared more outlined. Figure 38b shows a low-magnification view of the fracture cross-section from the 760°C specimen. At higher magnifications, a dendritic cast structure dominated by lamellar M_3B_2 phase of this high-boron alloy was observed.

CRM-6D. Cross-sections from the 870°C, 117 MPa and 760°C, 193 MPa specimens were examined. Both the specimens showed an interdendritic fracture. No significant difference in dendrite size or interdendritic precipitates was

noticed between the fracture edge and the areas away from it. A fine matrix precipitate existed in all the areas. Only a few side-edge or internal cracks were observed. These specimens showed two kinds of interdendritic phases--one with outline and the other without it. Figure 39a shows a view of the cross-section from the 870°C specimen. Figure 39b shows the interdendritic phases and matrix precipitates in a typical area from the 760°C specimen. The figure on the left-hand side of Fig. 39b is an enlargement of the area inside the insert on the right-hand side. These carbides showed a high-carbon high-chromium chemistry upon energy-dispersive X-ray analysis of individual particles.

SUMMARY OF RESULTS

Six iron-base superalloys were tested in air for creep rupture at 650° to 925°C. The rupture life (t_r), time to 1% creep strain ($t_{0.01}$), and minimum creep rate ($\dot{\epsilon}_m$) data were analyzed statistically. The analyses indicate the following:

- At the Reference Engine operating temperature of 870°C and 28 MPa stress level, N-155 strength was adequate while 19-9DL and IN 800H strengths were marginal, and A-286 strength was inadequate. Both XF-818 and CRM-6D exceeded the strength requirements for the Reference Engine.
- Rupture life activation energy was least for IN 800H (406 kJ/mole) and highest for A-286 (544 kJ/mole) with the other four alloy values in the range of 435 to 505 kJ/mole. The activation energies for minimum creep rate exceeded that of rupture life with the exception of IN 800H where the values were close.
- Both the temperature-compensated analysis as well as the simple power law analysis of $\dot{\epsilon}_m$ vs. σ at the 760° to 870°C level gave similar stress exponent values in the range of 6.5 to 7.5, indicative of a dislocation climb model (lattice diffusion control).⁴ The observed lower values of about 3 to 4 at the higher temperatures are indicative of viscous glide behavior while the much higher values of 9 to 12 at the lower temperatures may be indicative of dislocation climb (core diffusion control).⁴
- Both N-155 and 19-9DL showed total elongation in the 30 to 50% range at the intermediate temperature and stress levels. XF-818 showed better ductility than CRM-6D at all temperature levels, and both the cast alloys had less than one-half the ductility of the wrought alloys.
- In wrought alloys, the main fracture mechanism was dimple rupture with multiple location initiation in most cases. Dendritic patterns on relatively smooth facets were noted on the fracture surfaces of both the cast alloys.

REFERENCES

1. Joseph R. Stephens, "Hostile Environmental Conditions Facing Candidate Alloys for the Automotive Stirling Engine," Conference Proceedings on Environment Degradation of Engineering Materials in Hydrogen, Sept. 21-23, 1981, pp. 123-132, Virginia Polytechnic Institute, Blacksburg, Virginia 24061.
2. Walter R. Witzke and Joseph R. Stephens, "Creep-Rupture Behavior of Seven Iron-Base Alloys After Long-Term Aging at 760° in Low Pressure Hydrogen," NASA TM-81534, August 1980, NASA-Lewis Research Center, Cleveland, Ohio.
3. Joseph R. Stephens, NASA-Lewis. Private Communication, 1982.
4. H. J. Frost and M. F. Ashby, "Deformation-Mechanism Maps for Pure Iron, Two Austenitic Stainless Steels, and a Low-Alloy Ferritic Steel," Cambridge University Report, July 1975, Cambridge, U.K.
5. F. R. Larson and J. Miller, Trans. ASME, Vol. 74, 1952, p. 765.
6. S. S. Manson and A. M. Haford, "A Linear Time-Temperature Relation for Extrapolation and Creep and Stress-Rupture Data," NACA Technical Note 2890, March 1952.
7. S. S. Manson and W. R. Brown, Proc. ASTM, ASTEA, Vol. 53, 1953, p. 693.
8. O. D. Sherby, "Factors Affecting the High Temperature Strength of Polycrystalline Solids," Acta Met., Vol. 10, No. 2, 1962, pp. 135-147.
9. J. E. Dorn, "The Spectrum of Activation Energies for Creep," in Creep and Recovery, ASM, Metals Park, Ohio, 1957, pp. 255-283.
10. R. M. Goldhoff, "The Evaluation of Elevated Temperature Creep and Rupture Strength Data: An Historical Perspective," in Characterization of Materials for Service at Elevated Temperatures, G. V. Smith, ed., Publ. No. MPC-7. ASME, New York, 1978, pp. 247-265.

TABLE 1. NOMINAL CHEMICAL COMPOSITION OF IRON-BASE ALLOYS

Alloys	Nominal Composition, %													
	C	Mn	Si	Cr	Ni	Co	Mo	W	Cb	Ti	Al	B	Fe	Others
A-286	0.05	1.40	0.40	15	26	-	1.25	-	-	2.15	0.2	0.003	Ba1	0.03 V
Incoloy 800H	0.05	0.8	0.5	21	32.5	-	-	-	-	0.4	0.4	-	46	0.4 Cu
N-155	0.15	1.5	0.5	21	20	20	3.0	2.5	1.0	-	-	-	Ba1	0.15 N
19-9DL	0.30	1.10	0.60	19	9.0	-	1.25	1.20	0.40	0.30	-	-	Ba1	-
CRM-6D ^a	1.05	5.00	0.50	22	5.0	-	1.0	1.0	1.0	-	-	0.003	Ba1	-
XF-818 ^a	0.20	0.15	0.30	18	18	-	7.5	-	0.40	-	-	0.70	Ba1	0.12 N

^aHeat analyses of cast specimens. Sample No. 6365 (CRM-6D) and No. 6366 (XF-818):

CRM-6D	1.08	4.65	0.46	22.9	5.56	-	0.98	0.98	0.97	-	-	0.007	Ba1	0.069 N 0.008 P 0.013 S
XF-818	0.21	0.29	0.34	18.3	18.0	-	7.32	-	0.43	-	-	0.75	Ba1	0.106 N 0.007 P 0.010 S

ORIGINAL PAGE IS
OF POOR QUALITY

TABLE 2. ALLOY SPECIFICATIONS AND HEAT TREATMENT
CONDITION FOR TEST SPECIMENS

Alloy	Specification	Heat Treatment (in vacuum)
A-286	55250 ^a	Solution 1149°C (2100°F) ^{b,c} Age 718°C (1325°F)-16 hr/AC
Incoloy 800H	5871D ^d	Solution 1149°C (2100°F) ^{b,c}
N-155	5532C ^e or 5585B ^f	Solution 1177°C (2150°F) ^{b,c}
19-9DL	5526E ^g	Solution 1204°C (2200°F)-10 min ^c
CRM-6D	(None available)	Age 650°C (1200°F)-100 h
XF-818	(None available)	None specified

^aAMS 5525D revised 10/15/79 supersedes AMS 5525C.

^bSolution annealing time of 142 s/mm (1 hr/in.) thickness minimum.

^cRapid cool or quench from solution temperature.

^dAMS 5871D issued 5/15/72.

^eAMS 5532C revised 7/15/77 supersedes AMS 5532B.

^fAMS 5585B revised 1/15/78 supersedes AMS 5585A.

^gAMS 5526E revised 1/15/78 supersedes AMS 5526D.

ORIGINAL PAGE IS
OF POOR QUALITY

TABLE 3. AIR CREEP-RUPTURE TEST DATA FOR ALLOY A-286

(1)	(2)	(3)	(4)	(5)	(6)	(7)	(8)	(9)
A1R	A2R	650	483	36.2	5.54E-07	11.4	0.2	22.0
A1R	A2R	650	414	568.1	3.03E-09	4.4	340.	260.
A1R	A2R	650	310		9.72E-11			
A1R	A2R	705	379	35.0	1.25E-07	13.8	13.0	7.0
A1R	A2R	705	276	706.6	1.49E-09	21.0	542.	460.
A1R	A2R	705	234	1222.	1.22E-10	3.4	1095	600.
A1R	A2R	705	179		1.53E-10			
A1R	A2R	760	345	5.4	5.54E-06	26.3	0.3	
A1R	A2R	760	276	27.2	2.04E-07	25.9	10.5	7.0
A1R	A2R	760	207	126.0	1.02E-08	23.4	76.0	60.0
A1R	A2R	760	179	254.8	5.54E-09	18.0	156.	110.
A1R	A2R	760	124	1181.0	1.21E-10	8.2	500.	250.
A1R	A2R	760	83					325.
A1R	A2R	815	138	0.9		44.6	8.1	6.0
A1R	A2R	815	110	49.7	3.45E-08	25.4	27.5	15.0
A1R	A2R	815	83	206.4	1.11E-08	16.0	70.0	60.0
A1R	A2R	815	62	439.5	6.42E-09	11.8	102.	90.0
A1R	A2R	815	55	1030.		10.7	234.	340.
A1R	A2R	815	41		2.20E-09		521.	170.
A1R	A2R	870	55	15.0	1.04E-05	59.2	0.3	5.0
A1R	A2R	870	41	59.8	1.85E-06	87.2	1.5	30.0
A1R	A2R	870	31	160.0	7.03E-07	49.5	4.0	85.0
A1R	A2R	870	21	6222.0	1.72E-07	29.8	19.5	4500
A1R	A2R	925	28	53.0	2.33E-06	58.4	1.0	30.0
A1R	A2R	925	21	171.9	6.24E-07	42.9	3.5	140.
A1R	A2R	925	17	2214.0		38.7	7.0	
A1R	A2R	925	9.0		4.17E-08		70.0	

Col.	Explanation
1	Environment: AIR, HYD (Hydrogen) - not yet included.
2	Alloy code: A28 - A-286; IN8 - IN 800H; N15 - N155; 199 - 19-9DL; CRM - CRM-6D; XF8 - XF-818
3	Test temperature: (T), °C
4	Applied initial stress (σ), MPa
5	Rupture life (t_r), hr
6	Minimum creep rate ($\dot{\epsilon}_m$), s ⁻¹
7	Total elongation (ϵ), %
8	Time to reach 1% creep elongation ($t_{0.01}$), hr
9	Time to reach tertiary creep stage (t_{ter}), hr

TABLE 4. AIR CREEP-RUPTURE TEST DATA FOR ALLOY IN ROOM

(1)	(2)	(3)	(4)	(5)	(6)	(7)	(8)	(9)
AIR	IN8	650	276	54.8	2.64E-07	32.2	3.0	19.0
AIR	IN8	650	248	101.4	1.39E-07	26.3	5.0	25.0
AIR	IN8	650	207	309.0	6.94E-08	15.0	8.7	120.
AIR	IN8	650	186				63.0	1100
AIR	IN8	705	186	46.2	6.25E-07	26.8	1.0	16.0
AIR	IN8	705	124	848.1	3.61E-08	36.8	50.0	275.
AIR	IN8	705	110	1475.0	2.28E-08	19.6		400.
AIR	IN8	760	152	4.7	8.72E-06	46.8		2.0
AIR	IN8	760	124	28.9	1.71E-06	53.0	0.5	6.0
AIR	IN8	760	103	132.2	5.47E-07	43.7	3.0	70.0
AIR	IN8	760	76	1265.0	2.78E-08	28.1	68.0	475.
AIR	IN8	760	70	4490.0	7.58E-09	29.5		4300
AIR	IN8	815	110	14.6	4.44E-06	59.6	0.2	4.0
AIR	IN8	815	82	37.5	1.03E-06	22.3	1.8	13.5
AIR	IN8	815	83	72.6		32.1	4.0	20.0
AIR	IN8	815	76	83.2	4.89E-07	23.3	4.5	40.0
AIR	IN8	815	62	780.6		18.1	78.0	250.
AIR	IN8	815	52		4.67E-08	29.0		300.
AIR	IN8	815	52	636.0	3.03E-08	23.6		435.
AIR	IN8	815	45	2862.0	1.11E-08	18.7		2400
AIR	IN8	815	41					
AIR	IN8	870	76	19.3	1.39E-06	32.2	2.1	4.5
AIR	IN8	870	62	39.3	4.81E-07	15.0	5.5	12.0
AIR	IN8	870	48	161.0	1.50E-07	18.1	10.0	40.0
AIR	IN8	870	34	451.6	9.92E-08	23.1		370.
AIR	IN8	870	31		1.31E-09			
AIR	IN8	870	26	1724.0	2.22E-09	16.9		1005
AIR	IN8	925	48	53.0	1.75E-07	24.0	10.0	11.0
AIR	IN8	925	41	130.5	5.50E-08	23.2	38.5	22.0
AIR	IN8	925	31	292.2		19.7	48.0	62.0
AIR	IN8	925	21		1.39E-09		675.	280.

Col.	Explanation
1	Environment: AIR, HYD (Hydrogen) - not yet included.
2	Alloy code: A28 - A-286; IN8 - IN ROOM, N15 - N155; 199 - 19-9DL; CRM - CRM-6D; XFB - XF-818
3	Test temperature: (T), °C
4	Applied initial stress (σ), MPa
5	Rupture life (t_r), hr
6	Minimum creep rate ($\dot{\epsilon}_m$), s^{-1}
7	Total elongation (ϵ), %
8	Time to reach 1% creep elongation ($t_{0.01}$), hr
9	Time to reach tertiary creep stage (t_{ter}), hr

ORIGINAL PAGE IS
OF POOR QUALITY

TABLE 5. AIR CREEP-RUPTURE TEST DATA FOR ALLOY N-155

(1)	(2)	(3)	(4)	(5)	(6)	(7)	(8)	(9)
ATR	N15	650	414	2.7	4.63E-06	23.6	0.5	0.2
ATR	N15	650	379	14.8	7.45E-07	19.9	1.7	13.0
ATR	N15	650	276	968.7	2.78E-08	26.2	20.0	475.
ATR	N15	705	276	42.5	6.72E-07	28.3	0.8	20.0
ATR	N15	705	193	527.8	6.11E-08	46.0	16.0	200.
ATR	N15	705	159	3667.0	6.87E-09	29.2	89.0	1670
ATR	N15	760	241	9.0	1.85E-06	42.7	0.2	
ATR	N15	760	193	36.8	1.25E-06	44.0	1.0	12.0
ATR	N15	760	165	115.3	4.14E-07	51.5	4.0	50.0
ATR	N15	760	124	573.6	5.00E-08	71.1	16.0	290.
ATR	N15	760	97	4523.0	4.17E-09	18.0	144.	1100
ATR	N15	815	165	7.5	4.14E-06	58.3	0.2	
ATR	N15	815	124	42.5	1.50E-06	53.2	1.3	20.0
ATR	N15	815	110	128.8	2.92E-07	46.8	3.0	50.0
ATR	N15	815	83	457.3	5.28E-08	25.0	19.0	180.
ATR	N15	815	76	931.3	2.94E-08	34.7	30.0	325.
ATR	N15	815	63	2536.0	7.51E-09	12.1	170.	1800
ATR	N15	870	110	8.9	6.67E-06	65.0	0.2	2.1
ATR	N15	870	93	55.6		59.6		11.0
ATR	N15	870	83	58.0	9.92E-07	46.0	2.5	24.0
ATR	N15	870	69	212.2	2.11E-07	35.9	7.0	83.0
ATR	N15	870	59	436.7	5.56E-08	26.7	29.0	220.
ATR	N15	870	47	2497.0	1.36E-08	26.3	85.0	1210
ATR	N15	925	69	32.7		38.8		8.5
ATR	N15	925	59	49.2	1.07E-06	43.3	2.0	16.0
ATR	N15	925	41	354.2	9.17E-08	27.7	29.0	120.

Col.	Explanation
1	Environment: AIR, HYD (Hydrogen) - not yet included.
2	Alloy code: A28 - A-286; IN8 - IN 800H; N15 - N155; 199 - 19-9DL; CRM - CRM-60; XF8 - XF-818
3	Test temperature: (T), °C
4	Applied initial stress (σ), MPa
5	Rupture life (t_r), hr
6	Minimum creep rate ($\dot{\epsilon}_m$), s^{-1}
7	Total elongation (c), %
8	Time to reach 1% creep elongation ($t_{0.01}$), hr
9	Time to reach tertiary creep stage (t_{ter}), hr

ORIGINAL PAGE IS
OF POOR QUALITY

TABLE 6. AIR CREEP-RUPTURE TEST DATA FOR ALLOY 19-9DL

(1)	(2)	(3)	(4)	(5)	(6)	(7)	(8)	(9)
ATR	199	650	414	1.1	4.72E-06	18.8		0.6
ATR	199	650	310	27.9	9.29E-08	10.1	1.9	22.5
ATR	199	650	276	135.9	3.58E-08	11.9	32.0	55.0
ATR	199	705	276	10.9	5.97E-07	16.9	0.7	
ATR	199	705	172	268.5	5.69E-08	24.2	50.0	65.0
ATR	199	705	131	1342.0	1.14E-08	12.1	152.	650.
ATR	199	760	193	8.5	1.35E-06	30.0		
ATR	199	760	172	20.2	6.95E-07	31.0	2.5	14.5
ATR	199	760	138	101.0	3.22E-07	37.4	9.0	34.0
ATR	199	760	100	739.1	1.86E-08	18.8	89.0	280.
ATR	199	760	86	1687.0	5.77E-09	12.1	300.	425.
ATR	199	815	134	2.8	2.22E-05	44.8		1.9
ATR	199	815	124	14.2	3.33E-06	33.4	0.4	11.0
ATR	199	815	103	66.4	4.33E-07	29.2	4.0	22.0
ATR	199	815	83	173.1	1.44E-07	32.3	11.0	62.0
ATR	199	815	72	324.1	6.03E-08	25.0	40.0	105.
ATR	199	815	59	1118.0	5.72E-09	19.1	330.	350.
ATR	199	870	103	1.8	1.89E-05	61.6		0.5
ATR	199	870	83	10.2	5.00E-06	42.4	0.4	3.2
ATR	199	870	69	38.0	1.60E-06	36.4	1.2	17.0
ATR	199	870	55	107.9	3.47E-07	34.3	8.0	45.0
ATR	199	870	41	406.3	3.19E-08	28.8	82.0	130.
ATR	199	870	33	799.0	2.00E-08		89.0	290.
ATR	199	870	29	1300.0	6.94E-09	12.3	279.	120.
ATR	199	925	69	4.1	1.58E-05	47.6	0.2	1.8
ATR	199	925	55	16.3	3.06E-06	37.1	0.7	4.5
ATR	199	925	35	177.2	1.25E-07	27.5	10.5	55.0

Col.	Explanation
1	Environment: AIR, HYD (Hydrogen) - not yet included.
2	Alloy code: A28 - A-286; IN8 - IN 80GH; N15 - N155; 199 - 19-9DL; CRM - CRM-6D; XF8 - XF-818
3	Test temperature: (T), °C
4	Applied initial stress (σ_i), MPa
5	Rupture life (t_r), hr
6	Minimum creep rate ($\dot{\epsilon}_m$), s ⁻¹
7	Total elongation (ϵ_t), %
8	Time to reach 1% creep elongation ($t_{0.01}$), hr
9	Time to reach tertiary creep stage (t_{ter}), hr

**ORIGINAL PAGE IS
OF POOR QUALITY**

TABLE 7. AIR CREEP-RUPTURE TEST DATA FOR ALLOY CRM-6D

(1)	(2)	(3)	(4)	(5)	(6)	(7)	(8)	(9)
A1R	CRM	650	343	190.7	3.67E-04	5.6	30.0	115.
A1R	CRM	650	374	305.0	1.42E-04	4.2	36.0	150.
A1R	CRM	705	315	49.1		7.6	6.0	20.0
A1R	CRM	705	310	147.4	1.06E-07	8.6	12.0	70.0
A1R	CRM	705	276	427.4	1.32E-08	8.2	53.0	175.
A1R	CRM	705	255		4.44E-09		90.0	
A1R	CRM	760	290	11.5	1.01E-06	7.0	1.6	6.5
A1R	CRM	760	276	23.6	6.28E-07	10.7	2.9	14.0
A1R	CRM	760	255	56.0	2.06E-07	7.6	2.9	20.5
A1R	CRM	760	241	140.2	5.61E-08	9.9	12.0	60.0
A1R	CRM	760	221	354.4	3.28E-08	10.3	20.0	240.
A1R	CRM	760	207	796.7	6.03E-09	8.7	59.0	610.
A1R	CRM	760	193		3.41E-09		63.0	
A1R	CRM	760	193	1708.0	4.08E-09	7.7	95.0	1100
A1R	CRM	815	241	7.1	1.16E-06	13.0	0.6	4.2
A1R	CRM	815	193	78.6	1.48E-07	11.8	6.5	40.0
A1R	CRM	815	172	281.9	2.86E-08	10.6	19.0	175.
A1R	CRM	815	152	768.0	6.11E-09	7.6	58.0	440.
A1R	CRM	815	131		1.32E-09		560.	
A1R	CRM	815	131	1808.0	1.54E-09	4.6	682.	1300
A1R	CRM	870	172	11.0	6.28E-07	11.1	2.0	5.5
A1R	CRM	870	152	29.7	2.94E-07	11.7	6.0	17.0
A1R	CRM	870	138	19.1		21.7		8.0
A1R	CRM	870	117	430.5	7.64E-09	5.6	80.0	230.
A1R	CRM	870	117	461.0	9.81E-09	6.6	125.	215.
A1R	CRM	870	97		1.00E-09		498.	470.
A1R	CRM	870	97	1334.0	1.30E-09	2.8	1110	1000
A1R	CRM	925	117	28.4	1.79E-07	12.5	8.5	12.0
A1R	CRM	925	103	55.4	4.28E-08	9.6	22.0	32.0
A1R	CRM	925	90	237.3	1.13E-08	5.5	146	130.

Col.	Explanation
1	Environment: AIR, HYD (Hydrogen) - not yet included.
2	Alloy code: A28 - A-286; IN8 - IN 80CH; N15 - N155; 199 - 19-9DL; CRM - CRM-6D; XF8 - XF-818
3	Test temperature: (T), °C
4	Applied initial stress (σ), MPa
5	Rupture life (t_r), hr
6	Minimum creep rate ($\dot{\epsilon}_m$), s^{-1}
7	Total elongation (ϵ), %
8	Time to reach 1% creep elongation ($t_{0.01}$), hr
9	Time to reach tertiary creep state (t_{ter}), hr

TABLE 8. AIR CREEP-RUPTURE TEST DATA FOR ALLOY XF-818

(1)	(2)	(3)	(4)	(5)	(6)	(7)	(8)	(9)
AIR	XFB	650	414	143.2	6.72E-08	7.5	11.0	100.
AIR	XFB	650	393	300.8	3.11E-08	8.0	17.0	220.
AIR	XFB	705	414	3.1	1.60E-06	6.7	0.3	
AIR	XFB	705	379	20.9	3.97E-07	7.2	3.5	11.0
AIR	XFB	705	331	103.0	9.02E-08	10.1	10.5	50.0
AIR	XFB	705	283	541.0	1.52E-08	9.0	130.	160.
AIR	XFB	760	345	2.3	0.12E-06	8.2	0.3	
AIR	XFB	760	262	38.4	3.50E-07	12.7	4.5	17.0
AIR	XFB	760	221	132.3	1.16E-07	13.6	14.0	50.0
AIR	XFB	760	207	261.7	5.67E-08	12.7	31.5	80.0
AIR	XFB	760	152	2497.0	4.58E-09	11.4	300.	860.
AIR	XFB	815	241	4.2	2.77E-06	13.1	0.5	3.3
AIR	XFB	815	172	62.5	3.50E-07	22.3	5.0	24.0
AIR	XFB	815	138	199.5	8.33E-08	14.1	14.5	95.0
AIR	XFB	815	117	1104.0	1.78E-08	18.0	60.0	550.
AIR	XFB	815	103	3115.0	4.87E-09	23.8	200.	742.
AIR	XFB	870	172	4.1	5.15E-06	16.0	0.8	1.0
AIR	XFB	870	117	58.5	3.64E-07	20.6	4.5	22.0
AIR	XFB	870	97	194.0	9.00E-08	19.0	14.0	65.0
AIR	XFB	870	63	2198.0	6.78E-09	17.0	205.	640.
AIR	XFB	925	103	11.8	2.11E-06	25.2	0.8	5.0
AIR	XFB	925	69	128.5	1.46E-07	23.1	15.0	42.0
AIR	XFB	925	55	316.4	5.36E-08	18.4	20.0	120.

Col.	Explanation
1	Environment: AIR, HYD (Hydrogen) - not yet included.
2	Alloy code: A28 - A-286; IN8 - IN 800H; N15 - N155; 199 - 19-9DL; CRM - CRM-6D; XFB - XF-818
3	Test Temperature: (T), °C
4	Applied initial stress (σ), MPa
5	Rupture life (t_r), hr
6	Minimum creep rate ($\dot{\epsilon}_m$), s^{-1}
7	Total elongation (ϵ), %
8	Time to reach 1% creep elongation ($t_{0.01}$), hr
9	Time to reach tertiary creep stage (t_{ter}), hr

ORIGINAL PAGE IS
OF POOR QUALITY

**ORIGINAL PAGE IS
OF POOR QUALITY**

**TABLE 9. BASIC TEMPERATURE AND STRESS RANGES FOR DIRECT
CORRELATION OF INITIAL STRESS WITH RUPTURE LIFE (t_r),
TIME TO 1% STRAIN ($t_{0.01}$), AND MINIMUM CREEP RATE ($\dot{\epsilon}_m$)**

Alloy	Key Temp., °C	Test Conditions
<u>ln σ vs. ln t_r</u>		
A-286	760	705° to 925°C, and $\sigma = 25$ to 300 MPa and 925°C, 21 MPa
IN 800H	815	650° to 925°C, and $\sigma = 40$ to 300 MPa
N-155	760	650° to 925°C, and $\sigma = 50$ to 300 MPa
19-9DL	760	650° to 925°C, and $\sigma = 40$ to 400 MPa
CRM-6D	760	650° to 925°C, and $\sigma = 80$ to 400 MPa
XF-818	815 705	760° to 870°C, and $\sigma = 90$ to 300 MPa 650°, 705°C, and $\sigma > 300$ MPa
<u>ln σ vs. ln $t_{0.01}$</u>		
A-286	870	705° to 925°, and $\sigma = 9$ to 300 MPa
IN 800H	870 815	870°, 925°C, and $\sigma = 20$ to 80 MPa 650° to 815°C, and $\sigma = 60$ to 300 MPa
N-155	760	650° to 925°C, and $\sigma < 300$ MPa
19-9DL	760	650° to 925°C, and $\sigma = 40$ to 300 MPa
CRM-6D	760	650° to 925°C, and $\sigma = 80$ to 350 MPa
XF-818	815 705	760° to 870°C, and $\sigma = 80$ to 300 MPa 650°, 705°C, and $\sigma > 300$ MPa
<u>ln σ vs. ln $\dot{\epsilon}_m$</u>		
A-286	925 760	815° to 925°C, and $\sigma = 9$ to 110 MPa 650° to 760°C, and $\sigma = 120$ to 420 MPa
IN 800H	815	650° to 925°C, and $\sigma = 20$ to 300 MPa
N-155	815	650° to 925°C, and $\sigma < 300$ MPa
19-9DL	870	650° to 925°C, and $\sigma = 30$ to 350 MPa and $\dot{\epsilon}_m < 2 \times 10^{-5} \text{ s}^{-1}$
CRM-6D	815	705° to 925°C, and $\sigma = 80$ to 350 MPa
XF-818	815 705	760° to 925°C, and $\sigma = 50$ to 300 MPa 650° to 705°C, and $\sigma > 300$ MPa

TABLE 10. TEMPERATURE-COMPENSATED ANALYSIS DATA SUBSET CONDITIONS
FOR SIX IRON-BASE SUPERALLOYS TESTED IN AIR

Alloy	Analyzed Parameter	Subset Conditions		
		Case 2A	Case 2B	Case 2C
A-286	Minimum creep rate ($\dot{\epsilon}_m$)	Temp. 870°-925°C	Stress 40-250 MPa Temp. 705°-815°C	Stress 100-450 MPa
	Rupture life (t_r)	Temp. 870°-925°C	Stress 25-300 MPa Temp. 705°-925°C	Stress 250-450 MPa
	Time to 1% strain ($t_{0.01}$)	Temp. 870°-925°C	Stress 40-300 MPa Temp. 705°-815°C	Stress >300 MPa
IN 800H	Minimum creep rate ($\dot{\epsilon}_m$)	Temp. 870°-925°C	Stress 40-300 MPa	Stress >150 MPa
	Rupture life (t_r)	Stress <45 MPa	Stress 40-300 MPa	Stress >150 MPa
	Time to 1% strain ($t_{0.01}$)	Stress 20-80 MPa Temp. 870°-925°C	Stress 60-300 MPa Temp. 650°-815°C	Stress >150 MPa
N-155	Minimum creep rate ($\dot{\epsilon}_m$)	Temp. 870°-925°C	Stress 50-200 MPa	Stress >150 MPa
	Rupture life (t_r)	Stress <65 MPa	Stress 50-200 MPa	Stress >200 MPa
	Time to 1% strain ($t_{0.01}$)	Stress <65 MPa	Stress 50-200 MPa	Stress >200 MPa
19-9DL	Minimum creep rate ($\dot{\epsilon}_m$)	Temp. 870°-925°C	Stress 50-250 MPa	Stress >250 MPa
	Rupture life (t_r)	Stress <50 MPa	Stress 50-250 MPa	Stress >250 MPa
	Time to 1% strain ($t_{0.01}$)	Stress <50 MPa	Stress 50-250 MPa	Stress >250 MPa
CRM-6D	Minimum creep rate ($\dot{\epsilon}_m$)	Temp. 870°-925°C	Stress 80-400 MPa	Stress >250 MPa
	Rupture life (t_r)	Stress <150 MPa	Stress 80-400 MPa	Stress >250 MPa
	Time to 1% strain ($t_{0.01}$)	Stress <150 MPa	Stress 80-400 MPa	Stress >250 MPa
XF-818	Minimum creep rate* ($\dot{\epsilon}_m$)	Temp. 870°-925°C	Stress 85-300 MPa	Stress >300 MPa
	Rupture life (t_r)	Stress <85 MPa	Stress 85-300 MPa	Temp. 650°-705°C
	Time to 1% strain ($t_{0.01}$)	Stress <85 MPa	Stress 85-300 MPa	Stress >300 MPa

*Special Cases: Case 2D, $\dot{\epsilon}_m > 1.0 \text{ E-09}$; Case 2E $\dot{\epsilon}_m < 3.0 \text{ E-06}$

ORIGINAL PAGE IS
OF POOR QUALITY

TABLE 11. STATISTICAL DATA ON TEMPERATURE-COMPENSATED ANALYSIS^a
OF SIX ALLOYS TESTED IN AIR

Alloy	Y	No. of Data	R ²	ln k	n	Q, kJ/K mole	90% Conf. Limits	
							Low	High
A-286	t _r	15	0.858	-38.4	-3.82	544	439	650
	t _{0.01}	12	0.946	-39.4	-3.54	535	465	605
	ε _m	9	0.767	35.9	3.09	-613	-847	-378
IN 800H	t _r	23	0.941	-10.8	-6.79	406	367	445
	t _{0.01}	14	0.886	-17.0	-8.86	515	424	607
	ε _m	22	0.849	-0.803	6.49	-384	-449	-320
N-155	t _r	19	0.976	-13.9	-6.28	435	407	463
	t _{0.01}	17	0.988	-17.4	-7.04	467	443	491
	ε _m	17	0.980	8.85	7.39	-527	-561	-493
19-9DL	t _r	19	0.975	-17.6	-6.44	461	430	492
	t _{0.01}	16	0.955	-26.8	-7.38	559	504	614
	ε _m	19	0.948	15.2	7.38	-573	-628	-518
CRM-6D	t _r	26	0.843	0.829	-9.12	461	392	530
	t _{0.01}	29	0.973	5.59	-10.6	468	439	498
	ε _m	28	0.947	-16.9	11.8	-551	-598	-504
XF-818	t _r	14	0.991	-13.2	-7.52	505	481	530
	t _{0.01}	14	0.988	-20.8	-6.86	522	494	550
	ε _m	14	0.990	6.85	7.47	-545	-573	-517
	ε _m ^b	23	0.897	0.700	6.92	-461	-521	-401
	ε _m ^b	21	0.855	0.524	6.83	-456	-531	-381

^aBasis: $\ln Y = \ln k + n \ln \sigma + Q/RT$, where $Y = t_r, t_{0.01},$ or ϵ_m .

^bSee footnote of Table 10 for these two cases.

ORIGINAL PAGE IS
OF POOR QUALITY

TABLE 12 . PREDICTED STRESS FOR 3500-HOUR RUPTURE LIFE IN AIR

Alloy	Temperature, °C (°F)		Estimated Stress, MPa (ksi)			
			Based on Temperature- Compensated Analysis	Based on Linear Regression at Each Temperature		
				Mean	90% Conf. Limits	
				Low	High	
A-286	705	(1300)	205 (29.7)	192 (27.8)	192	192
	760	(1400)	81 (11.7)	100 (14.5)	92.3	109
	815	(1500)	35 (5.05)	43.3 (6.28)	32.9	57.1
	870	(1600)	16 (2.37)	16.8 (2.44)	11.8	24.1
IN 800H	705	(1300)	96 (13.9)	94.2 (13.7)	64.2	138
	760	(1400)	65 (9.39)	59.8 (8.67)	40.5	88.5
	815	(1500)	46 (6.60)	42.5 (6.16)	36.4	49.7
	870	(1600)	33 (4.80)	29.8 (4.32)	18.3	48.5
N-155	705	(1300)	150 (21.7)	149 (21.6)	87.0	257
	760	(1400)	95 (13.9)	98.3 (14.3)	92.3	108
	815	(1500)	63 (9.18)	63.5 (9.21)	57.2	70.5
	870	(1600)	44 (6.35)	46.3 (6.72)	40.9	52.4
19-9DL	705	(1300)	121 (17.6)	115 (16.7)	102	129
	760	(1400)	76 (11.0)	78.3 (11.4)	74.6	82.1
	815	(1500)	50 (7.22)	51.3 (7.44)	43.7	60.1
	870	(1500)	34 (4.94)	32.5 (4.71)	27.5	38.5
CRM-6D	705	(1300)	223 (32.4)	243 (35.2)	217	272
	760	(1400)	161 (23.3)	183 (26.5)	181	186
	815	(1500)	119 (17.3)	137 (19.9)	116	162
	870	(1600)	91 (13.2)	97.7 (14.2)	82.3	116
XF-818	705	(1300)	225 (32.7)	265 (38.4)	223	316
	760	(1400)	145 (21.1)	146 (21.2)	141	151
	815	(1500)	98 (14.2)	99.7 (14.5)	92.4	108
	870	(1600)	68 (9.92)	68.7 (9.96)	50.5	93.6

ORIGINAL PAGE IS
OF POOR QUALITY

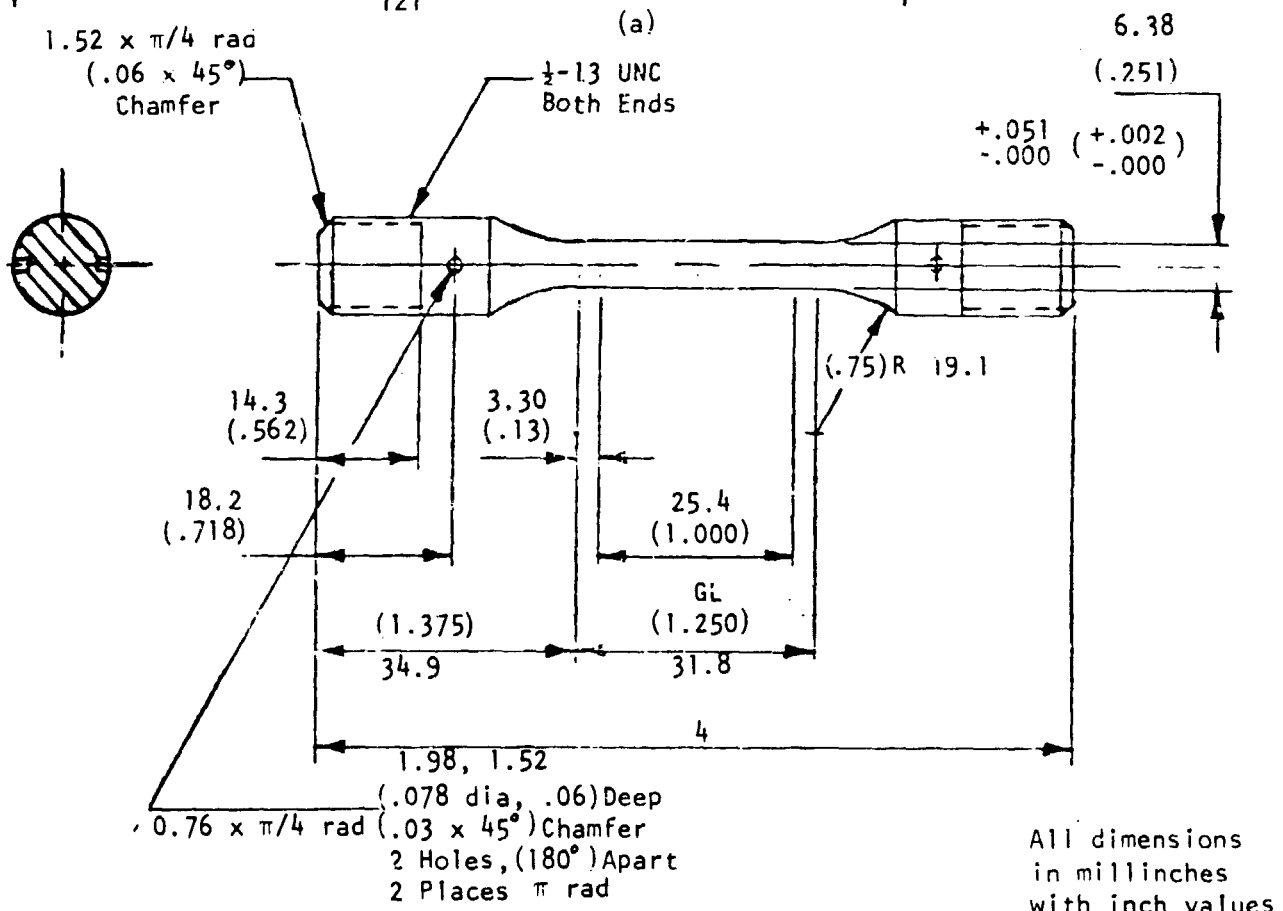
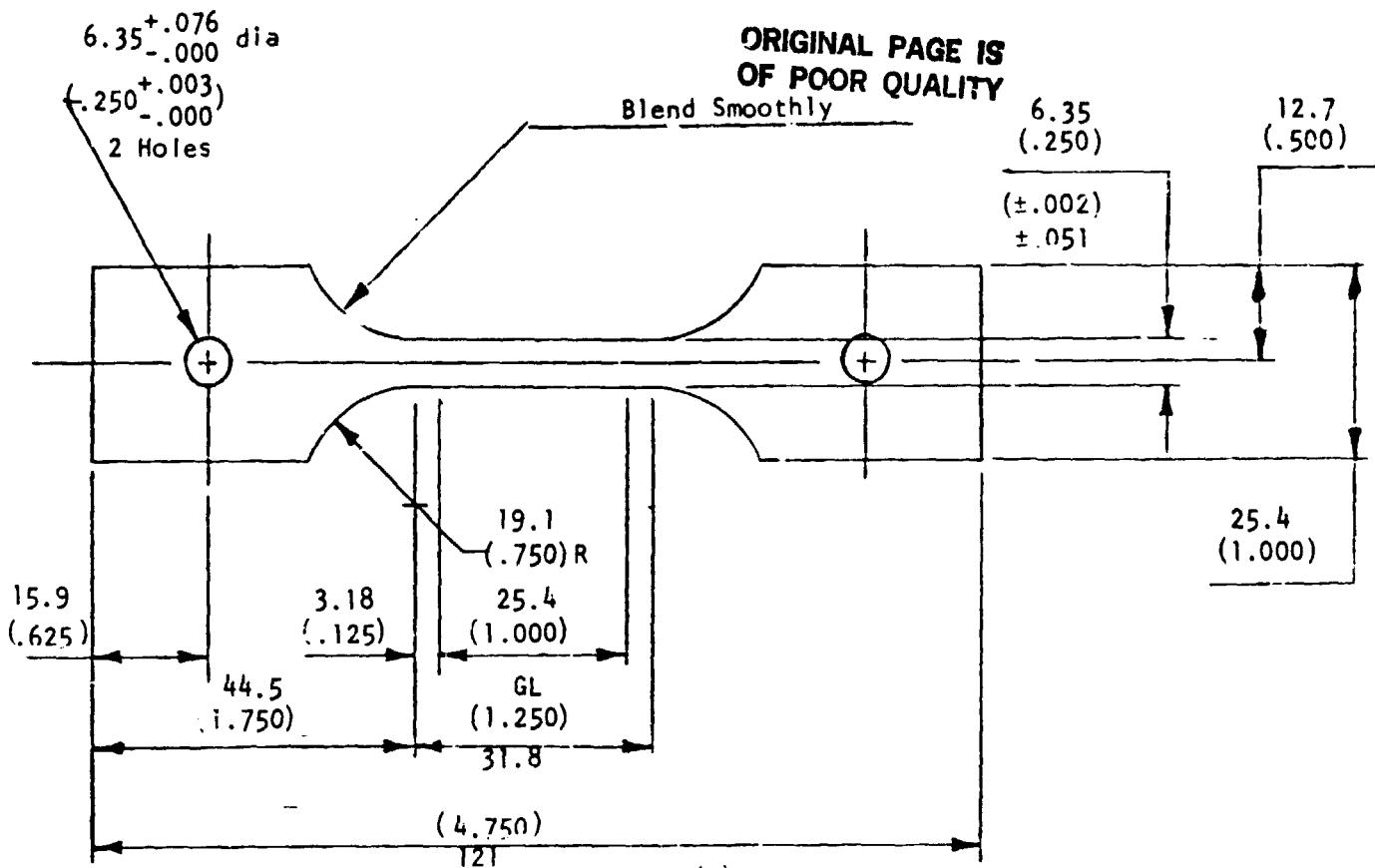
TABLE 13. PREDICTED STRESS TO 1% CREEP IN 3500 HOURS IN AIR

Alloy	Temperature, °C (°F)		Based on Temperature- Compensated Analysis	Estimated Stress, MPa (ksi)			
				Based on Linear Regression at Each Temperature			
				Mean	90% Conf. Limits		
			Low	High			
A-286	705	(1300)	173 (25.1)	178 (25.8)	178	178	
	760	(1400)	64 (9.31)	79.5 (11.5)	57.5	110	
	815	(1500)	26 (3.82)	30.9 (4.48)	23.9	40.0	
	870	(1600)	12 (1.71)	6.25 (0.91)	5.53	7.17	
IN 800H	705	(1300)	75 (10.9)	82.6 (12.0)	82.6	82.6	
	760	(1400)	51 (7.42)	51.7 (7.50)	49.5	54.1	
	815	(1500)	36 (5.27)	41.6 (6.03)	38.0	45.5	
	870	(1600)	27 (3.87)	16.2 (2.35)	16.2	16.2	
N-155	705	(1300)	93 (13.5)	88.9 (12.9)	51.8	153	
	760	(1400)	60 (8.71)	60.3 (8.75)	55.2	66.0	
	815	(1500)	41 (5.89)	40.0 (5.80)	37.9	42.3	
	870	(1600)	29 (4.14)	28.5 (4.13)	25.7	31.7	
19-9DL	705	(1300)	98 (14.2)	85.5 (12.4)	43.5	168	
	760	(1400)	60 (8.66)	59.4 (8.61)	55.8	63.3	
	815	(1500)	38 (5.54)	37.5 (5.44)	29.8	47.1	
	870	(1600)	26 (3.71)	22.7 (3.29)	19.8	26.0	
CRM-6D	705	(1300)	183 (26.6)	179 (26.0)	167	191	
	760	(1400)	137 (19.9)	133 (19.3)	124	142	
	815	(1500)	106 (15.3)	104 (15.1)	94.0	116	
	870	(1600)	83 (12.1)	87.8 (11.9)	75.8	88.4	
XF-818	705	(1300)	170 (24.6)	230 (33.4)	162	327	
	760	(1400)	103 (15.0)	102 (14.8)	89.4	116	
	815	(1500)	66 (9.56)	65.2 (9.46)	59.4	71.5	
	870	(1600)	44 (6.38)	44.4 (6.44)	35.0	56.3	

ORIGINAL PAGE IS
OF POOR QUALITY

TABLE 14. FRACTOGRAPHY AND MICROSTRUCTURAL ANALYSIS
OF SPECIMENS TESTED IN AIR

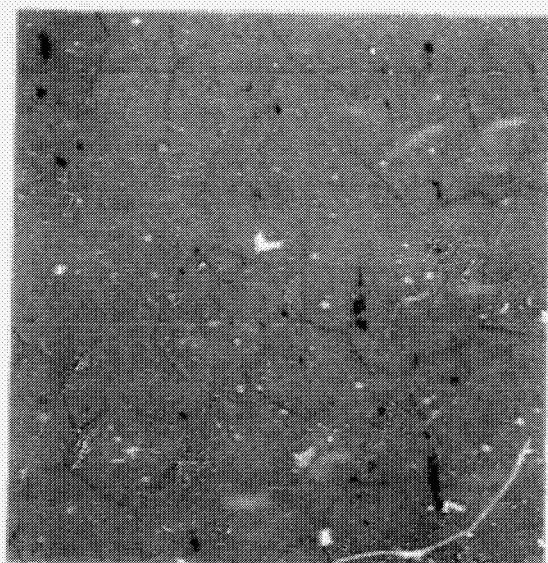
Alloy	Temp., °C	Stress, MPa	Rupture Life, h	Type of Examination	
				Fracture	Cross- Section
19-9DL	705	131	1342	X	
	760	86	1687	X	
	815	59	1118	X	X
	815	124	14.2	X	
	870	29	1300	X	X
A-286	705	379	35.0	X	
	815	55	1030	X	X
	870	41	59.8	X	
N-155	760	165	115.3	X	
	815	63	2536	X	X
	870	47	2897	X	X
	925	59	49.2	X	
IN 800H	650	207	309	X	
	760	70	4490	X	X
	760	124	28.9	X	
	825	45	2862	X	X
	925	48	53.0	X	
XF-818	705	414	3.1	X	
	815	103	3115	X	X
	815	138	199.5	X	X
	870	97	194.0	X	X
	760	152	2497	X	X
	925	103	11.8	X	
CRM-6D	705	310	147.4	X	X
	760	193	1708	X	X
	760	241	140.2	X	
	870	117	401.9	X	X
	925	117	28.4	X	X



All dimensions
in millinches
with inch values
given in
parentheses

Figure 1. Creep-rupture specimen design. (a) Wrought (sheet), (b) cast.

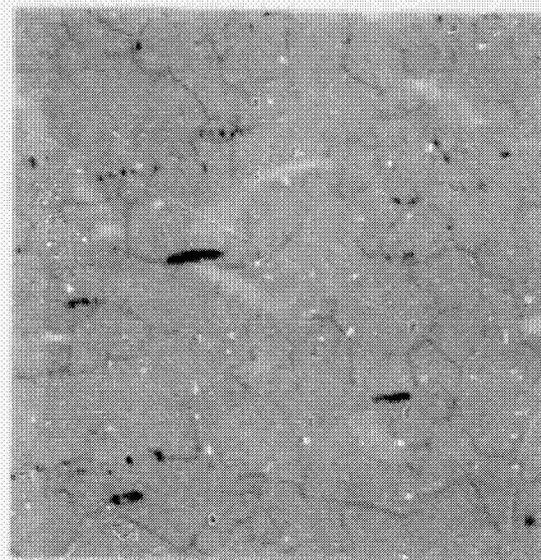
ORIGINAL PAGE IS
OF POOR QUALITY



Neg. No. 52209

100X

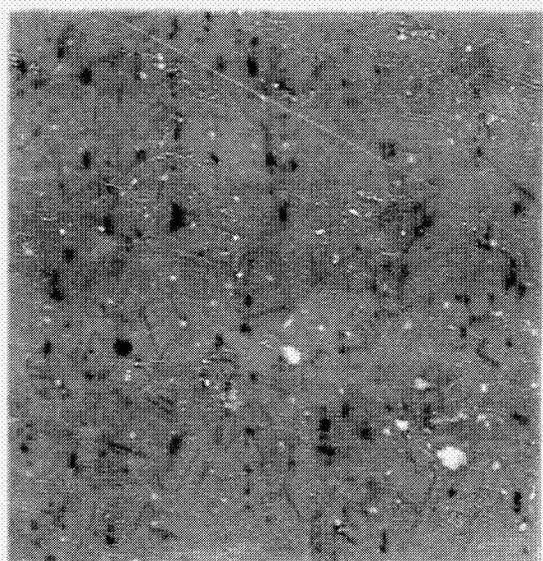
(a)



Neg. No. 52207

100X

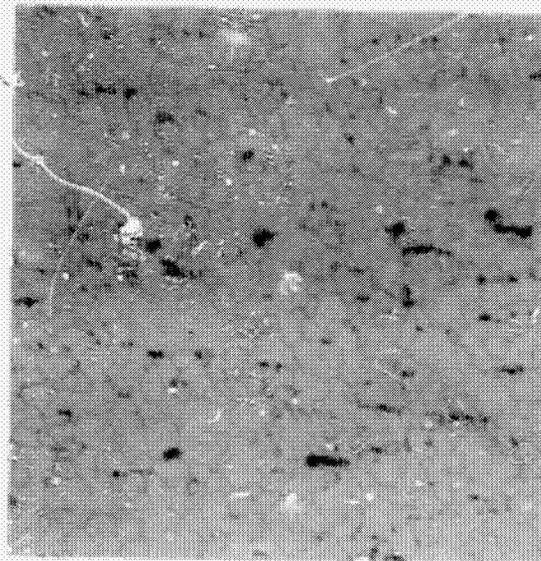
(b)



Neg. No. 52208

100X

(c)



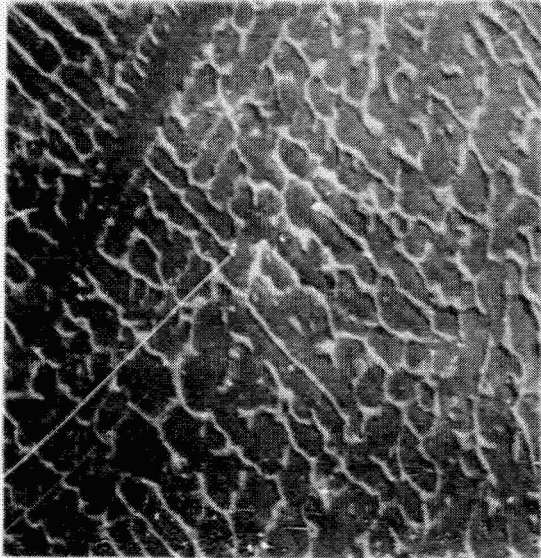
Neg. No. 52206

100X

(d)

Figure 2. Optical photomicrographs of wrought sheet alloys. (a) A-286, (b) Incoloy 800H, (c) N-155, (d) 19-9DL. Etchant: 10% oxalic acid, electrolytic.

ORIGINAL PAGE IS
OF POOR QUALITY



SEM No. 5486

100X

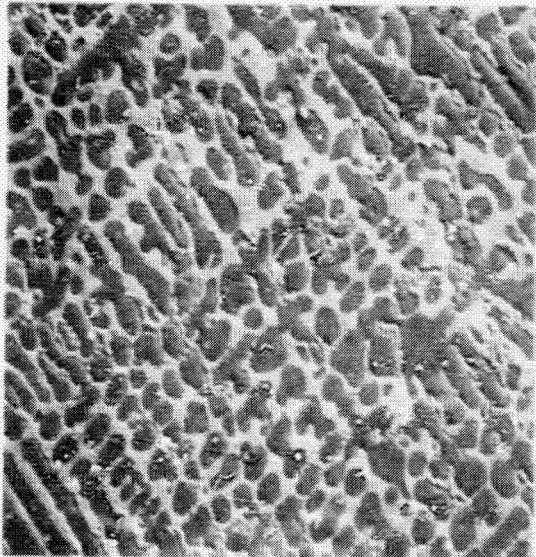
(a)



SEM No. 5488

1000X

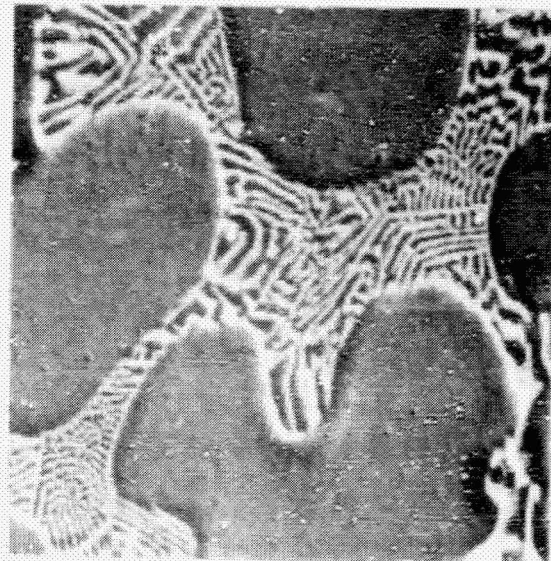
(b)



SEM No 5489

100X

(c)



SEM No. 549.

1000X

(d)

Figure 3. SEM microstructures of as-cast alloys showing interdentritic structure with carbide and boride dispersion. (a,b) CRM-6D. (c,d) XP-S18. Etchant: 10% oxalic acid, electrolytic.

ORIGINAL PAGE IS
OF POOR QUALITY

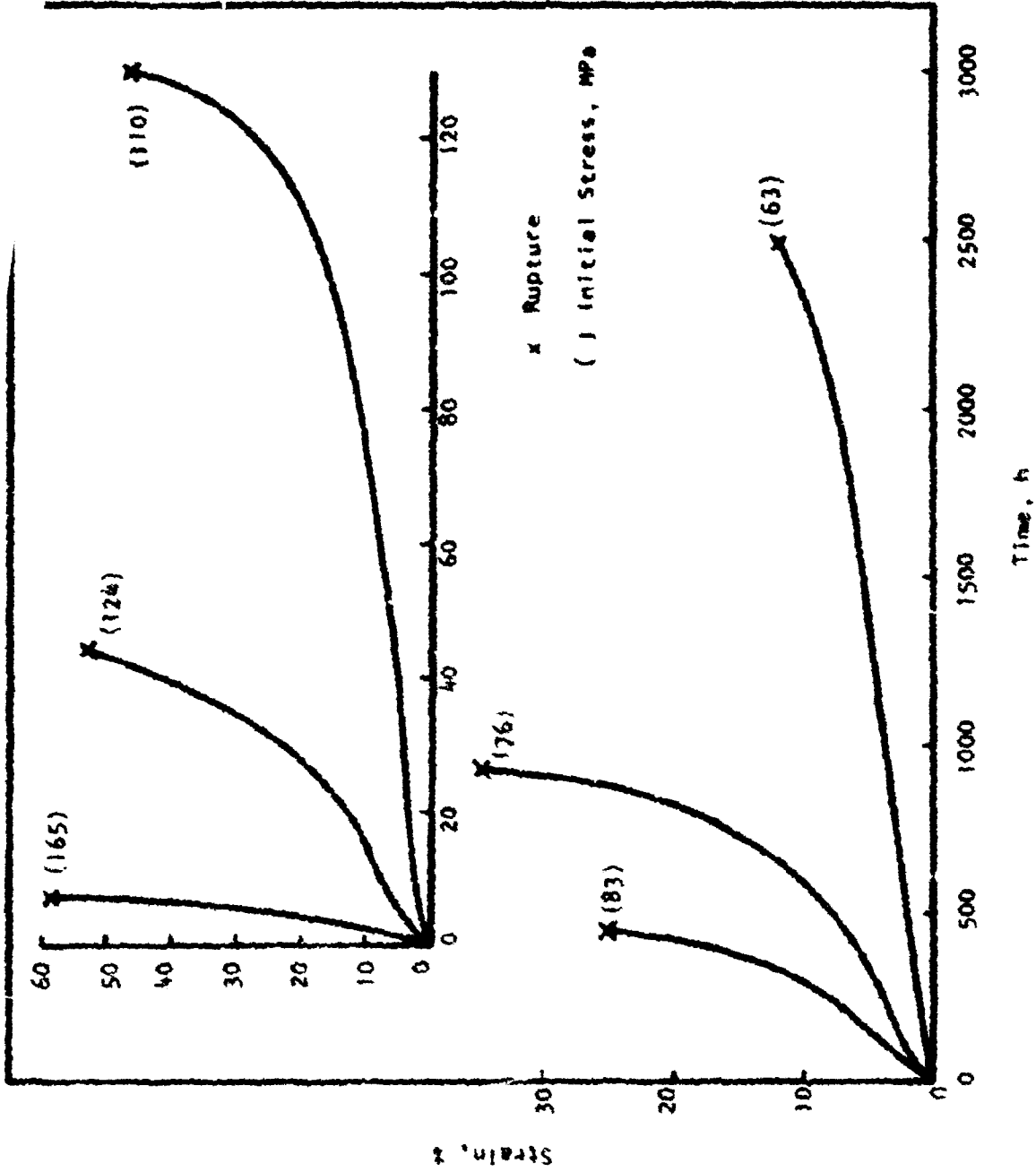


Figure 4. Creep curves for M-155 tested at 815°C in air.

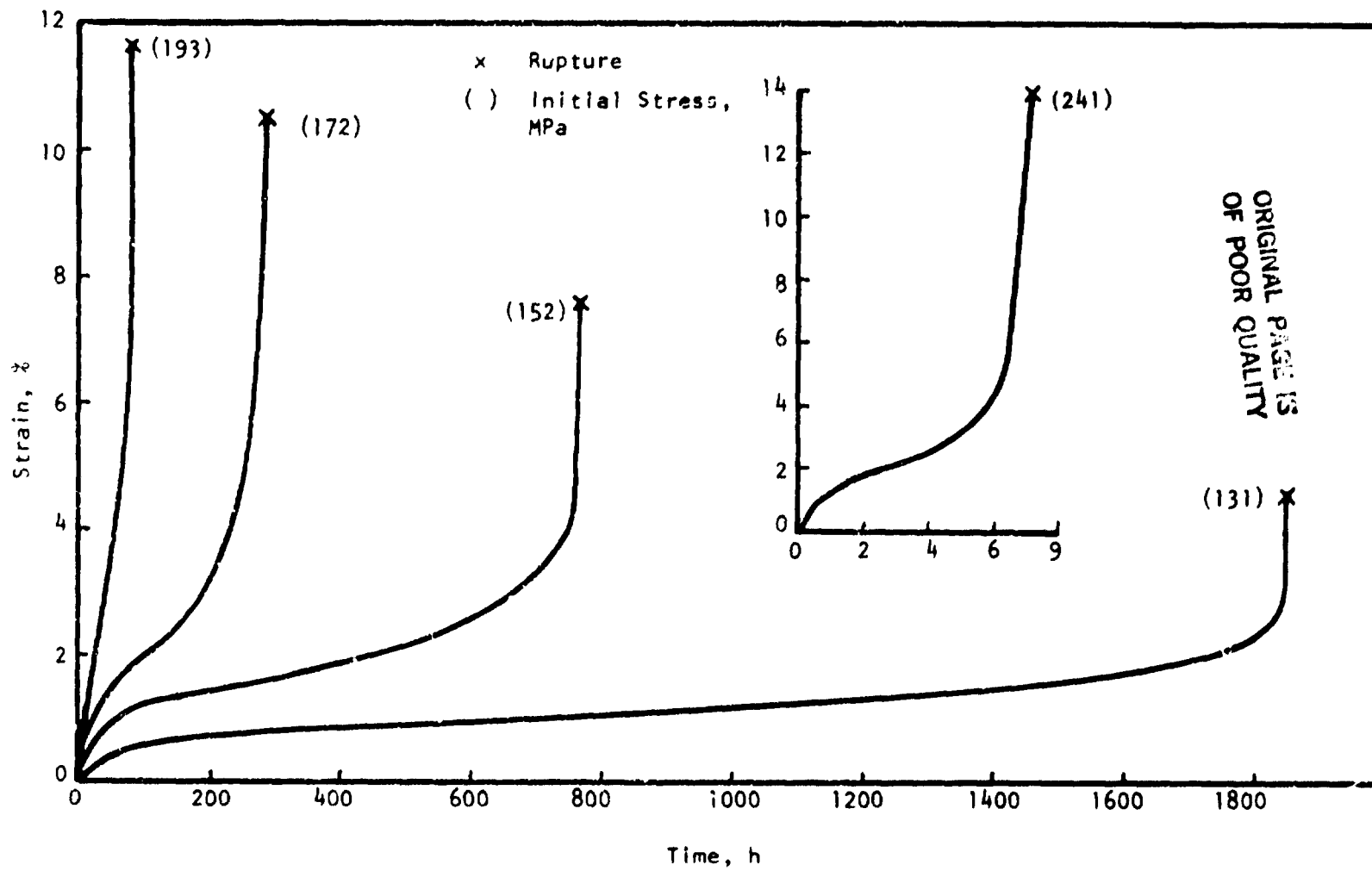


Figure 5. Creep curves for CRM-6D tested at 815°C in air.

A28 IN AIR

39

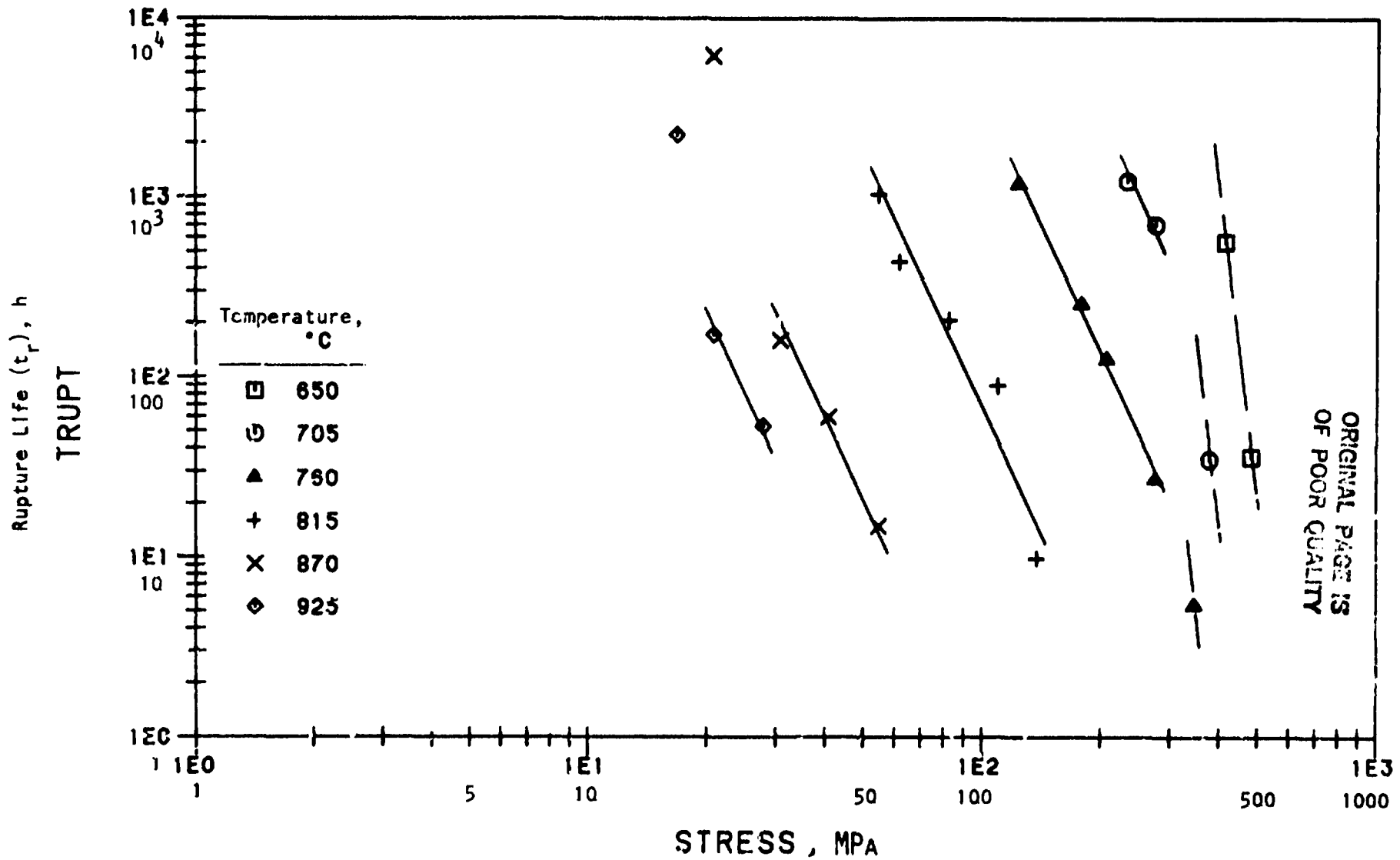


Figure 6. Stress vs. rupture life of A-286 in air.

IN8 IN AIR

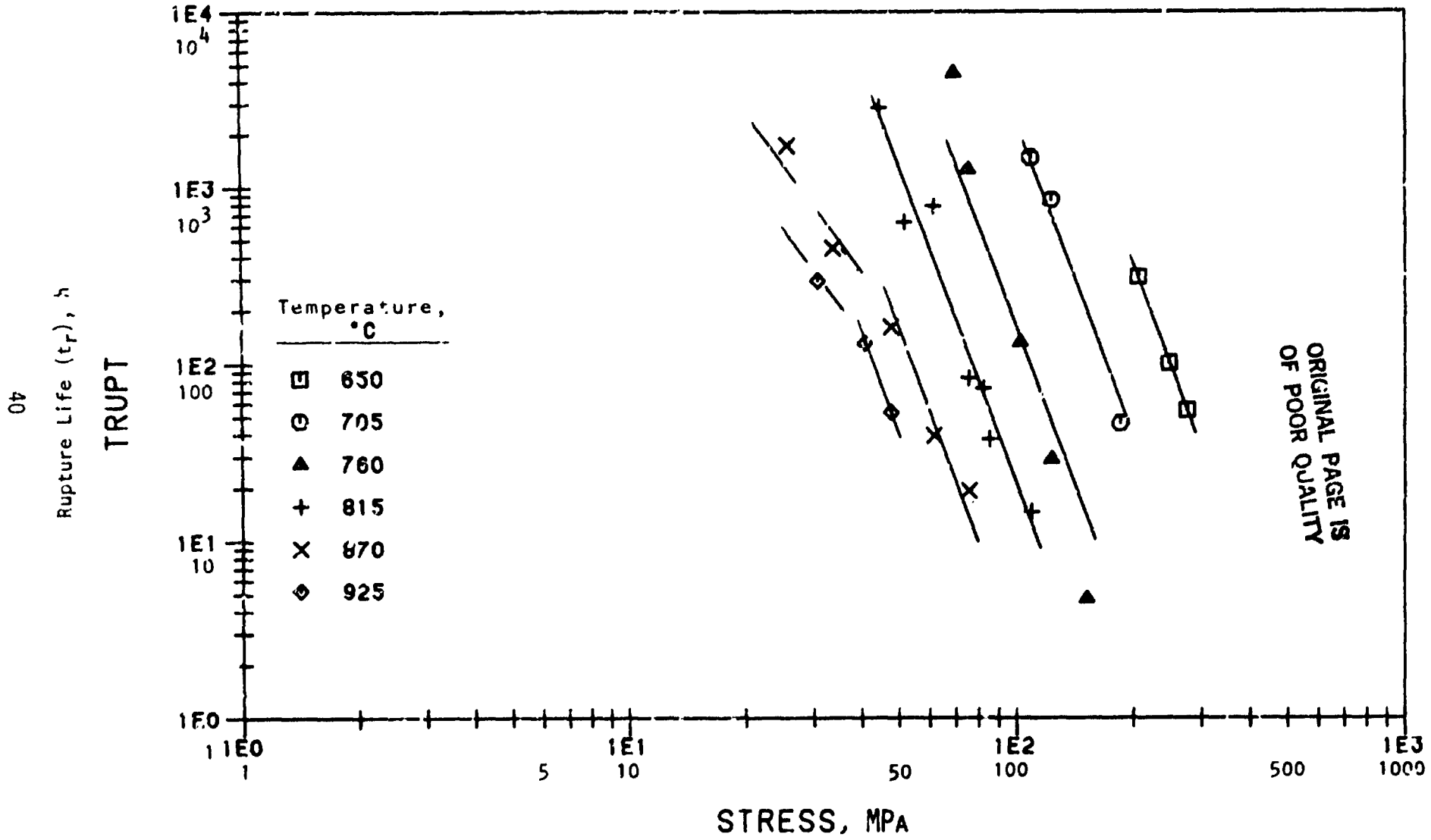


Figure 7. Stress vs. rupture life of IN 800H in air.

N15 IN AIR

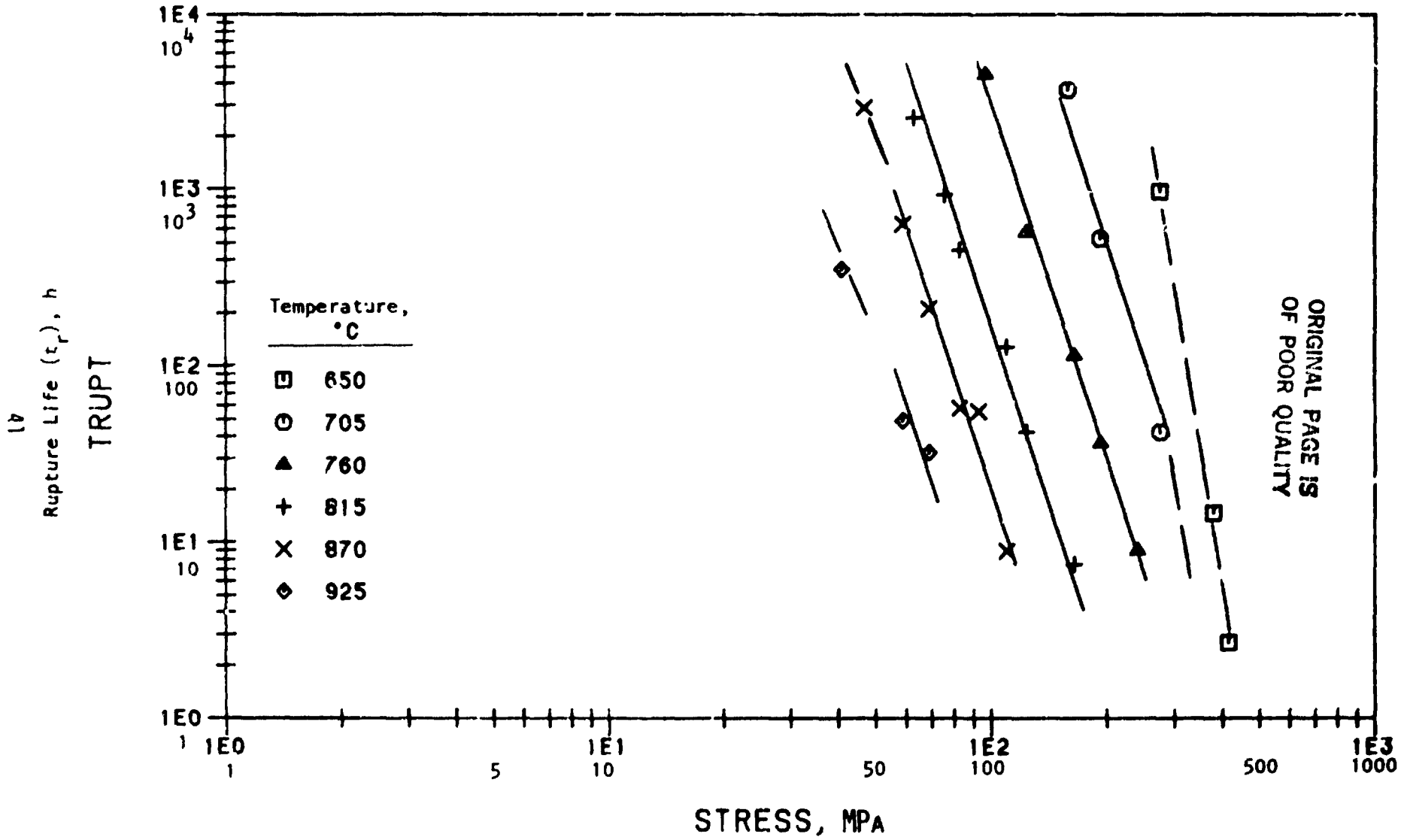


Figure 8. Stress vs. rupture life of N-155 in air.

199 IN AIR

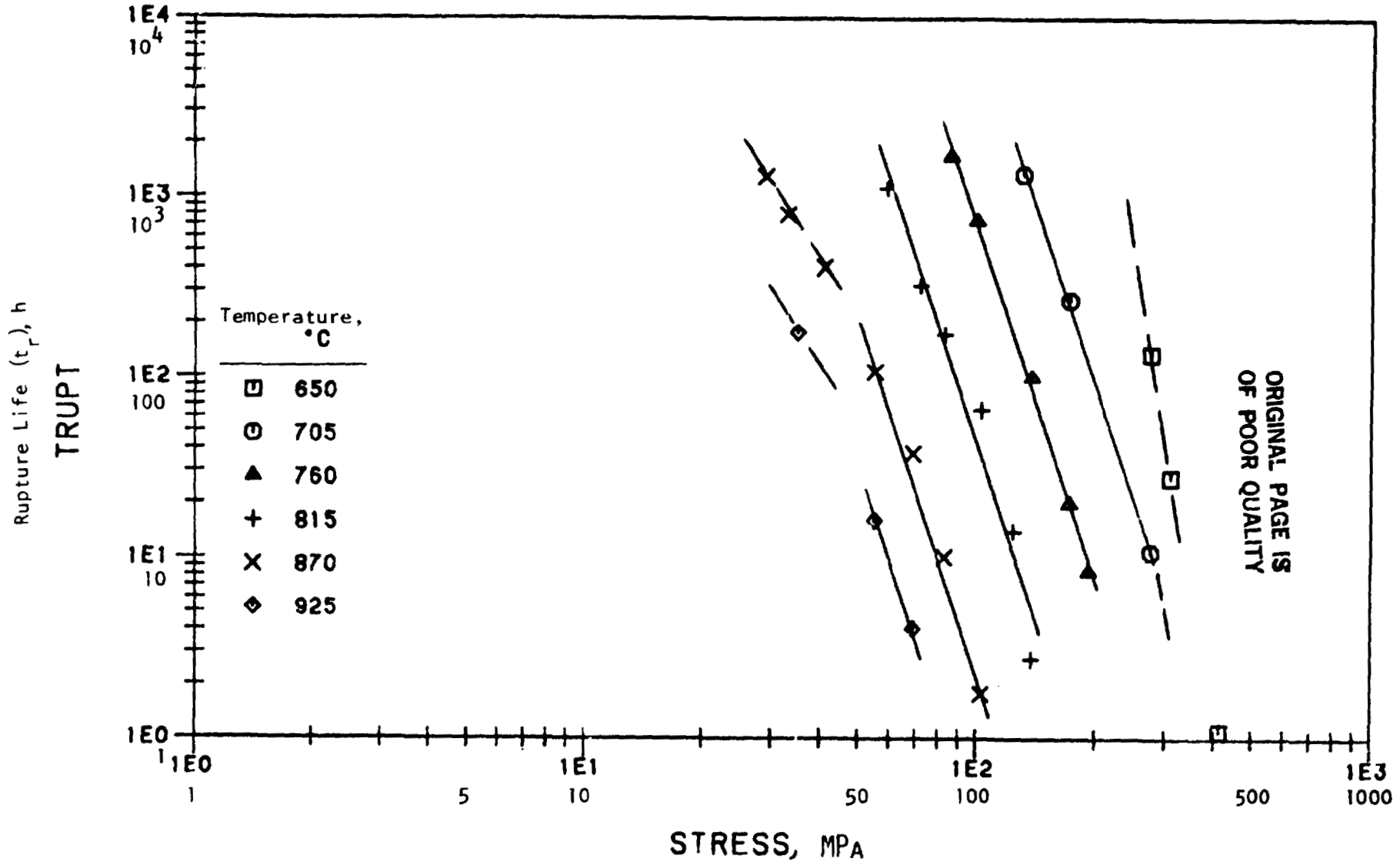


Figure 9. Stress vs. rupture life of 19-9DL in air.

CRM IN AIR

43

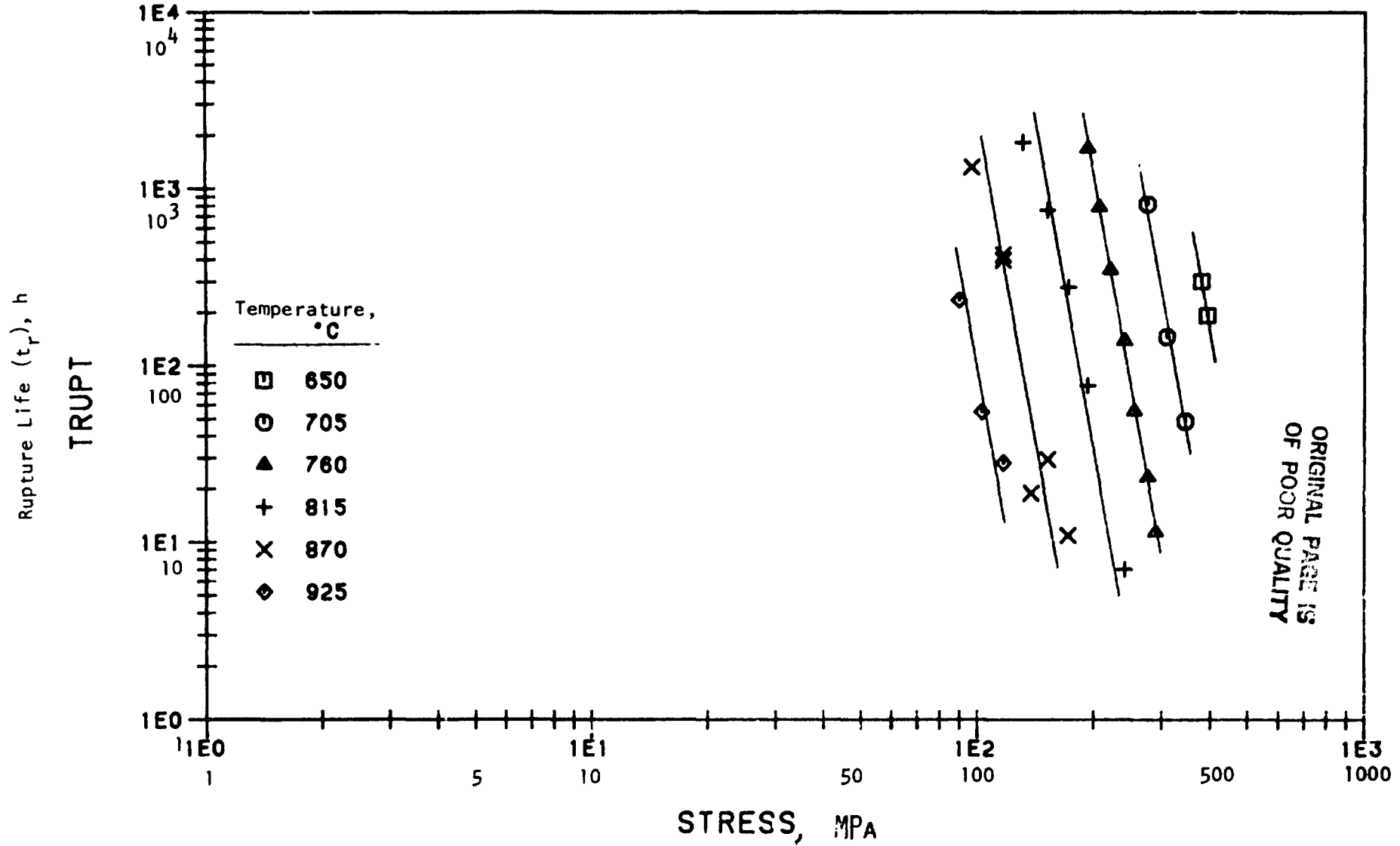


Figure 10. Stress vs. rupture life of CRM-6D in air.

XF8 IN AIR

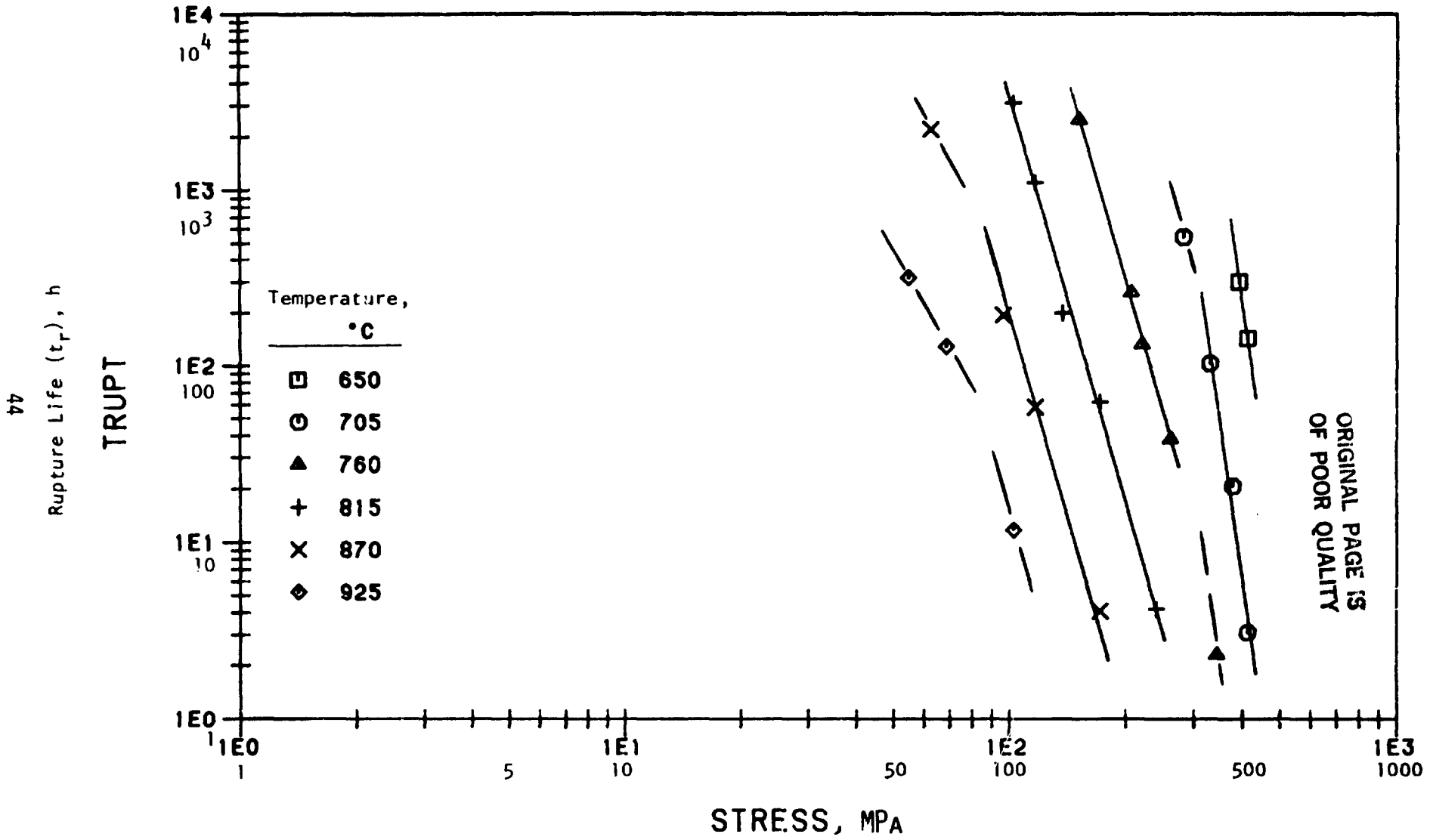


Figure 11. Stress vs. rupture life of XF-818 in air.

A28 IN AIR

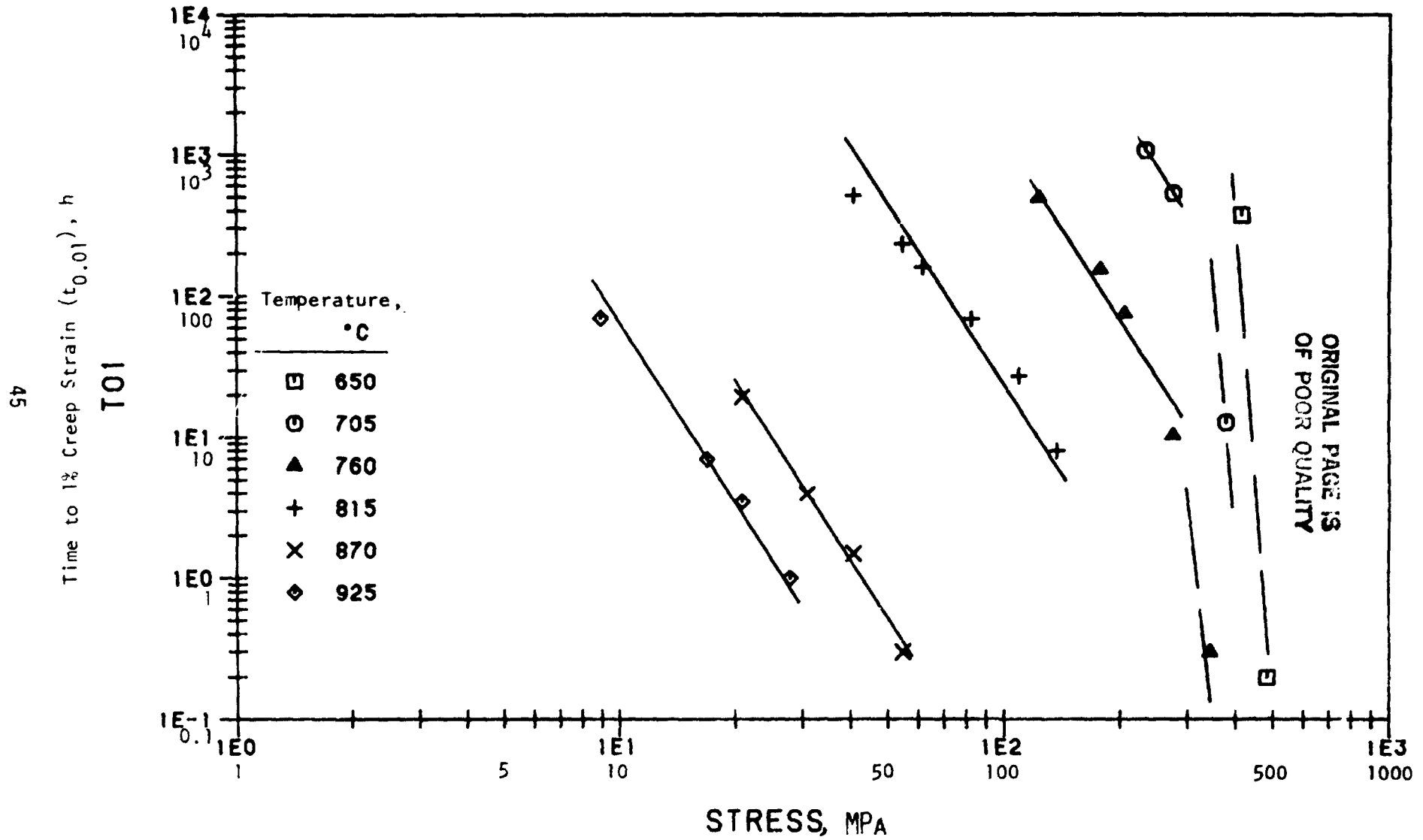


Figure 12. Stress vs. time to 1% creep strain of A-286 in air.

IN8 IN AIR

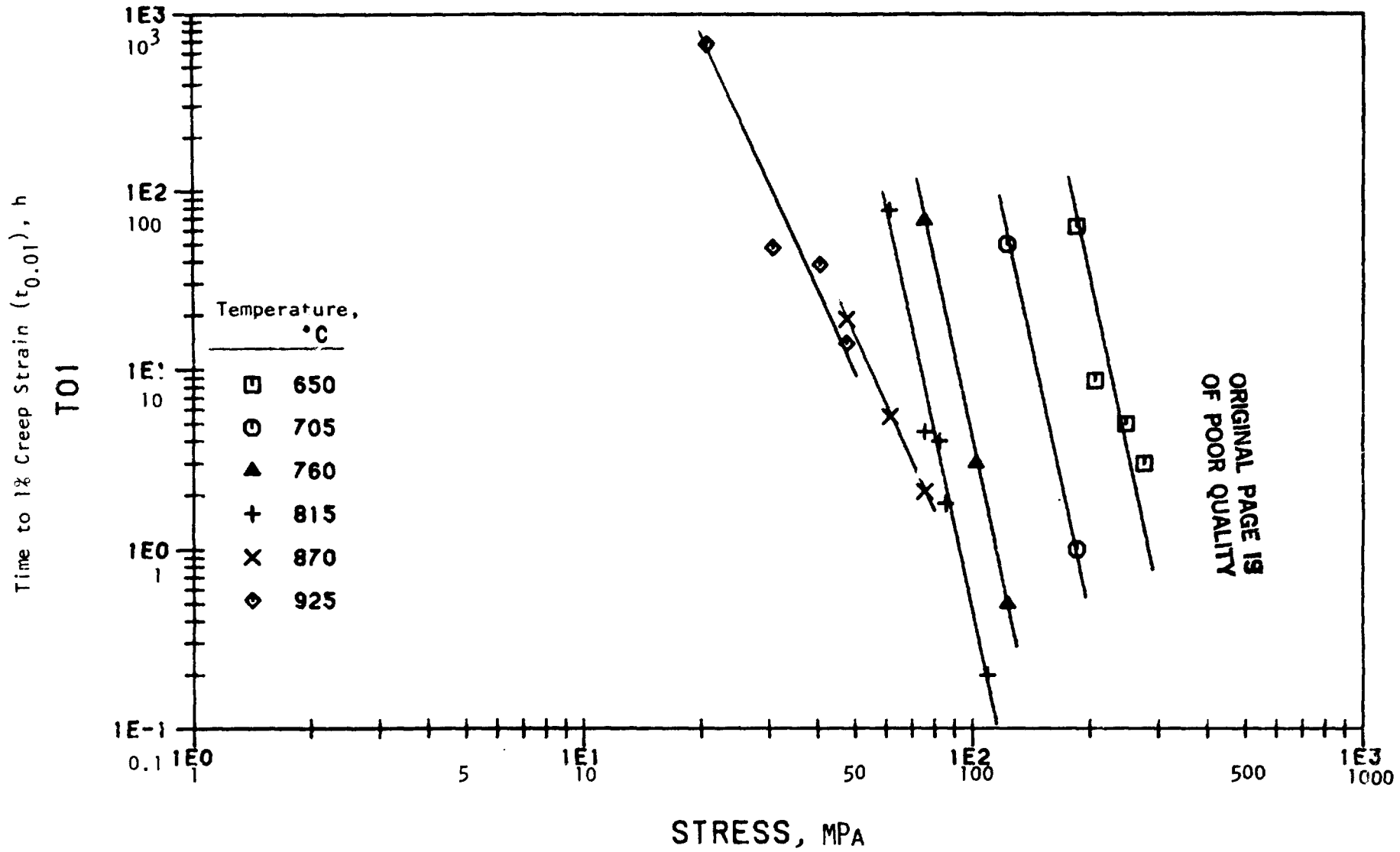


Figure 13. Stress vs. time to 1% creep strain of IN 800H in air.

N15 IN AIR

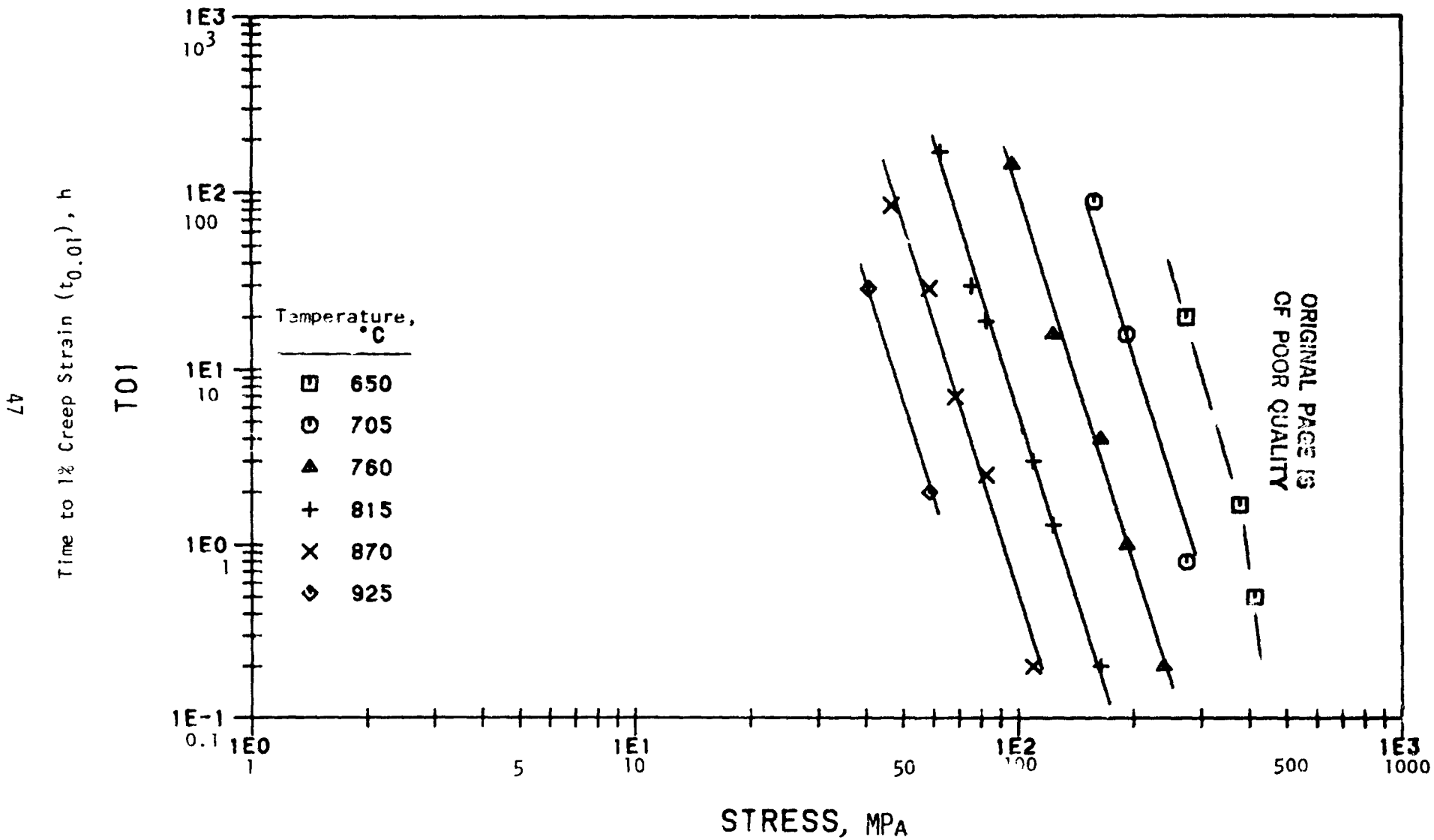


Figure 14. Stress vs. time to 1% creep strain of N-155 in air.

199 IN AIR

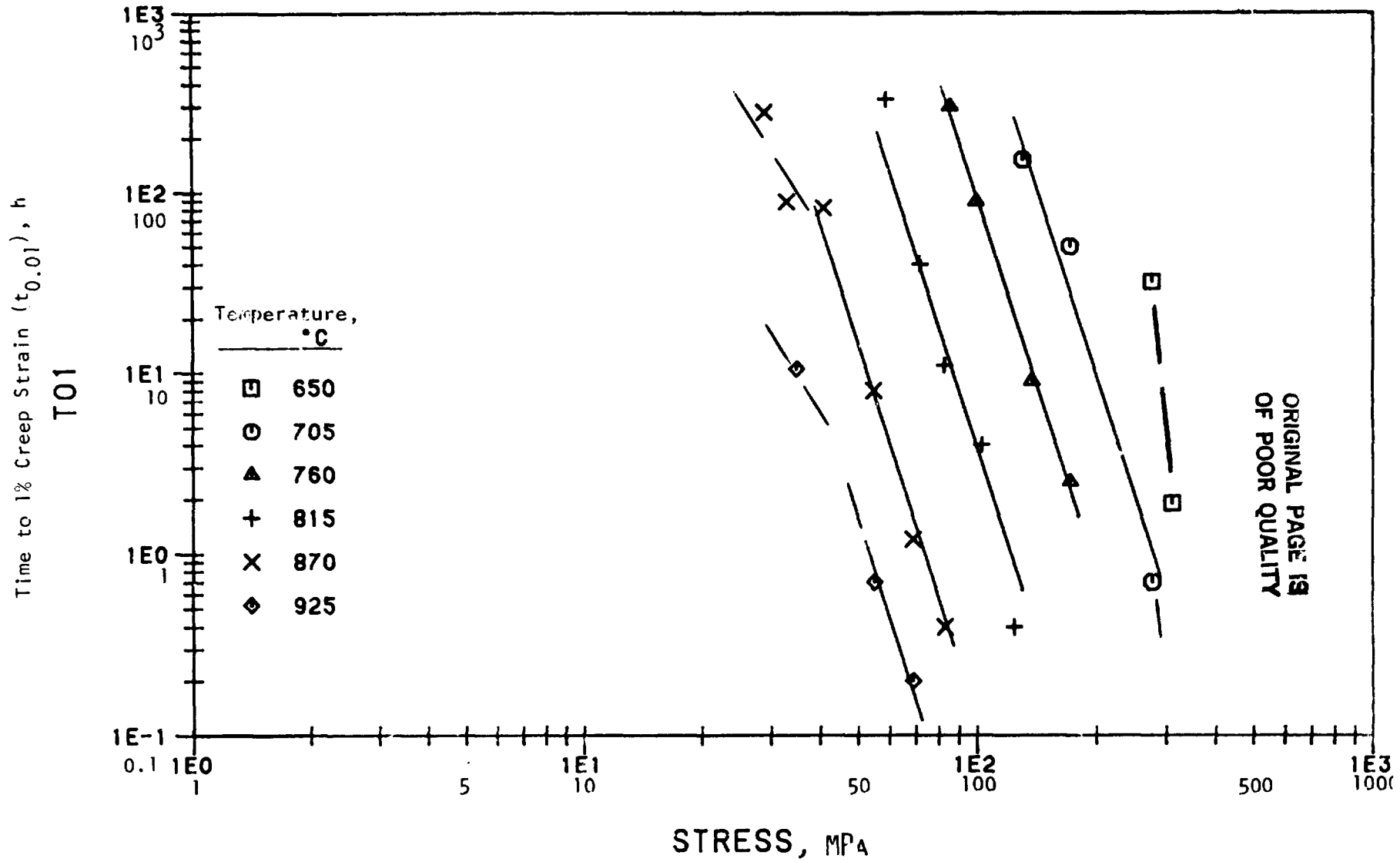


Figure 15. Stress vs. time to 1% creep strain of 19-9DL in air.

CRM IN AIR

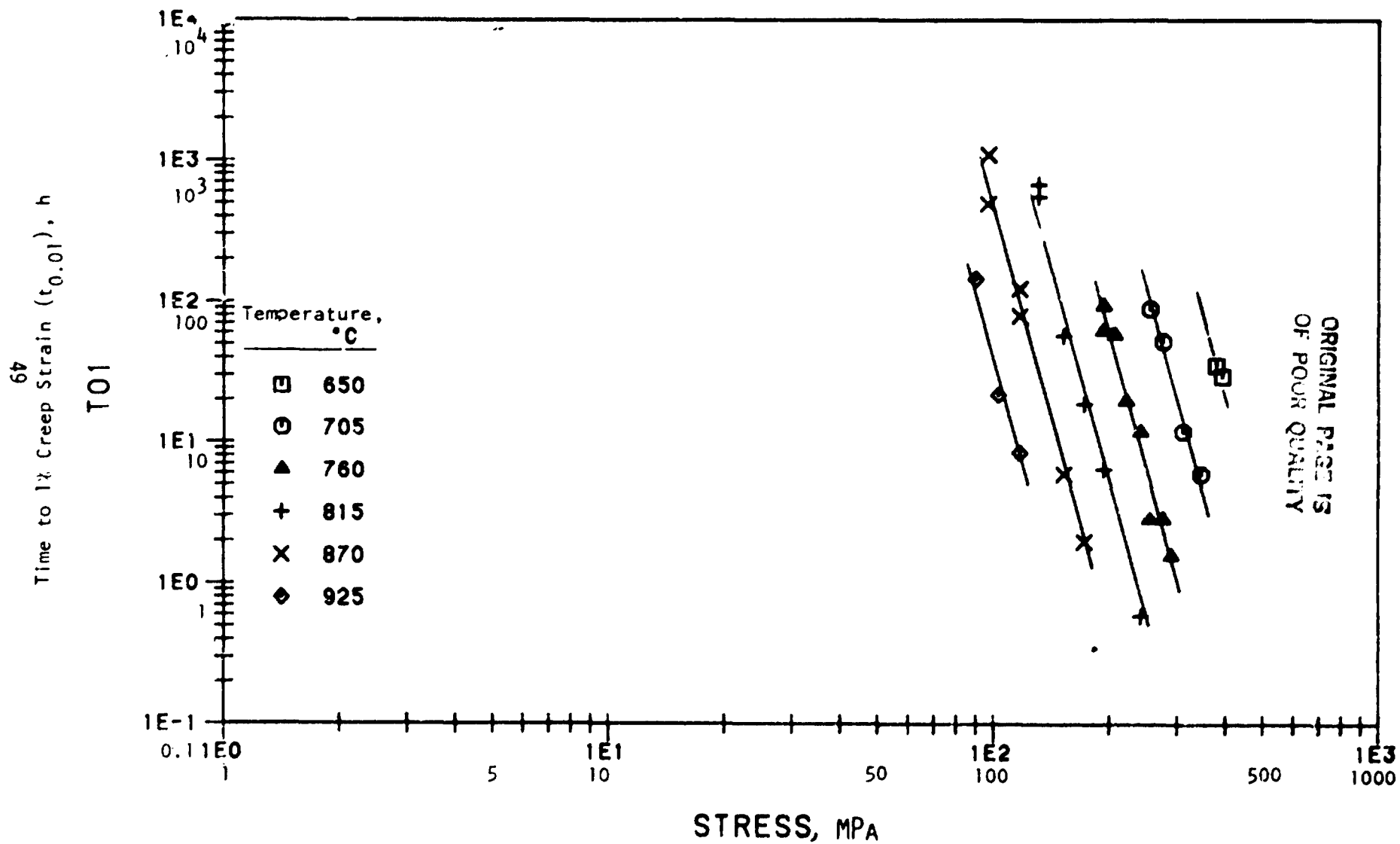


Figure 16. Stress vs. time to 1% creep strain of CRM-6D in air.

XF8 IN AIR

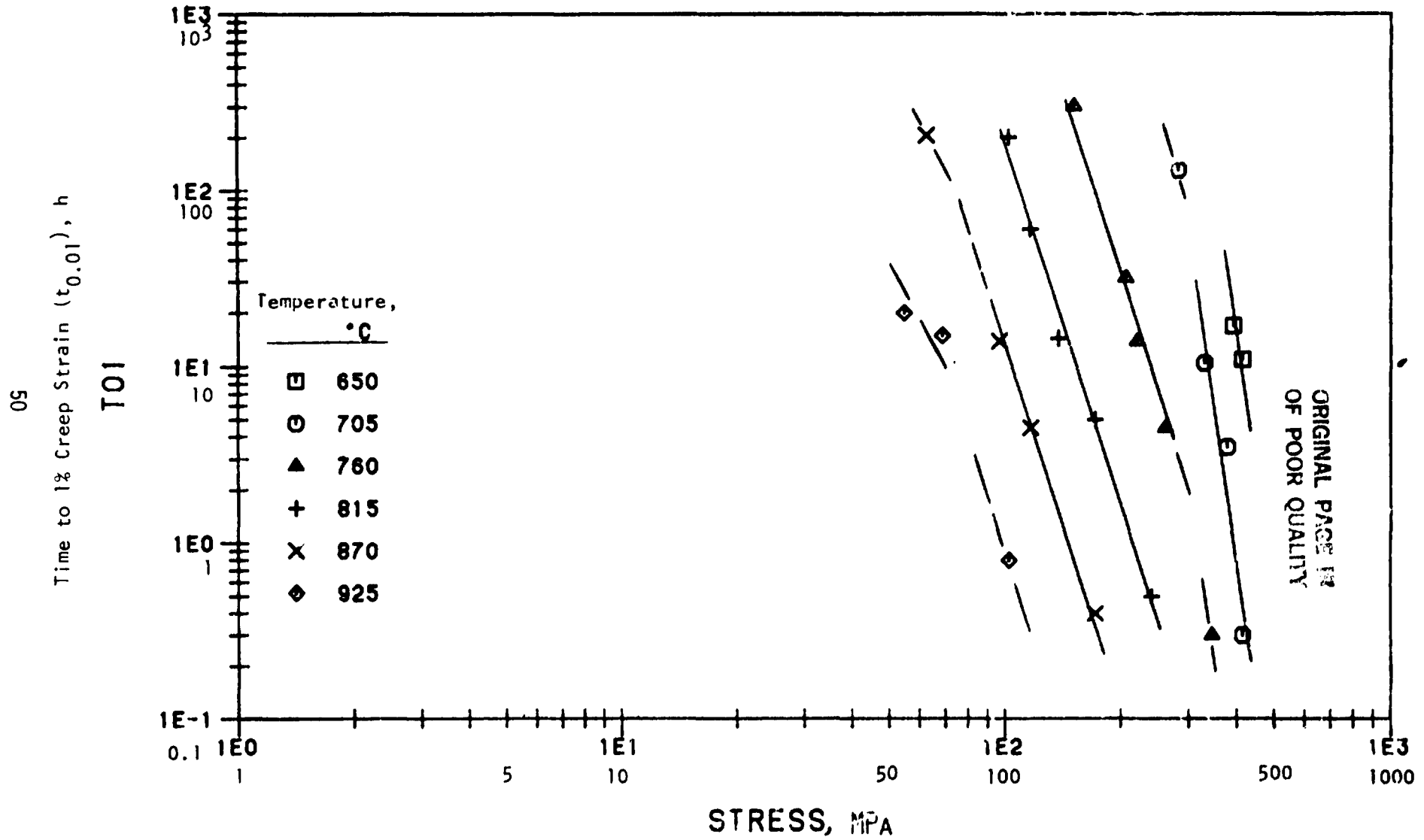


Figure 17. Stress vs. time to 1% creep strain of XF-818 in air.

A28 IN AIR

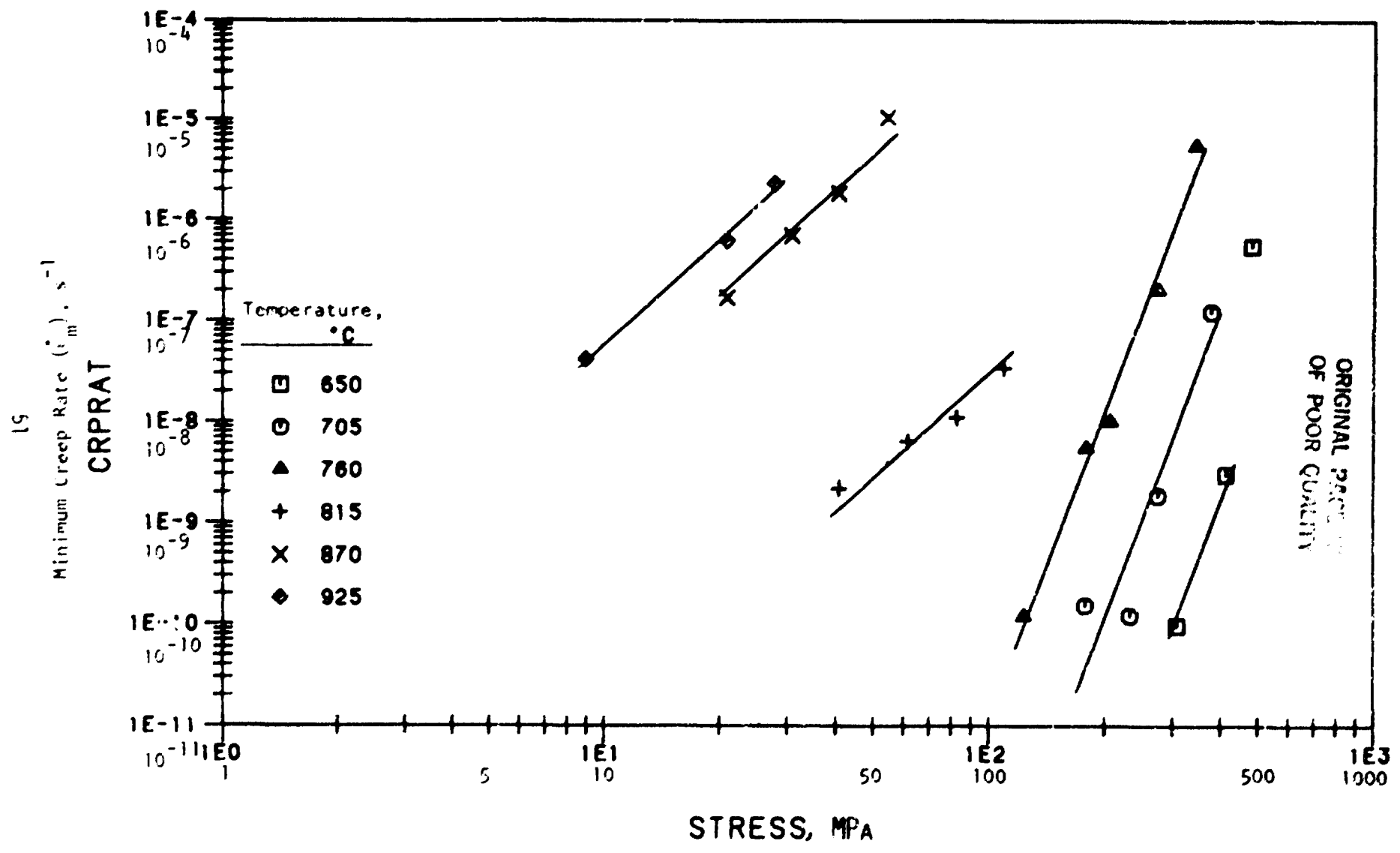


Figure 18. Stress vs. minimum creep rate of A-286 in air.

IN8 IN AIR

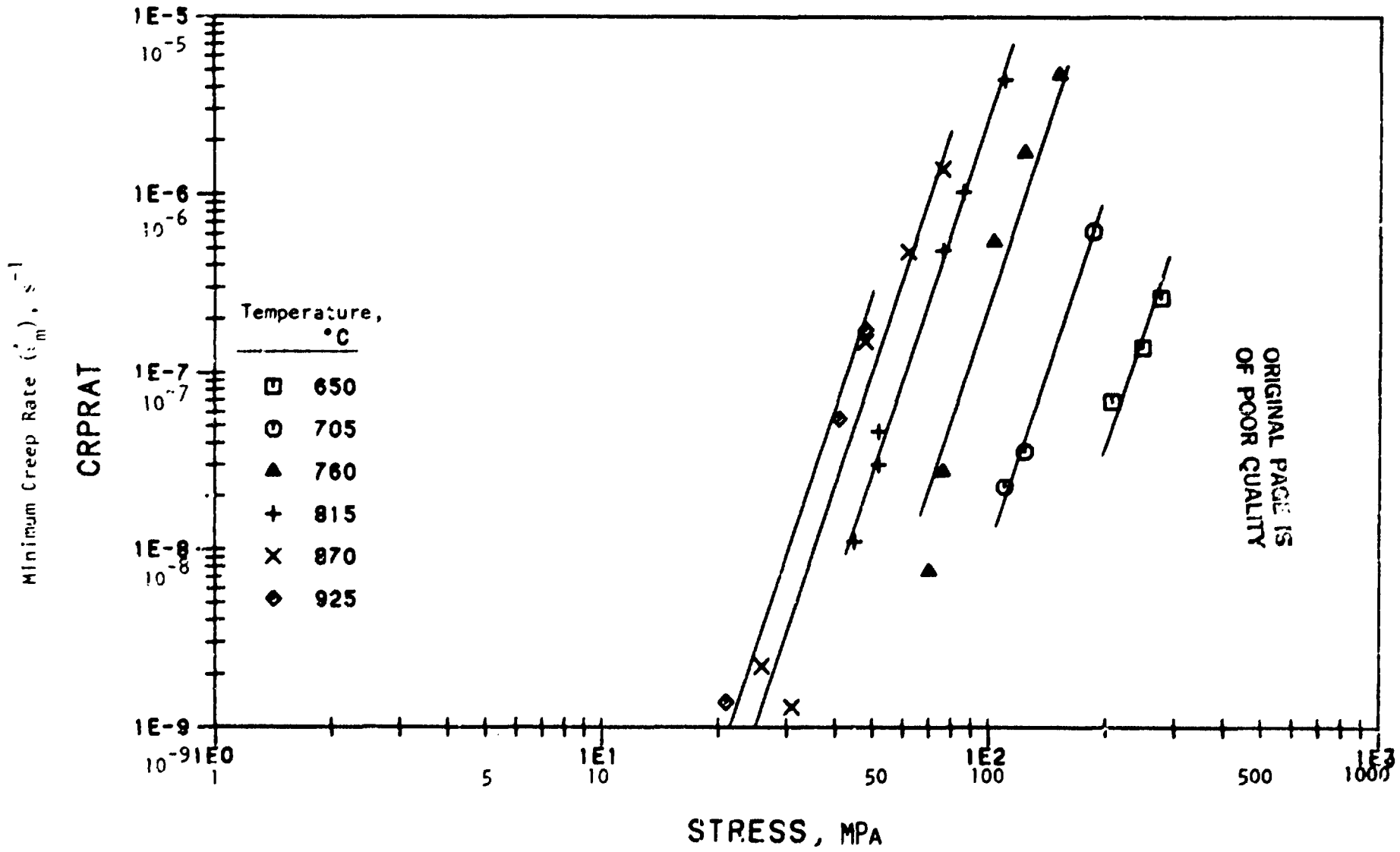


Figure 19. Stress vs. minimum creep rate of IN 800H in air.

N15 IN AIR

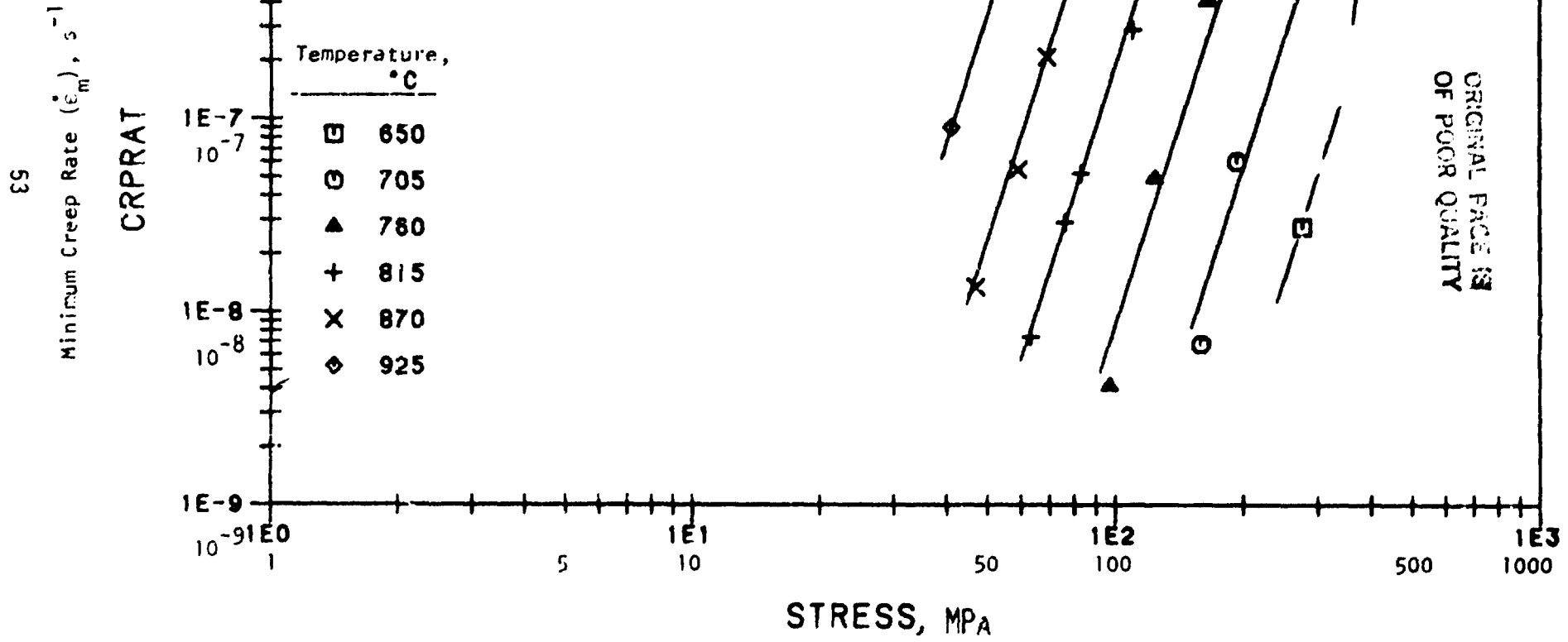


Figure 20. Stress vs. minimum creep rate of N-155 in air.

199 IN AIR

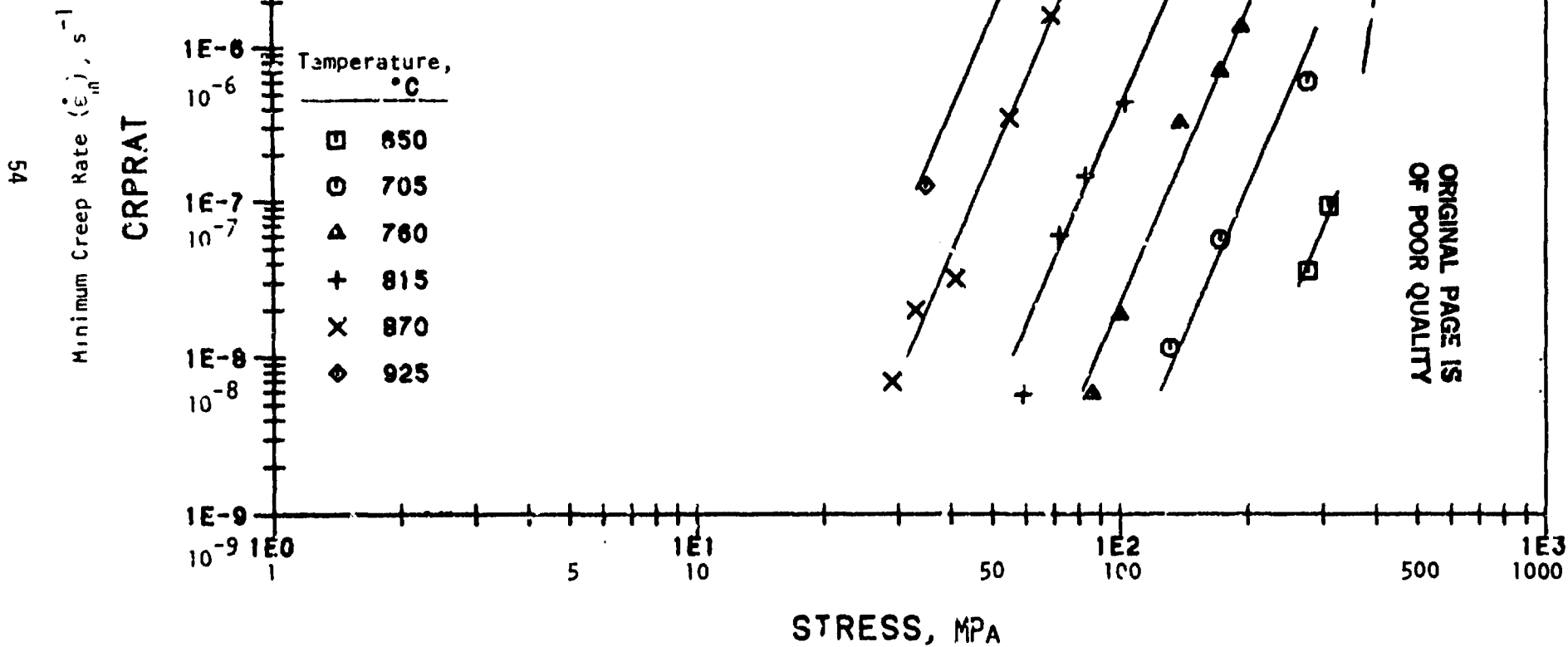


Figure 21. Stress vs. minimum creep rate of 19-9DL in air.

CRM IN AIR

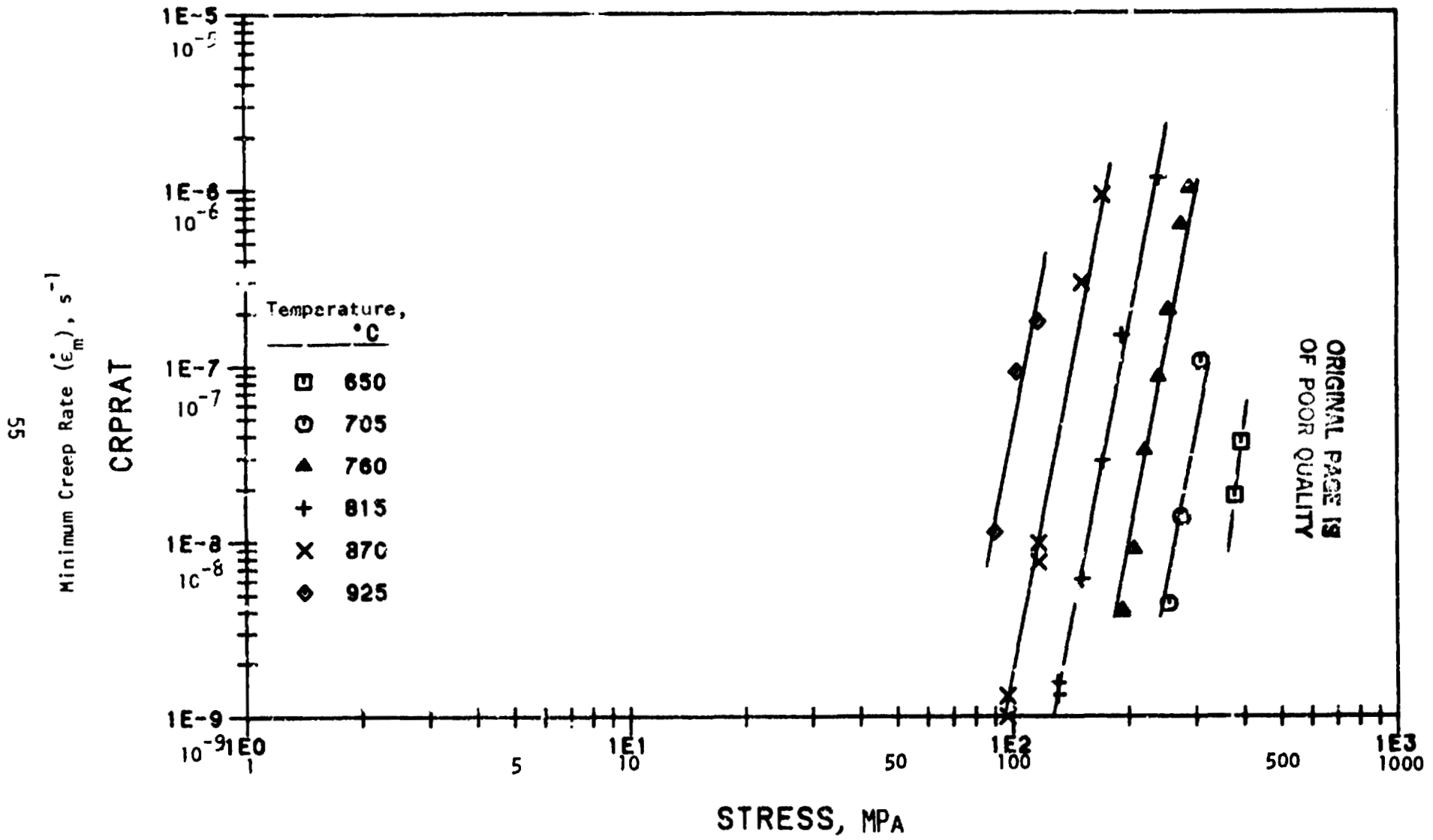


Figure 22. Stress vs. minimum creep rate of CRM-6D in air.

XF8 IN AIR

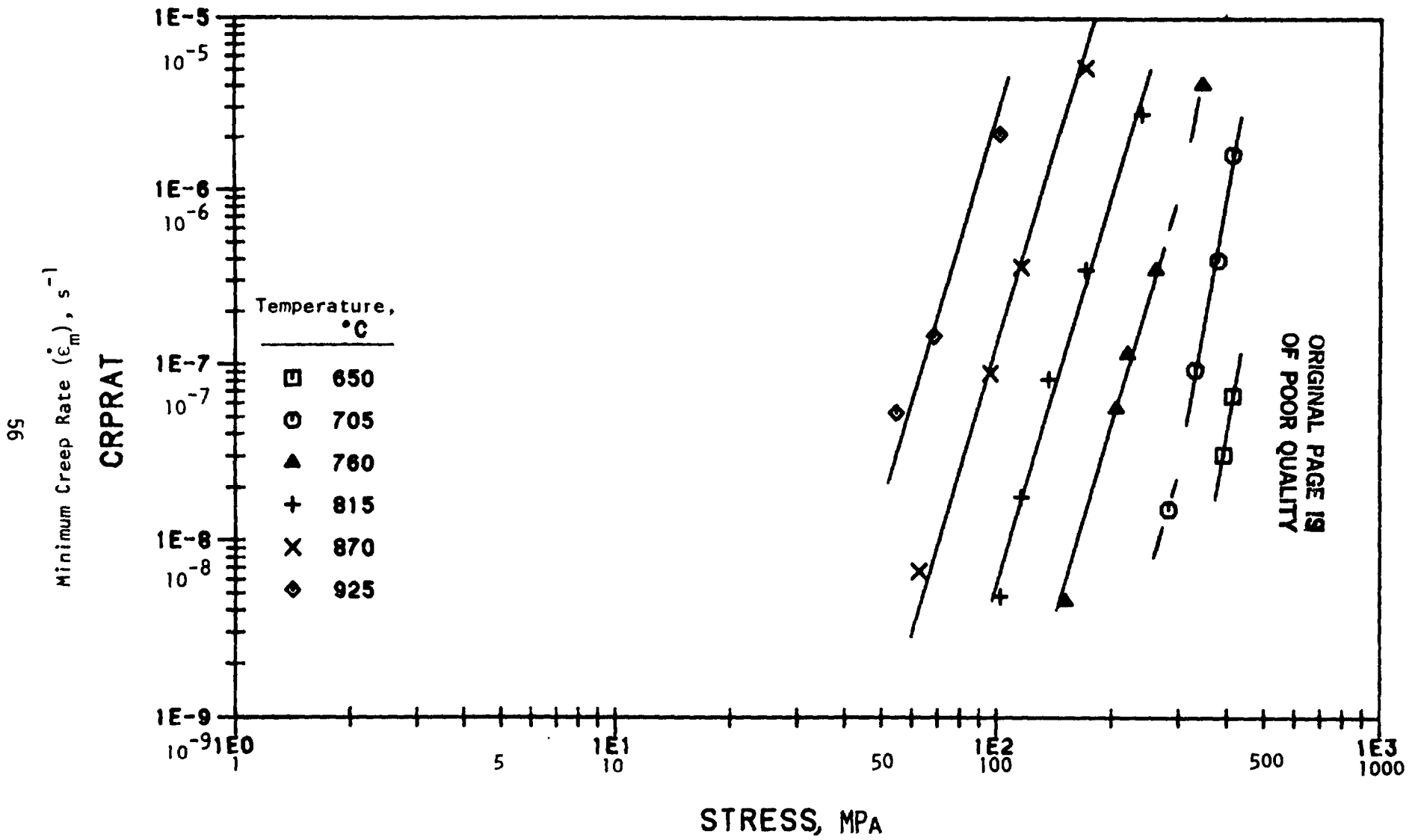


Figure 23. Stress vs. minimum creep rate of XF-818 in air.

ORIGINAL PAGE IS
OF POOR QUALITY

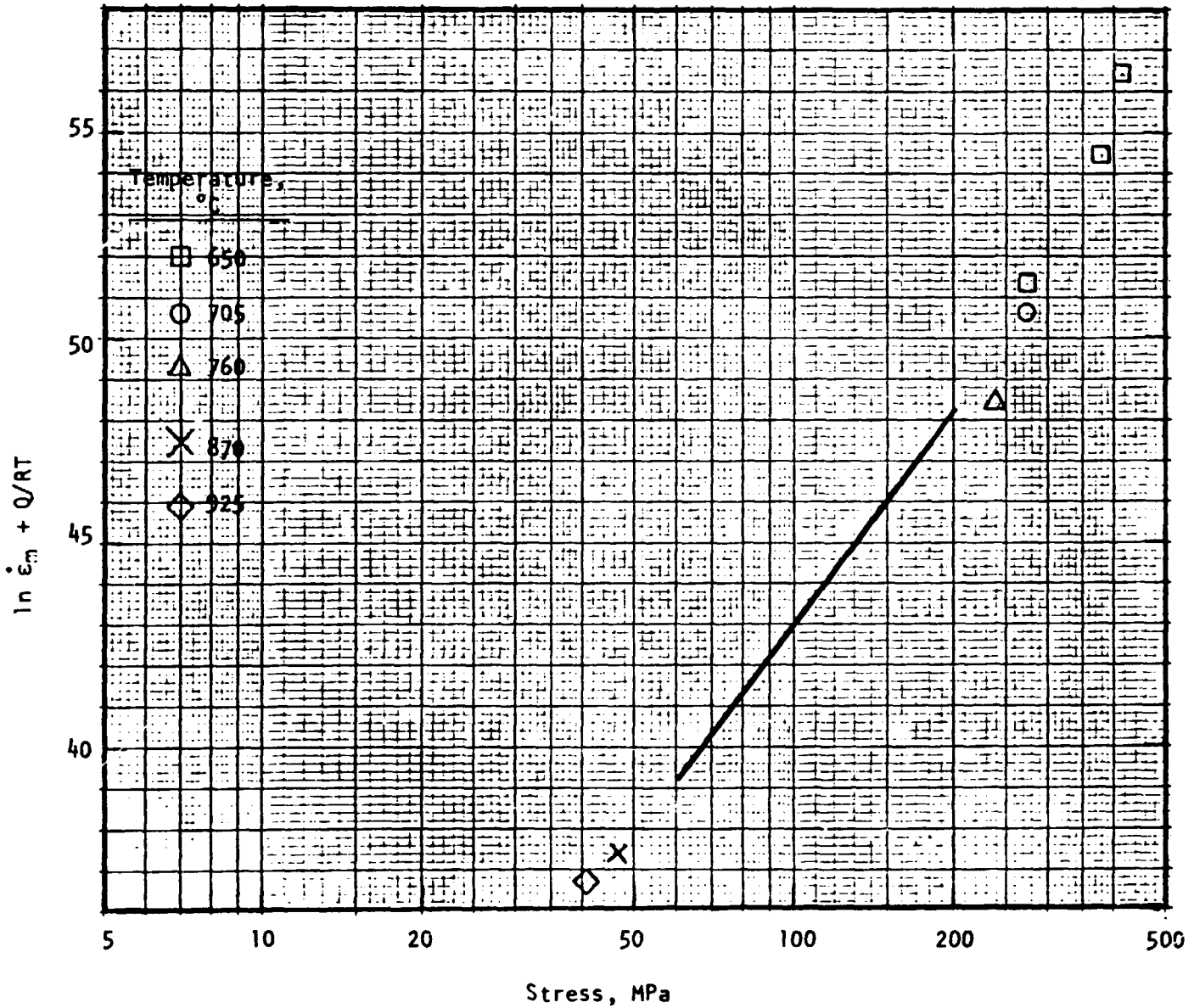


Figure 24. Temperature-compensated minimum creep rate vs. stress for N-155 tested in air (Case 2B, including Cases 2A and 2C shown separately).

ORIGINAL PAGE IS
OF POOR QUALITY

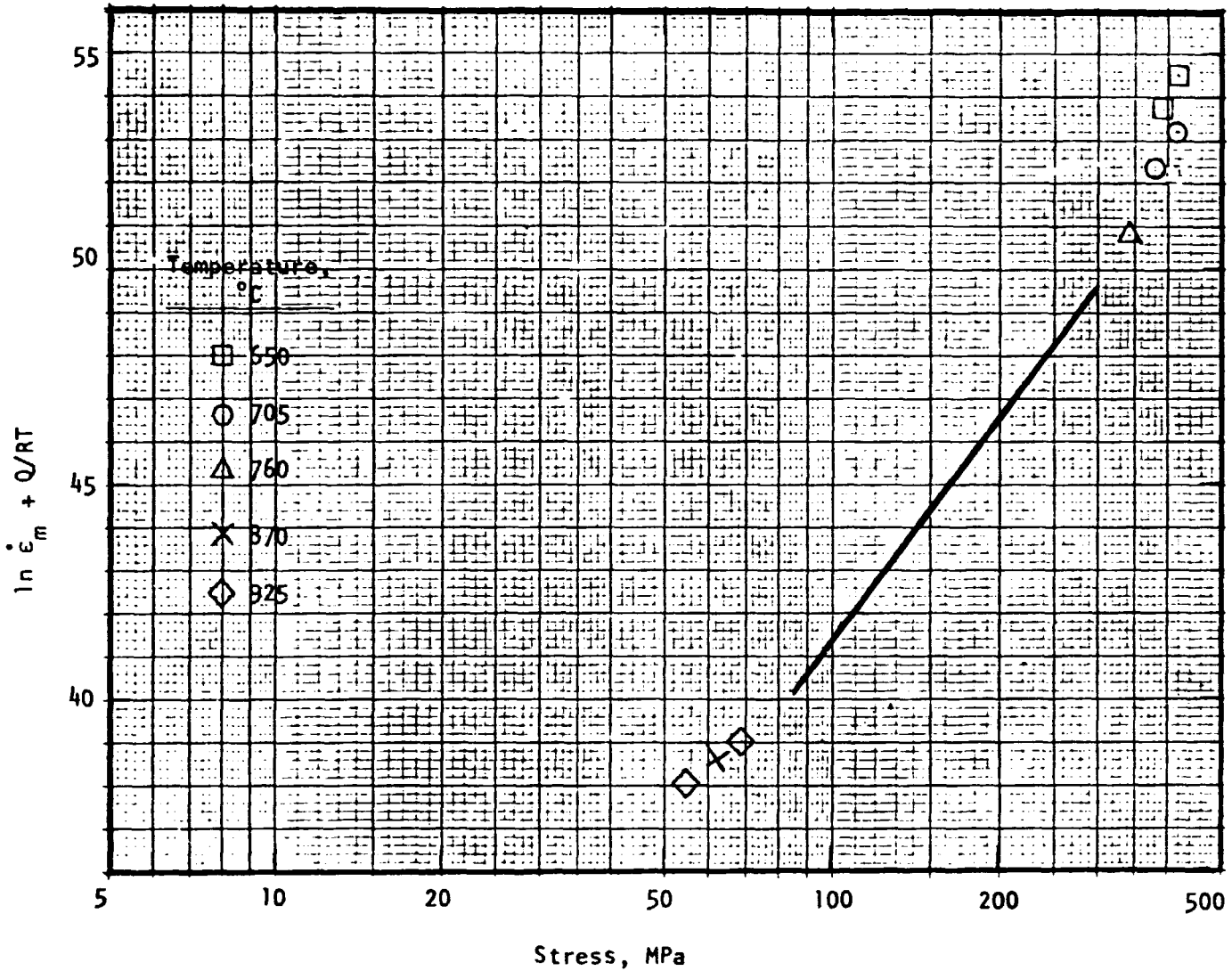


Figure 25. Temperature-compensated minimum creep rate vs. stress for XF-818 tested in air (Case 2B, including Cases 2A and 2C shown separately).

ORIGINAL FIGURE IS
OF POOR QUALITY

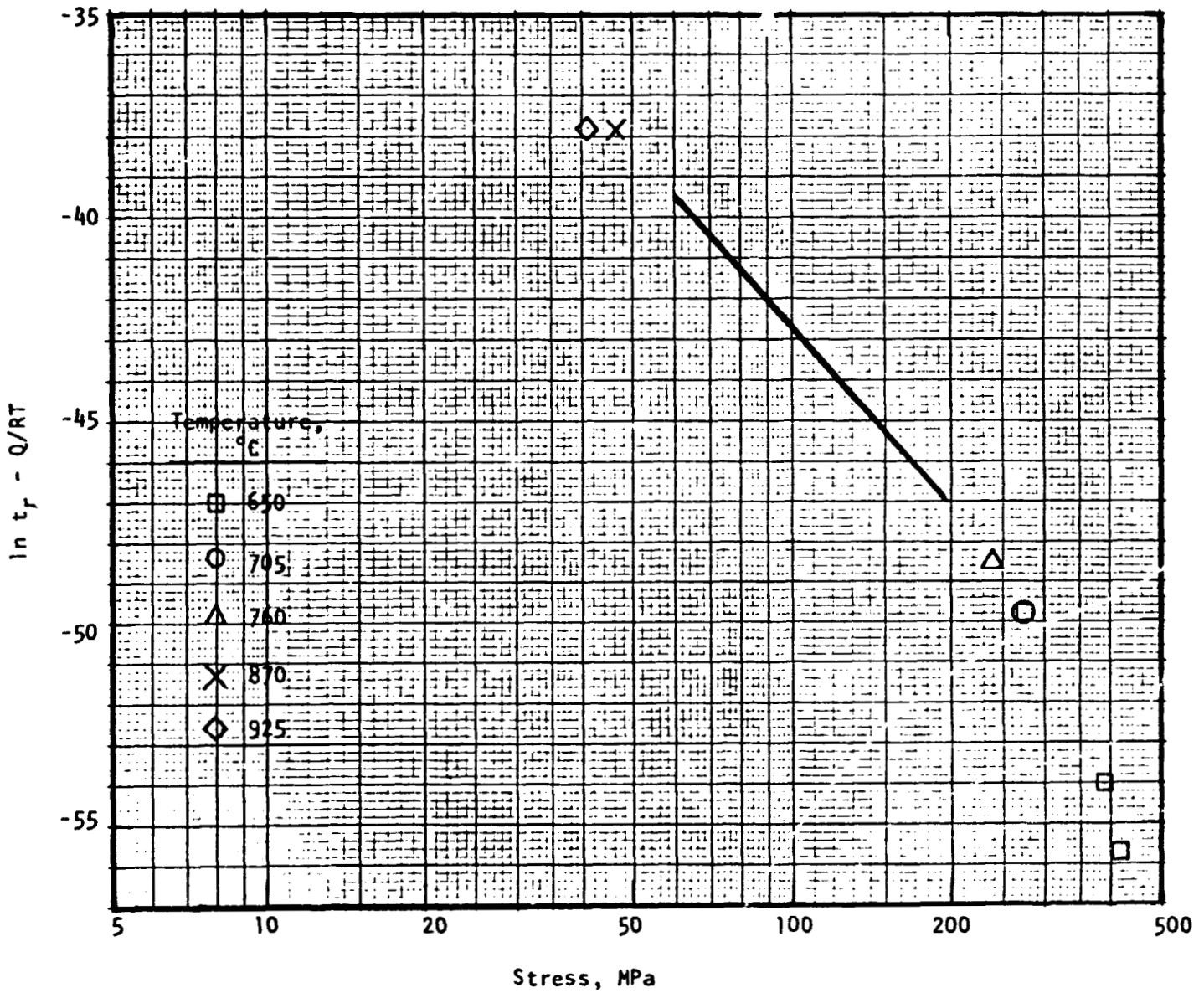


Figure 26. Temperature-compensated rupture life vs. stress for N-155 tested in air (Case 2B, including Cases 2A and 2C data shown separately).

ORIGINAL PAGE IS
OF POOR QUALITY

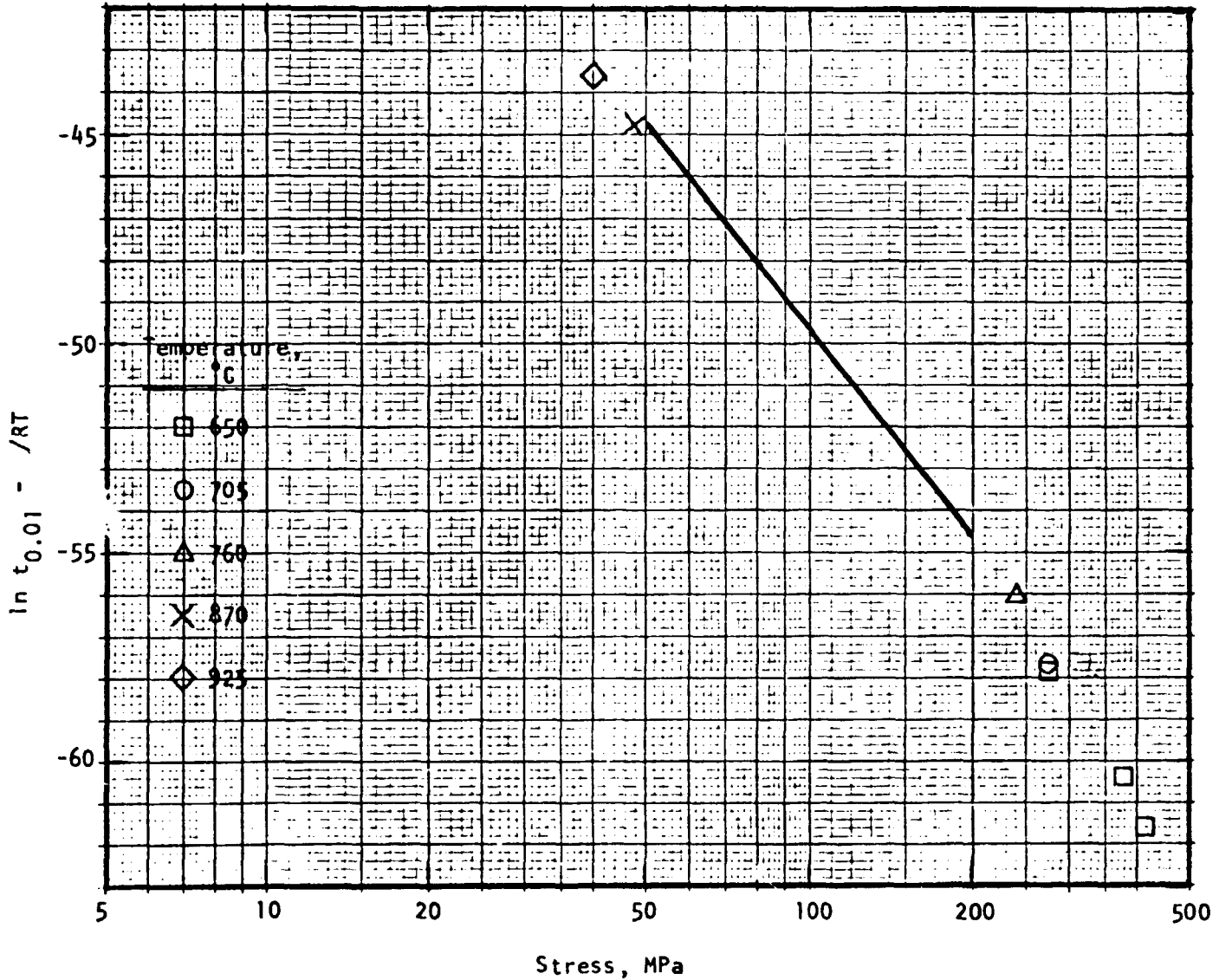


Figure 27. Temperature-compensated time to 1% creep strain vs. stress for N-155 tested in air (Case 2B, including Cases 2A and 2C shown separately).

ORIGINAL PAGE IS
OF POOR QUALITY

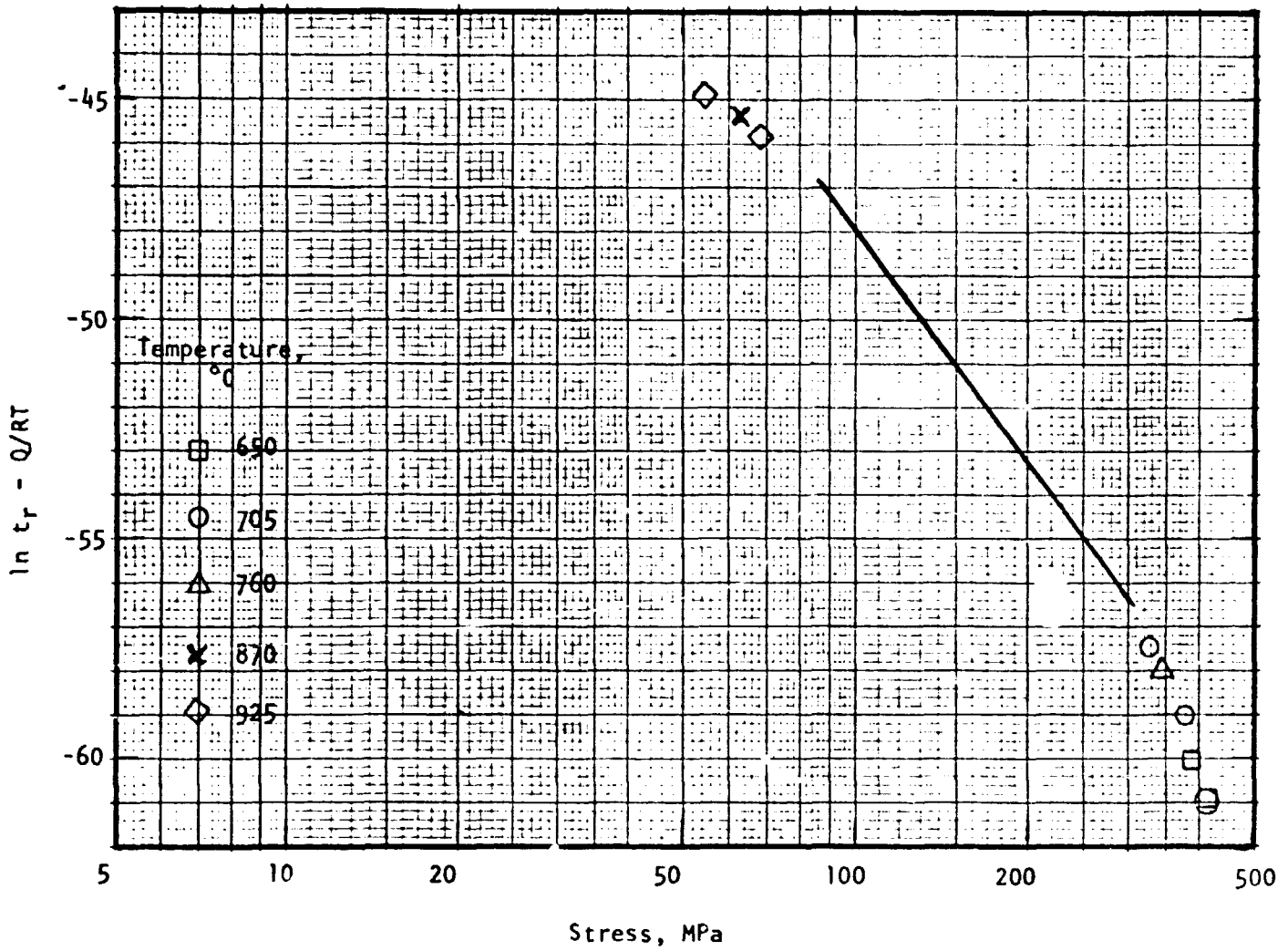


Figure 28. Temperature-compensated rupture life vs. stress for XF-818 tested in air (Case 2B, including Cases 2A and 2C data shown separately).

ORIGINAL PAGE IS
OF POOR QUALITY

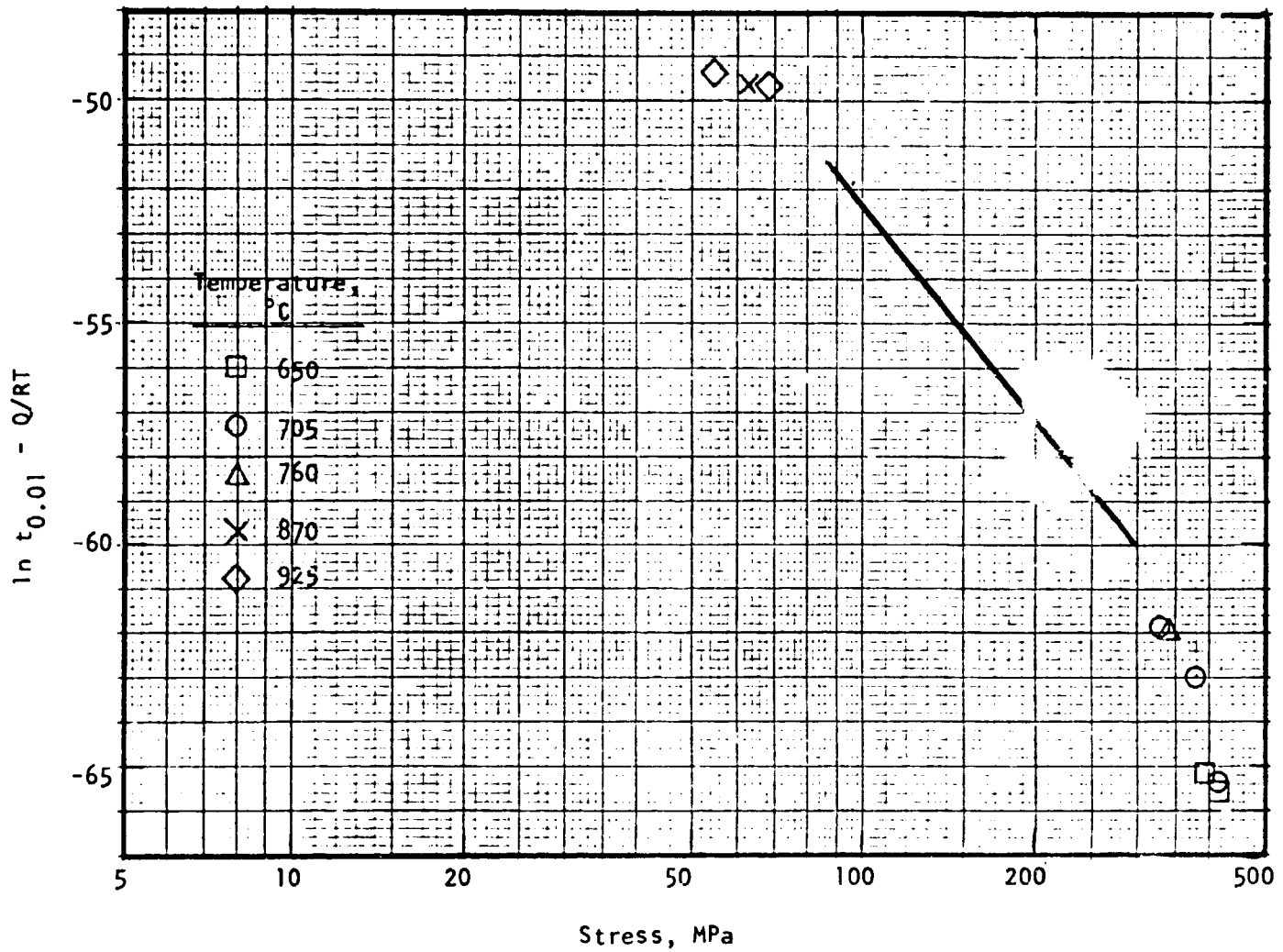


Figure 29. Temperature-compensated time to 1% creep strain vs. stress for XF-818 tested in air (Case 2B, including Cases 2A and 2C shown separately).

ORIGINAL PAGE IS
OF POOR QUALITY

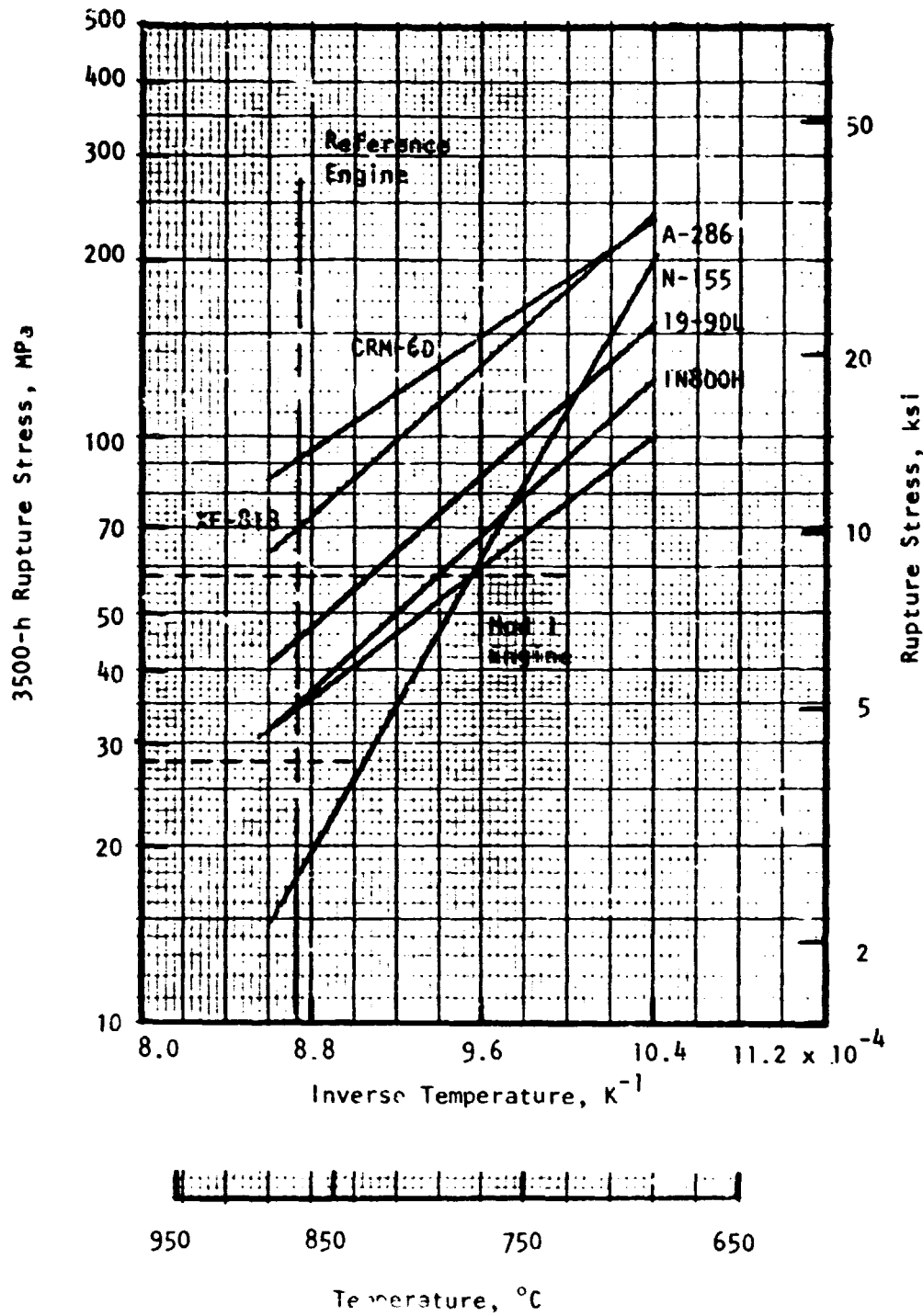
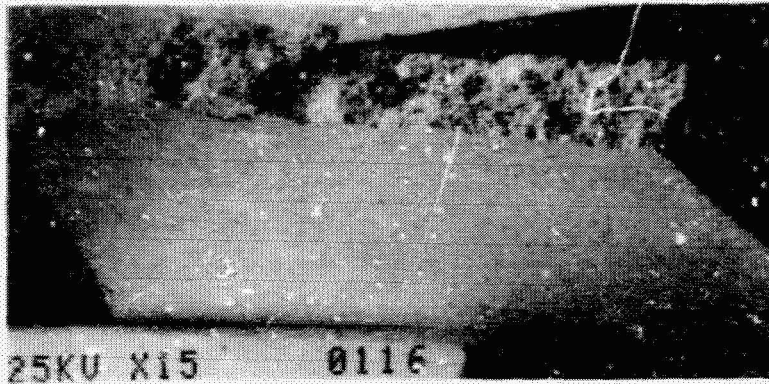


Figure 30. Estimated 3500-hour rupture stress of six alloys tested in air.

ORIGINAL PAGE IS
OF POOR QUALITY



(a)



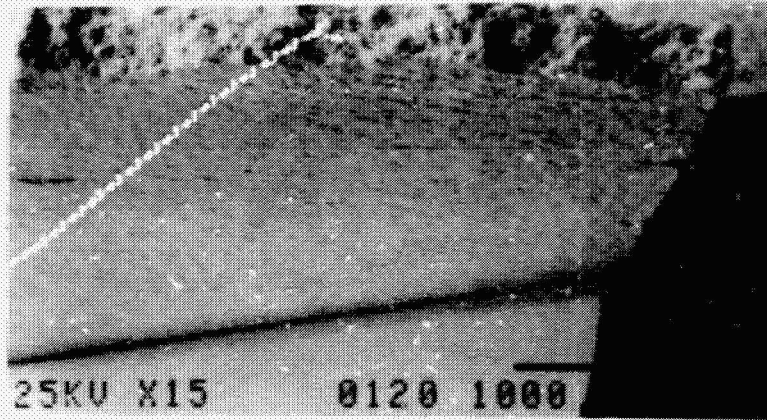
(b)



(c)

Figure 31. Typical macrofractographs of wrought specimens creep-rupture tested in air. (a) 19-9DL, 815°C, 59 MPa; (b) 19-9DL, 870°C, 29 MPa; (c) A-286, 815°C, 55 MPa; (d) N-155, 870°C, 47 MPa; (e) N-155, 815°C, 63 MPa; (f) IN 800H, 760°C, 70 MPa; and (g) IN 800H, 815°C, 45 MPa. (All 15X)

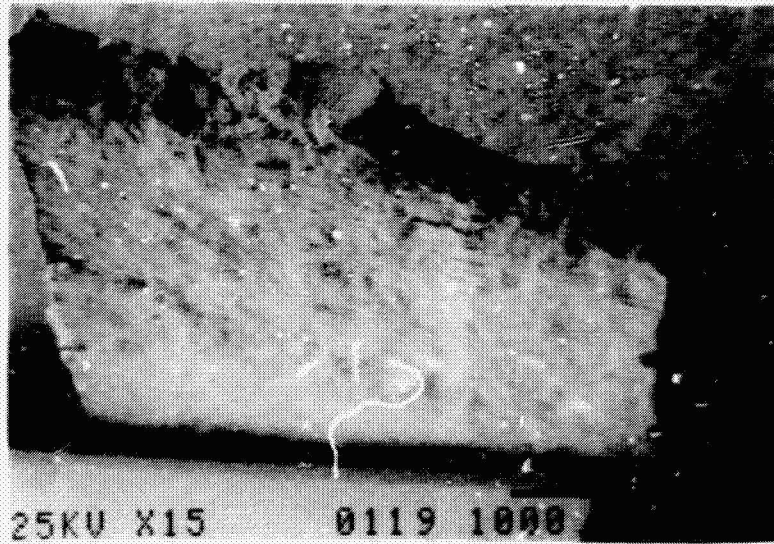
ORIGINAL PAGE IS
OF POOR QUALITY



(d)



(e)



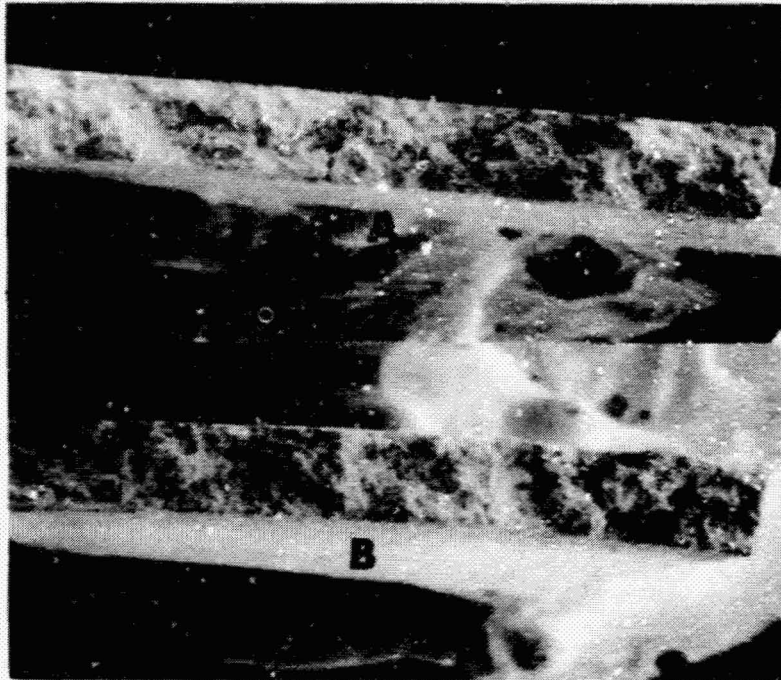
(f)



(g)

Figure 31 (cont.)

ORIGINAL PAGE IS
OF POOR QUALITY



SEM No. 6486, 6487

~15X

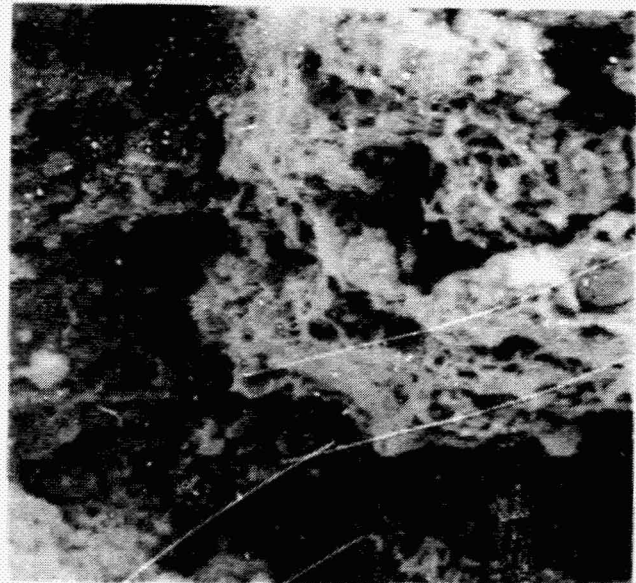
(a)



SEM No. 6492

~15X

(b)



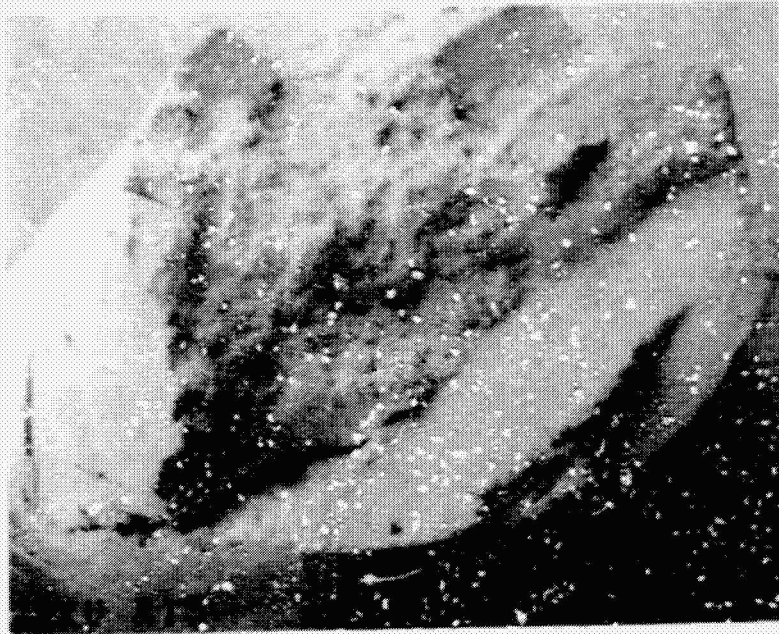
SEM No. 6490

500X

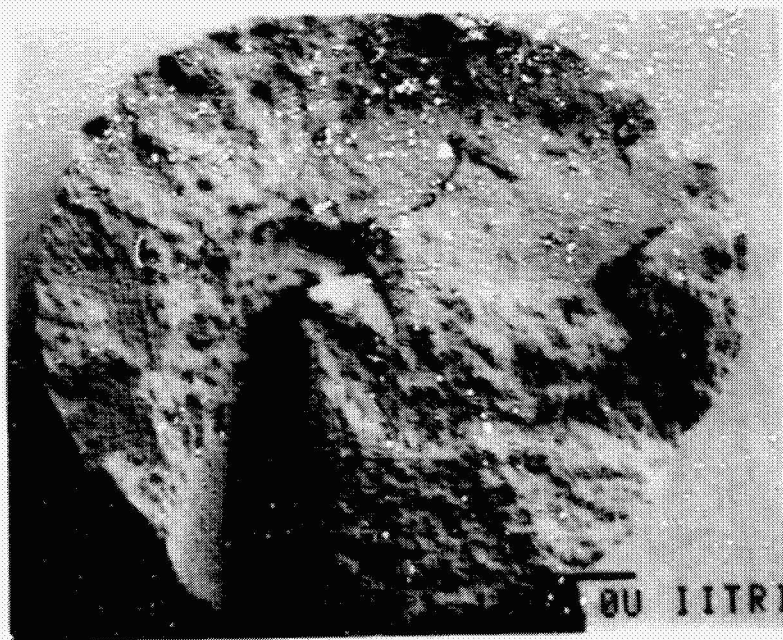
(c)

Figure 32. Typical macro- and microfractographs of the 19-9DL specimen creep-rupture tested at 870°C and 41 MPa. (a) Macrofractographs of the mating fracture surfaces; (b) side view of fracture surface in Fig. 38a (B); and (c) microfractograph from the center of fracture surface in Fig. 33a (B).

ORIGINAL PAGE 13
OF POOR QUALITY



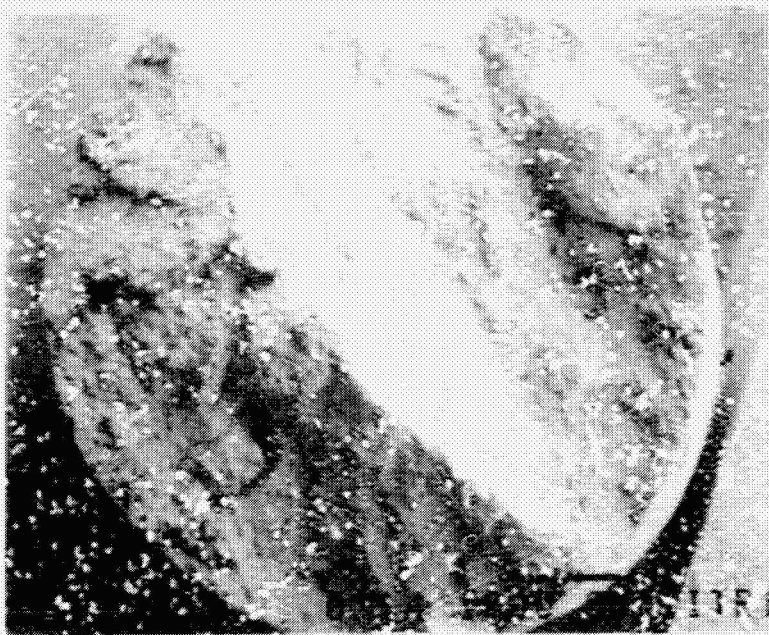
(a)



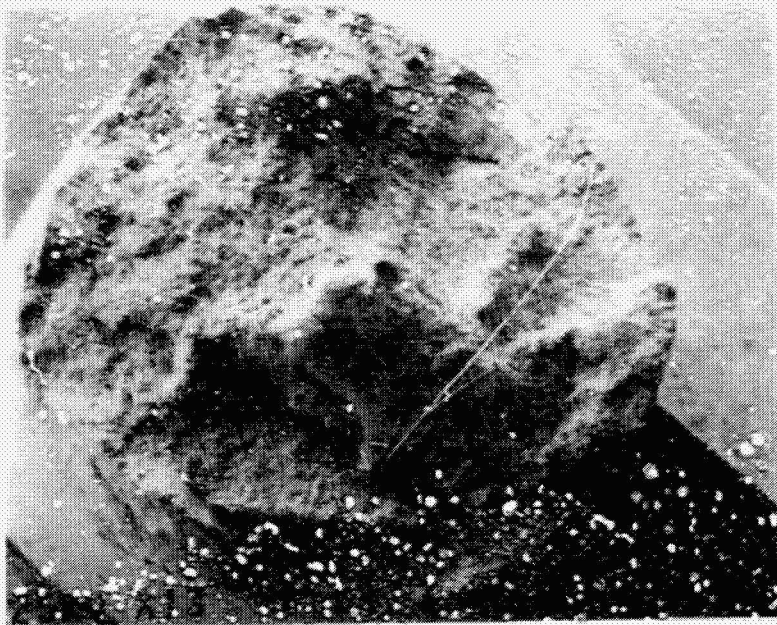
(b)

Figure 33. Typical macrofractographs of the cast specimens creep-rupture tested in air. (a) XF-818, 760°C, 152 MPa; (b) XF-818, 815°C, 103 MPa; (c) CRM-6D, 760°C, 193 MPa; and (d) CRM-6D, 870°C, 117 MPa.

ORIGINAL PAGE IS
OF POOR QUALITY



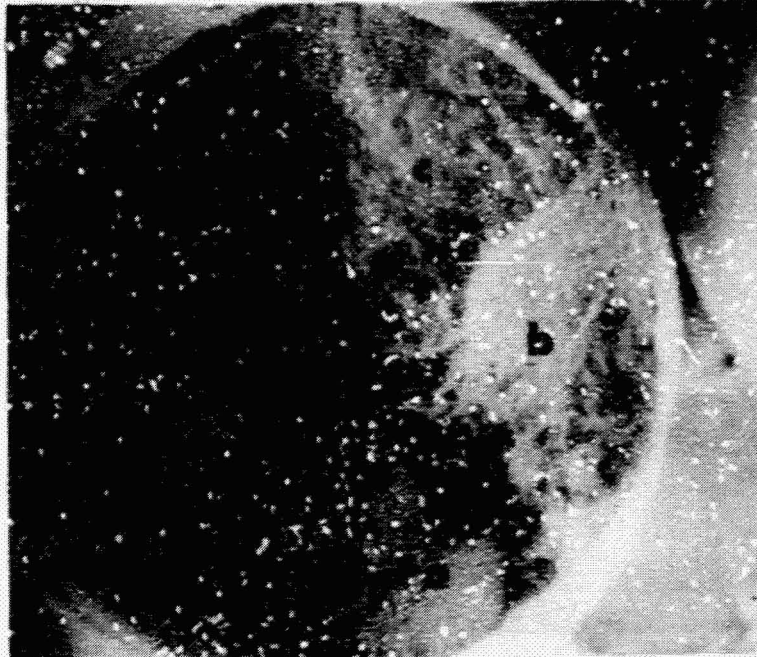
(c)



(d)

Figure 33 (cont.)

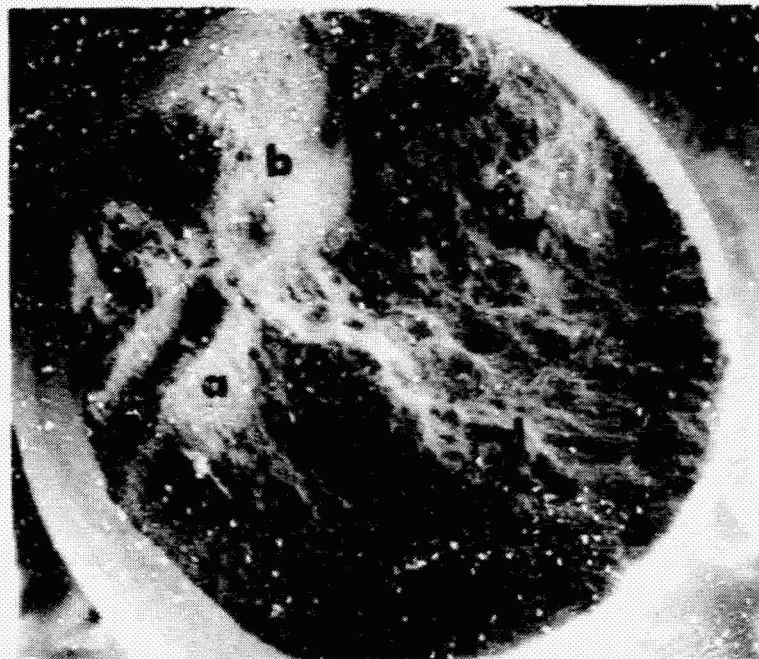
ORIGINAL PAGE IS
OF POOR QUALITY



SEM No. 6494

~20X

(a)



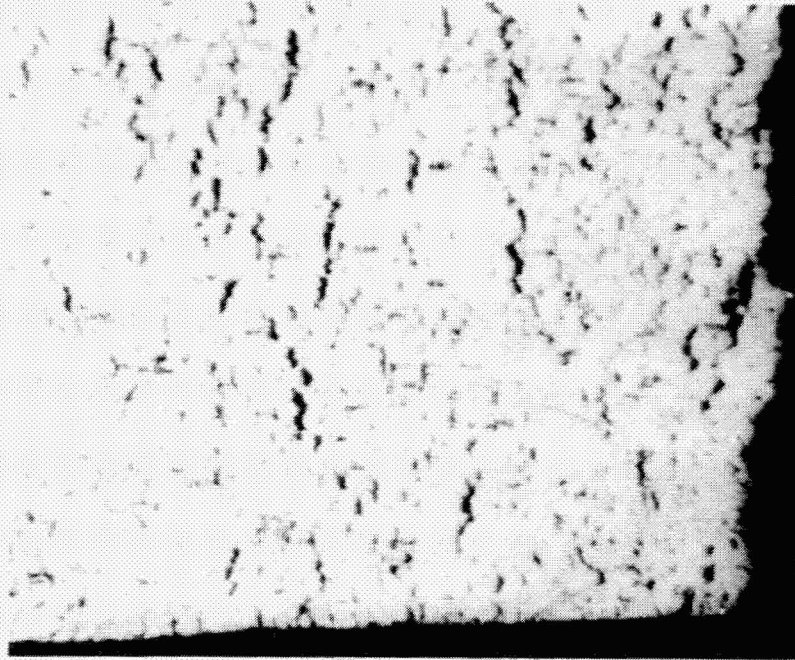
SEM No. 6493

20X

(b)

Figure 34. Typical macrofractographs of XF-818 specimen creep-rupture tested at 815°C and 138 MPa. Corresponding areas of mating fracture surfaces are indicated.

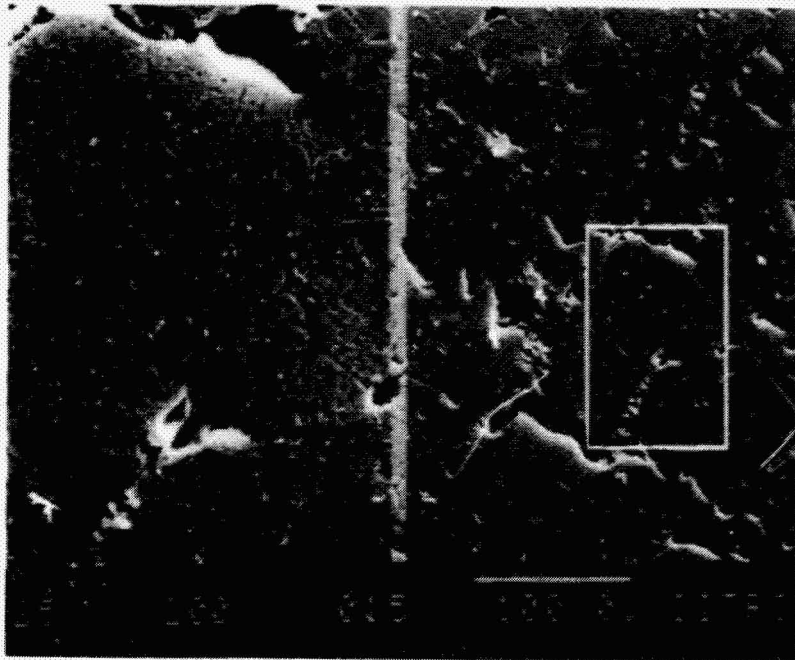
ORIGINAL PAGE IS
OF POOR QUALITY



Neg. No. 54596

50X

(a)



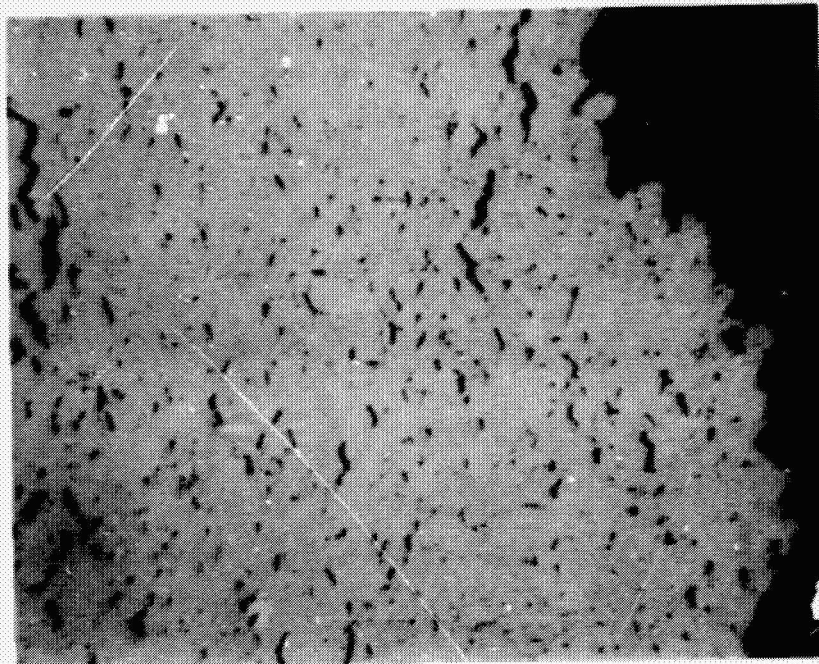
SEM No. 150

60X, 200X

(b)

Figure 35. Typical optical and SEM photomicrographs of cross-sections from 19-9DL specimen creep-rupture tested in air. (a) Optical, 870°C, 29 MPa; and (b) SEM, 815°C, 59 MPa.

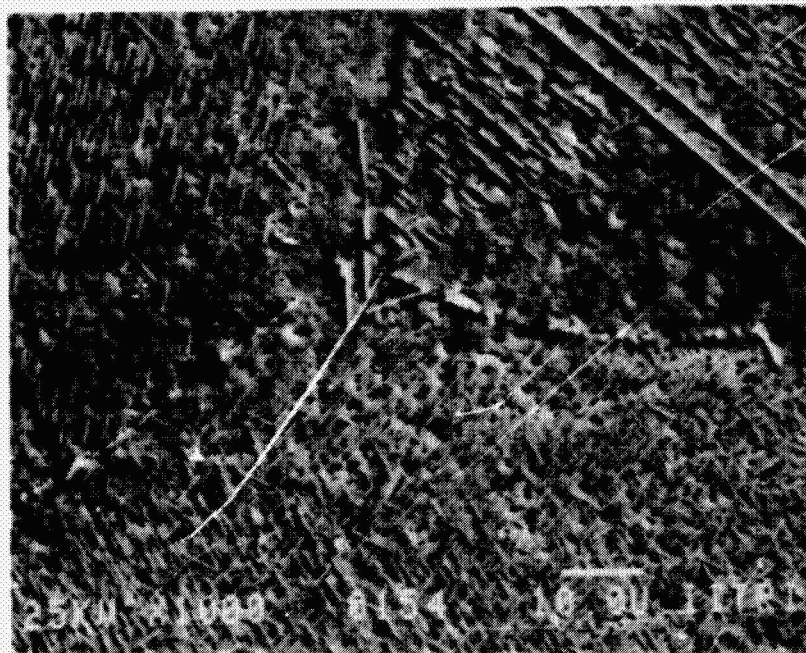
ORIGINAL PAGE IS
OF POOR QUALITY



Neg. No. 54597

20X

(a)



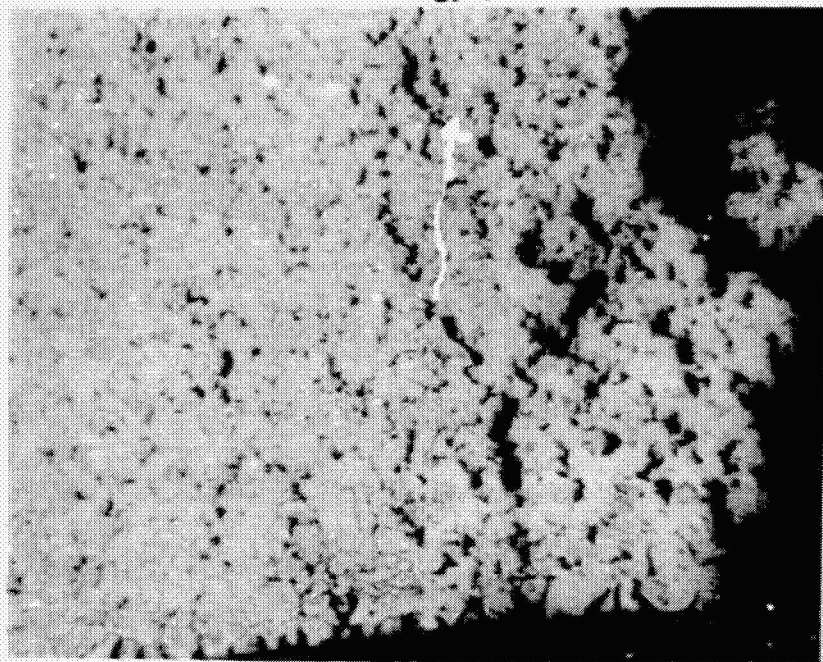
SEM No. 154

1000X

(b)

Figure 36. Typical optical and SEM photomicrographs of cross-sections from A-286 specimen creep-rupture tested in air, 815°C, 55 MPa. (a) Optical, (b) SEM.

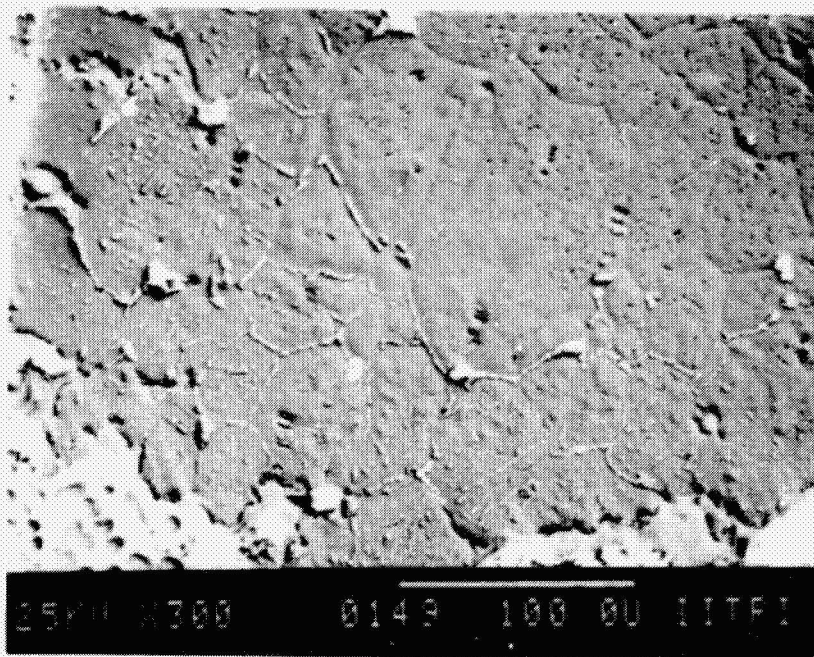
ORIGINAL PAGE IS
OF POOR QUALITY



Neg. No. 54598

50X

(a)



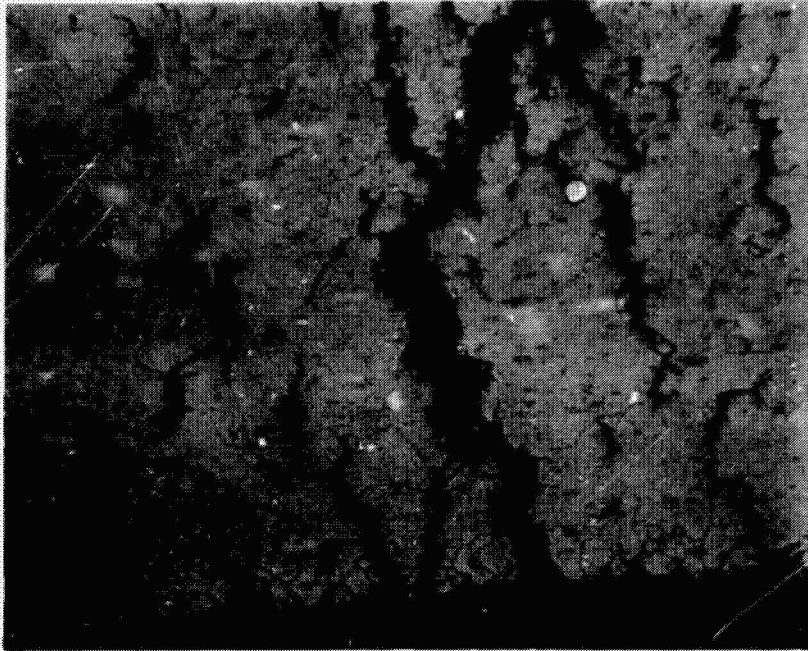
SEM No. 149

300X

(b)

Figure 37. Typical optical and SEM photomicrographs of cross-sections from N-155 specimen creep-rupture tested in air, 870°C, 47 MPa. (a) Optical, (b) SEM.

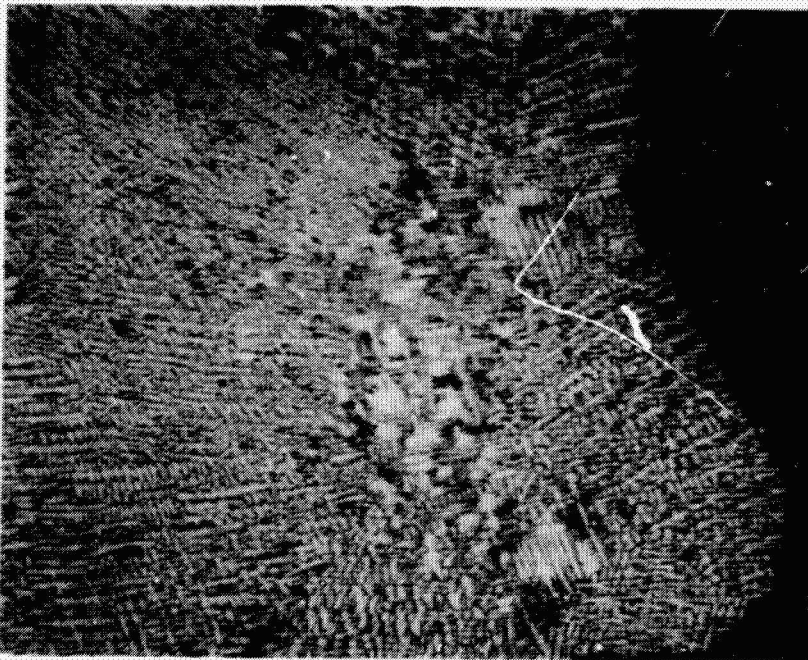
ORIGINAL PAGE IS
OF POOR QUALITY



Neg. No. 54599

20X

(a)



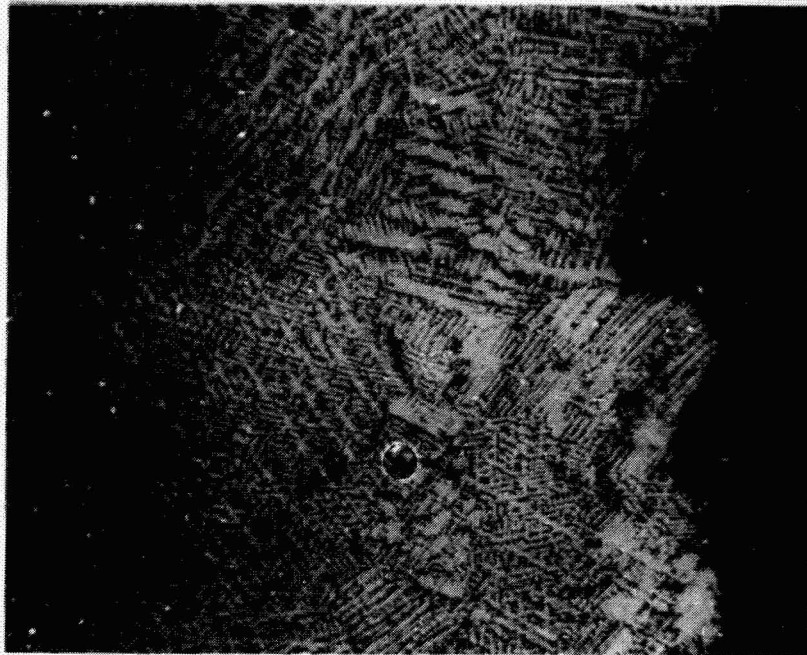
Neg. No. 54600

20X

(b)

Figure 38. Optical photomicrographs of cross-sections from IN 800H and XF-818 specimens creep-rupture tested in air. (a) IN 800H, 815°C, 45 MPa; and (b) XF-818, 760°C, 152 MPa.

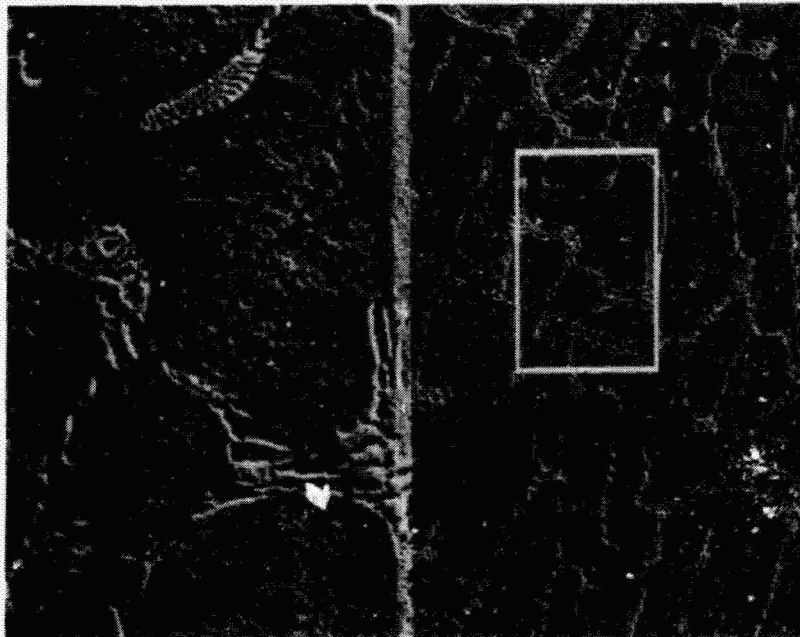
ORIGINAL PAGE IS
OF POOR QUALITY



Neg. No. 54601

20X

(a)



SEM No. 155

60X, 200X

(b)

Figure 39. Typical optical and SEM photomicrographs of cross-sections of CRM-6D specimens creep-rupture tested in air. (a) 870°C, 117 MPa; and (b) 760°C, 193 MPa.

APPENDIX A
COMPLETE AIR CREEP-RUPTURE DATA

APPENDIX A
COMPLETE AIR CREEP-RUPTURE

ORIGINAL PAGE IS
OF POOR QUALITY

(1)	(2)	(3)	(4)	(5)	(6)	(7)	(8)	(9)	(10)	(11)
AIR	A2R	650	463	36.2	5.56E-07	11.4	20.0		22.0	14.2
AIR	A2R	650	414	568.1	3.03E-09	8.4	200.	380.	260.	308.
AIR	A2R	650	310		9.72E-11					
AIR	A2R	705	379	35.0	1.25E-07	13.6	6.6	13.0	7.0	20.0
AIR	A2R	705	276	706.6	1.89E-09	21.0	460.	542.	460.	247.
AIR	A2R	705	234	1222.	1.22E-10	3.4	600.	1095	600.	622.
AIR	A2R	705	179		1.53E-10					
AIR	A2R	760	345	5.4	5.56E-06	26.3		0.3		
AIR	A2R	760	276	27.2	2.06E-07	25.0	6.4	10.5	7.0	20.2
AIR	A2R	760	207	126.0	1.02E-08	23.8	60.0	76.0	60.0	66.0
AIR	A2R	760	179	254.8	5.56E-09	18.0	100.	156.	110.	145.
AIR	A2R	760	124	1181.0	1.21E-10	8.7	250.	500.	250.	931.
AIR	A2R	760	83		2.39E-10		300.		325.	
AIR	A2R	815	134	9.9	3.47E-08	24.6	5.5	8.1	6.0	3.9
AIR	A2R	815	110	89.7	3.45E-08	25.4	12.0	27.5	15.0	74.7
AIR	A2R	815	83	206.4	1.11E-08	16.0	35.0	70.0	40.0	166.
AIR	A2R	815	62	439.5	6.42E-09	11.8	90.0	162.	90.0	350.
AIR	A2R	815	55	1030.	2.29E-08	10.7	110.	34.	340.	250.
AIR	A2R	815	41		2.20E-09		145.	20.	170.	
AIR	A2R	870	55	15.0	1.04E-05	59.2	4.5	0.3	5.0	10.0
AIR	A2R	870	41	59.8	1.25E-06	87.2	28.0	1.5	30.0	29.8
AIR	A2R	870	31	160.0	7.03E-07	49.5	85.0	4.0	85.0	75.0
AIR	A2R	870	21	6222.0	1.72E-07	29.8	3500	19.5	4500	1722
AIR	A2R	925	28	53.0	2.33E-06	58.4	28.0	1.0	30.0	23.0
AIR	A2R	925	21	171.4	6.28E-07	42.9	120.	3.5	140.	31.9
AIR	A2R	925	17	2214.0	6.95E-09	38.7		7.0		
AIR	A2R	925	9.0		4.17E-08			70.0		
AIR	INR	650	276	54.8	2.64E-07	32.2	16.0	3.0	19.0	35.8
AIR	INR	650	248	101.4	1.39E-07	26.3	20.0	5.0	25.0	76.4
AIR	INR	650	207	309.0	6.94E-08	15.0	110.	.7	120.	189.
AIR	INR	650	186		4.59E-09		900.	3.0	1100	
AIR	INR	705	186	46.2	6.25E-07	26.8	13.0	1.0	16.0	30.2
AIR	INR	705	124	848.1	3.61E-08	36.8	250.	50.0	275.	573.
AIR	INR	705	110	1475.0	2.28E-08	19.6	300.	25.0	400.	1075
AIR	INR	760	152	4.7	4.72E-06	46.8	1.6	0.4	2.0	2.7
AIR	INR	760	124	28.9	1.71E-06	53.0	5.0	0.5	6.0	22.9
AIR	INR	760	103	132.2	5.47E-07	43.7	60.0	3.0	70.0	62.2
AIR	INR	760	76	1265.0	2.78E-08	28.1	450.	68.0	475.	790.
AIR	INR	760	70	4490.0	7.58E-09	29.5	2600	11.5	4300	140.
AIR	INR	815	110	14.6	4.44E-06	59.6	2.5	0.2	4.0	10.6
AIR	INR	815	86	37.5	1.03E-06	22.3	12.5	1.8	13.5	24.0
AIR	INR	815	83	72.6		32.1	18.0	4.0	20.0	52.6
AIR	INR	815	76	83.2	4.84E-07	23.3	38.0	4.5	40.0	43.2
AIR	INR	815	62	780.6	1.74E-08	18.1	225.	78.0	250.	531.
AIR	INR	815	52	432.0	4.67E-08	29.0	125.	2.0	300.	132.
AIR	INR	815	52	636.0	3.03E-08	23.6	115.	1.7	435.	201.
AIR	INR	815	45	2862.0	1.11E-08	18.7	110	14.5	2400	1462
AIR	INR	815	41		1.36E-09					
AIR	INR	870	76	19.3	1.39E-06	32.2	4.5	2.1	4.5	14.8
AIR	INR	870	62	39.3	4.81E-07	15.9	11.0	5.5	12.0	27.3
AIR	INR	870	48	161.0	1.50E-07	18.1	44.0	19.0	44.0	117.

(cont.)

ORIGINAL PAGE IS
OF POOR QUALITY

(1)	(2)	(3)	(4)	(5)	(6)	(7)	(8)	(9)	(10)	(11)
AJR	INA	870	34	451.6	9.92E-08	23.1	276.	8.0	370.	81.6
AJR	INA	870	31		1.31E-09					
AJR	INA	870	26	1728.0	2.22E-09	16.9		14.9	1005	723.
AJR	INA	925	48	53.0	1.75E-07	24.0	11.0	14.0	11.0	42.0
AJR	INA	925	41	130.5	5.50E-08	23.2	22.0	38.5	22.0	109.
AJR	INA	925	31	292.2	5.56E-08	19.7	62.0	48.0	62.0	230.
AJR	INA	925	21		1.39E-09		260.	675.	280.	
AJR	N15	650	414	2.7	4.63E-06	23.6	0.7	0.5	0.8	2.2
AJR	N15	650	379	14.8	7.45E-07	19.9	9.0	1.7	13.0	1.8
AJR	N15	650	276	968.7	2.78E-08	26.2	325.	20.0	475.	493.
AJR	N15	705	276	42.5	6.72E-07	28.4	13.0	0.8	20.0	22.5
AJR	N15	705	193	527.8	6.11E-08	46.0	160.	16.0	200.	328.
AJR	N15	705	159	3667.0	6.87E-09	29.2	1570	89.0	1670	1997
AJR	N15	760	241	9.0	1.85E-06	42.7		0.2		
AJR	N15	760	193	36.8	1.25E-06	44.0	10.0	1.0	12.0	24.8
AJR	N15	760	165	115.3	4.14E-07	51.5	45.0	0.0	50.0	65.3
AJR	N15	760	124	573.6	5.00E-08	30.1	240.	16.0	290.	284.
AJR	N15	760	97	4523.0	4.17E-09	18.0	850.	144.	1100	3423
AJR	N15	815	165	7.5	4.44E-06	58.3		0.2		
AJR	N15	815	124	42.5	1.50E-06	53.2	19.0	1.3	20.0	22.5
AJR	N15	815	110	128.8	2.92E-07	46.8	45.0	3.0	50.0	78.8
AJR	N15	815	83	457.3	5.28E-08	25.0	140.	19.0	180.	277.
AJR	N15	815	76	931.3	2.94E-08	34.7	300.	30.0	325.	606.
AJR	N15	815	63	2536.0	7.51E-09	12.1	1600	170.	1800	736.
AJR	N15	870	110	8.9	6.67E-06	65.0	1.9	0.2	2.1	6.8
AJR	N15	870	93	55.6	1.94E-07	59.6	11.0	12.0	11.0	44.6
AJR	N15	870	83	58.0	9.92E-07	46.9	23.0	2.5	24.0	34.0
AJR	N15	870	69	212.2	2.11E-07	35.9	73.0	7.0	83.0	129.
AJR	N15	870	59	636.7	5.56E-08	26.7	200.	29.0	220.	414.
AJR	N15	870	47	2897.0	1.36E-08	26.3	1110	85.0	1210	1687
AJR	N15	925	69	32.7	4.86E-07	38.8	8.0	5.0	8.5	24.2
AJR	N15	925	59	49.2	1.07E-06	43.3	15.0	2.0	16.0	33.2
AJR	N15	925	41	354.2	9.17E-08	27.7	120.	29.0	120.	234.
AJR	199	650	414	1.1	4.72E-06	18.8	0.4	0.6	0.6	0.5
AJR	199	650	310	27.9	9.29E-08	10.1	17.5	1.9	22.5	5.4
AJR	199	650	276	135.9	3.58E-08	11.9	50.0	32.0	55.0	80.9
AJR	199	705	276	10.9	5.97E-07	16.9	9.9	0.7		
AJR	199	705	172	268.5	5.69E-08	24.2	60.0	50.0	65.0	204.
AJR	199	705	131	1342.0	1.14E-08	12.1	500.	152.	650.	692.
AJR	199	760	193	8.5	1.35E-06	30.0	8.0	0.2		
AJR	199	760	172	20.2	6.95E-07	31.0	14.0	2.5	14.5	5.7
AJR	199	760	138	101.0	3.22E-07	37.4	33.0	9.0	34.0	67.0
AJR	199	760	100	739.1	1.86E-08	18.8	220.	89.0	280.	459.
AJR	199	760	86	1687.0	5.77E-09	12.1	375.	300.	425.	1262
AJR	199	815	138	2.8	2.22E-05	44.8	1.7	0.1	1.9	0.9
AJR	199	815	124	14.2	3.33E-06	33.4	10.0	0.4	11.0	3.2
AJR	199	815	103	5.4	4.33E-07	29.2	20.0	4.0	22.0	44.4
AJR	199	815	83	173.1	1.44E-07	32.3	57.0	11.0	62.0	111.
AJR	199	815	72	324.1	5.03E-08	25.0	95.0	40.0	105.	209.
AJR	199	815	59	1118.0	5.72E-09	10.1	310.	330.	350.	768.

(cont.)

ORIGINAL PAGE IS
OF POOR QUALITY

(1)	(2)	(3)	(4)	(5)	(6)	(7)	(8)	(9)	(10)	(11)
AIR	199	870	103	1.8	1.89E-05	61.6	0.4		0.5	1.3
AIR	199	870	83	10.2	5.00E-06	42.4	2.7	0.4	3.2	7.0
AIR	199	870	69	38.0	1.60E-06	36.4	16.0	1.2	17.0	21.0
AIR	199	870	55	107.9	3.47E-07	34.3	43.0	8.0	45.0	62.9
AIR	199	870	41	406.3	3.19E-08	20.8	120.	82.0	130.	276.
AIR	199	870	33	799.0	2.00E-08		265.	89.0	290.	509.
AIR	199	870	27	1200.0	6.94E-09	12.3	90.0	279.	120.	1180
AIR	199	925	64	4.1	1.58E-05	47.6	1.8	0.2	1.8	2.3
AIR	199	925	55	16.3	3.06E-06	37.1	4.0	0.7	4.5	11.8
AIR	199	925	35	177.2	1.25E-07	27.5	45.0	10.5	55.0	122.
AIR	CRM	650	393	194.7	3.67E-08	5.6	85.7	30.0	115.	79.7
AIR	CRM	650	379	305.0	1.82E-08	4.2	120.	36.0	180.	125.
AIR	CRM	705	345	49.1	1.59E-08	7.8	14.0	6.0	20.0	29.1
AIR	CRM	705	310	147.4	1.06E-07	8.6	60.0	12.0	70.0	77.4
AIR	CRM	705	276	827.4	1.37E-08	8.2	325.	53.0	475.	352.
AIR	CRM	705	255		4.44E-09			90.0		
AIR	CRM	760	290	11.5	1.01E-06	7.9	6.0	1.6	6.5	9.9
AIR	CRM	760	276	23.6	6.28E-07	10.7	12.0	2.9	14.0	9.6
AIR	CRM	760	255	56.0	2.06E-07	7.6	14.5	2.9	29.5	26.5
AIR	CRM	760	241	140.2	8.61E-08	9.9	65.0	12.0	80.0	60.2
AIR	CRM	760	221	354.4	3.28E-08	10.3	200.	20.0	240.	154.
AIR	CRM	760	207	796.7	9.03E-09	8.7	510.	59.0	610.	187.
AIR	CRM	760	193		3.91E-09			63.0		
AIR	CRM	760	193	1708.0	4.08E-09	7.7	900.	95.0	1100	608.
AIR	CRM	815	241	7.1	1.16E-06	13.9	3.2	0.6	4.2	2.9
AIR	CRM	815	193	78.6	1.49E-07	11.8	30.0	6.5	40.0	38.6
AIR	CRM	815	172	281.9	2.86E-08	10.6	135.	19.0	175.	107.
AIR	CRM	815	152	768.0	6.11E-09	7.6	320.	58.0	440.	328.
AIR	CRM	815	131		1.32E-09			560.		
AIR	CRM	815	131	1848.0	1.54E-09	4.6	1200	682.	1300	548.
AIR	CRM	870	172	11.0	9.28E-07	11.1	5.0	2.0	5.5	5.5
AIR	CRM	870	152	29.7	2.94E-07	11.7	13.0	6.0	17.0	12.7
AIR	CRM	870	138	19.1	1.20E-06	21.7	7.0	0.7	8.0	11.1
AIR	CRM	870	117	430.5	7.64E-09	5.6	150.	80.0	230.	201.
AIR	CRM	870	117	401.9	9.81E-09	6.6	175.	125.	215.	187.
AIR	CRM	870	97		1.00E-09		245.	498.	470.	
AIR	CRM	870	97	1334.0	1.30E-09	2.8	900.	1110	1000	234.
AIR	CRM	925	117	28.4	1.79E-07	12.5	8.0	8.5	12.0	16.4
AIR	CRM	925	103	55.4	9.28E-08	9.6	28.0	22.0	32.0	23.4
AIR	CRM	925	90	237.3	1.13E-08	5.5	100.	146.	130.	107.
AIR	XFB	650	414	143.2	6.72E-08	7.5	80.0	11.0	100.	33.2
AIR	XFB	650	393	300.8	3.11E-08	8.0	160.	17.0	220.	80.8
AIR	XFB	705	414	3.1	1.60E-06	6.7	2.5	0.3		
AIR	XF	705	379	20.9	3.97E-07	7.2	9.0	3.5	11.0	9.9
AIR	XFB	705	371	103.0	9.42E-08	10.1	40.0	10.5	50.0	53.0
AIR	XFB	705	371	541.0	1.52E-08	9.9	110.	130.	160.	381.
AIR	XFB	760	262	2.3	4.12E-06	8.2	2.0	0.3		
AIR	XFB	760	262	38.4	3.50E-07	12.7	15.0	4.5	17.0	21.4
AIR	XFB	760	221	132.3	1.16E-07	13.6	45.0	14.0	50.0	82.3
AIR	XFB	760	207	261.7	5.67E-08	12.7	65.0	31.5	80.0	182.
AIR	XFB	760	152	2497.0	4.58E-09	11.4	700.	300.	860.	1637

ORIGINAL PAGE IS
OF POOR QUALITY

(cont.)

(1)	(2)	(3)	(4)	(5)	(6)	(7)	(8)	(9)	(10)	(11)
A1R	XFB	A15	241	4.2	2.77E-06	13.1	2.8	0.5	3.3	0.9
A1R	XFB	B15	172	62.5	3.50E-07	22.3	21.0	5.0	24.0	38.5
A1R	XFB	B15	138	199.5	8.33E-08	14.1	75.0	14.5	95.0	105.
A1R	XFB	A15	117	1104.0	1.78E-08	18.9	500.	60.0	550.	554.
A1R	XFB	A15	103	3115.0	4.87E-09	23.8	542.	200.	742.	2373
A1R	XFB	B70	172	4.1	5.15E-06	16.9	1.6	0.4	1.9	2.2
A1W	XFB	A70	117	58.5	3.64E-07	20.6	18.0	4.5	22.0	36.5
A1R	XFB	B70	97	194.0	9.00E-08	19.0	55.0	14.0	65.0	129.
A1R	XFB	A70	63	2198.0	6.78E-09	12.9	490.	205.	640.	1558
A1R	XFB	925	103	11.8	2.11E-06	25.2	4.0	0.8	5.0	3.8
A1R	XFB	925	69	128.5	1.46E-07	23.1	37.0	15.0	42.0	86.5
A1R	XFB	925	55	316.4	5.36E-08	18.4	110.	20.0	120.	196.

Col.	Explanation	Col.	Explanation
1	Environment: AIR, HYD (Hydrogen) - not yet included.	7	Total elongation (ϵ), %
2	Alloy code: A28 - A-286; IN8 - IN 800H; N15 - N155; 199 - 19-9DL; CRM - CRM-6D; XFB - XF-818	8	Duration of secondary creep (t_{sc}), hr
3	Test temperature: (T), °C	9	Time to reach 1% creep elongation ($t_{0.01}$), hr
4	Applied initial stress (σ), MPa	10	Time to reach tertiary creep stage (t_{ter}), hr
5	Rupture life (t_r), hr	11	Effective life ($t_r - t_{ter}$), hr
6	Minimum creep rate ($\dot{\epsilon}_m$), s ⁻¹		

ORIGINAL PAGE IS
OF POOR QUALITY

APPENDIX B

CORRELATIONAL ANALYSIS OF RUPTURE LIFE, TIME TO 1% CREEP STRAIN,
AND MINIMUM CREEP RATE AS A FUNCTION OF INITIAL STRESS
FOR SIX IRON-BASE SUPERALLOYS TESTED IN AIR AT 650° TO 925°C

		<u>Table Nos.</u>
$\ln t_r$	$= k_1 + n_1 \ln \sigma$	B-1
$\ln t_{0.01}$	$= k_2 + n_2 \ln \sigma$	B-2
$\ln \dot{\epsilon}_m$	$= k_3 + n_3 \ln \sigma$	B-3

PRECEDING PAGE BLANK NOT FILMED

ORIGINAL PAGE IS
OF POOR QUALITY

TABLE B-1. STATISTICAL ANALYTICAL DATA FOR RUPTURE LIFE VERSUS STRESS OF SIX IRON-BASE SUPERALLOYS TESTED IN AIR

Alloy	Temp., C	No. of Points	R ²	Constant (k)	Slope (n)
A-286	760	4	0.995	29.8	-4.70
	925	2	-	19.5	-4.70
	870	3	0.993	21.4	-4.70
	815	5	0.931	25.9	-4.70
	705	2	-	32.8	-4.70
IN 800H	815	7	0.950	30.5	-5.95
	925	2	-	27.0	-5.95
	870	3	0.985	28.3	-5.95
	760	5	0.995	32.5	-5.95
	705	3	0.995	35.2	-5.95
	650	3	1.000	37.4	-5.95
N-155	760	5	0.996	39.0	-6.71
	925	2	-	31.6	-6.71
	870	5	0.966	33.9	-6.71
	815	6	0.994	36.0	-6.71
	705	3	0.991	41.8	-6.71
19-9DL	760	5	0.997	36.7	-6.55
	925	2	-	29.1	-6.55
	870	5	0.979	31.0	-6.55
	815	6	0.960	33.9	-6.55
	705	3	0.999	39.2	-6.55
CRM-6D	760	7	0.998	72.2	-12.3
	925	3	0.963	61.2	-12.3
	870	6	0.908	64.5	-12.3
	815	5	0.984	68.6	-12.3
	705	3	0.989	75.7	-12.3
	650	2	-	78.7	-12.3
XF-818	815	5	0.993	43.4	-7.66
	870	3	1.000	40.6	-7.66
	760	4	0.998	46.3	-7.66
	705	3	0.971	93.8	-15.3
	650	2	-	97.4	-15.3

ORIGINAL PAGE IS
OF POOR QUALITY

TABLE B-2. STATISTICAL ANALYTICAL DATA FOR TIME TO 1% CREEP
STRAIN VERSUS STRESS OF SIX IRON-BASE SUPERALLOYS
TESTED IN AIR

Alloy	Temp., C	No. of Points	R ²	Constant (k)	Slope (n)
A-286	870	4	0.992	16.0	-4.25
	925	4	0.998	14.0	-4.25
	815	6	0.985	22.8	-4.25
	760	4	0.955	26.8	-4.25
	705	2	-	30.2	-4.25
IN 800H	870	3	1.000	21.5	-4.80
	925	4	0.923	21.0	-4.80
	815	5	0.975	46.1	-10.2
	760	3	1.000	48.3	-10.2
	705	2	-	53.1	-10.2
	650	4	0.844	57.5	-10.2
19-9PH	760	4	0.997	36.4	-6.92
	925	2	-	27.5	-6.92
	870	4	0.997	29.8	-6.92
	815	5	0.981	33.2	-6.92
	705	3	0.971	38.9	-6.92
N-155	760	5	0.992	36.9	-7.01
	925	2	-	29.4	-7.01
	870	5	0.937	31.7	-7.01
	815	6	0.996	34.0	-7.01
	705	3	1.000	39.6	-7.01
CRM-60	760	8	0.961	56.7	-9.94
	925	3	0.971	49.4	-9.94
	870	6	0.986	51.9	-9.94
	815	6	0.989	54.3	-9.94
	705	4	0.982	59.7	-9.94
XF-818	815	5	0.990	36.7	-6.84
	870	3	1.000	34.1	-6.84
	760	4	0.995	39.8	-6.84
	705	3	0.890	91.1	-15.3
	650	2	-	94.1	-15.3

ORIGINAL PAGE IS
OF POOR QUALITY

TABLE 8-3. STATISTICAL ANALYTICAL DATA FOR MINIMUM CREEP RATE
VERSUS STRESS OF SIX IRON-BASE SUPERALLOYS TESTED IN AIR

Alloy	Temp., C	No. of Points	R ²	Constant (k)	Slope (n)
A-286	925	3	0.994	-24.7	3.47
	870	4	0.982	-25.9	3.47
	815	4	0.981	-33.3	3.47
	760	5	0.985	-71.9	10.1
	705	4	0.850	-76.7	10.1
	650	2	-	-81.0	10.1
IN 800H	815	5	0.994	-43.4	6.64
	925	3	0.997	-41.1	6.64
	870	5	0.948	-42.1	6.64
	760	5	0.971	-45.8	6.64
	705	3	0.992	-49.0	6.64
	650	3	0.985	-52.2	6.64
N-155	815	6	0.994	-47.0	6.84
	925	2	-	-41.6	6.84
	870	5	0.997	-44.3	6.84
	760	5	0.953	-50.1	6.84
	705	3	0.980	-52.9	6.84
19-9DL	870	6	0.989	-40.3	6.35
	925	3	1.000	-38.2	6.35
	815	5	0.976	-44.0	6.35
	760	5	0.979	-46.9	6.35
	705	3	0.998	-49.6	6.35
	650	2	-	-52.8	6.35
CRM-50	815	6	0.995	-75.3	11.3
	925	3	0.952	-68.8	11.3
	870	6	0.995	-72.0	11.3
	760	8	0.997	-78.1	11.3
	705	3	0.997	-81.2	11.3
XF-818	815	5	0.987	-52.9	7.35
	925	3	0.991	-46.7	7.35
	870	4	0.998	-49.7	7.35
	760	4	0.995	-55.9	7.35
	705	3	0.998	-88.7	12.5
	650	2	-	-91.9	12.5

ORIGINAL PAGE IS
OF POOR QUALITY

APPENDIX C

TEMPERATURE-COMPENSATED RUPTURE LIFE, TIME TO 1% CREEP STRAIN,
AND MINIMUM CREEP RATE AS A FUNCTION OF INITIAL STRESS
FOR SIX IRON-BASE SUPERALLOYS TESTED IN AIR AT 650° TO 925°C

<u>Alloy</u>	<u>Figure Nos.</u>
A-286	C-1 to C-6
IN 800H	C-7 to C-12
N-155	C-13 to C-18
19-9DL	C-19 to C-24
CRM-6D	C-25 to C-30
XF-818	C-31 to C-36

A-286 IN AIR - CASE 2B
 $\ln(\text{TRUPT}) = \ln(K) + n \ln(\text{STRESS}) - Q/RT, Q = 544$

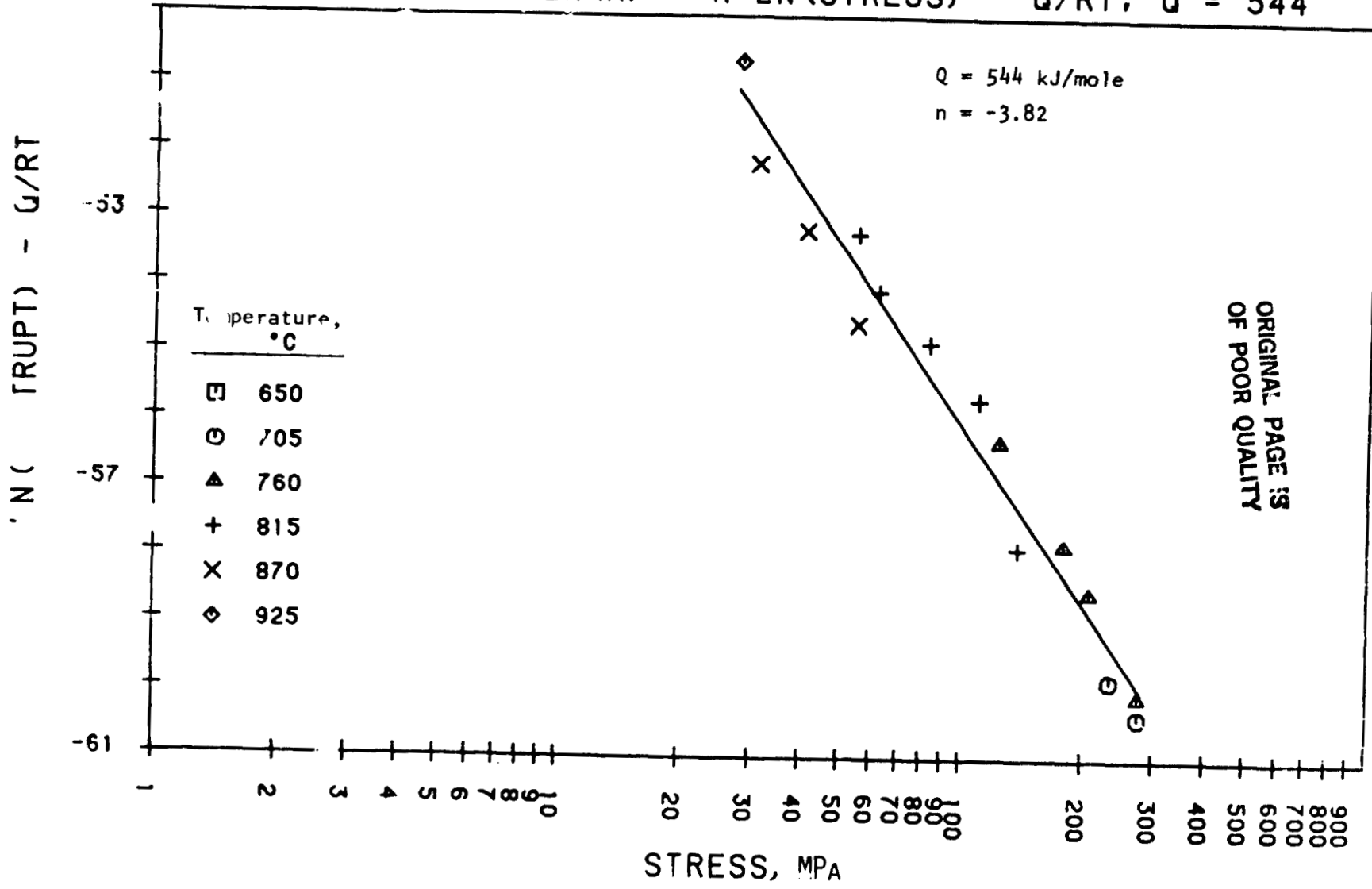


Figure C-1. Temperature-compensated rupture life vs. stress for A-286 tested in air (Case 2B).

ORIGINAL PAGE IS
OF POOR QUALITY

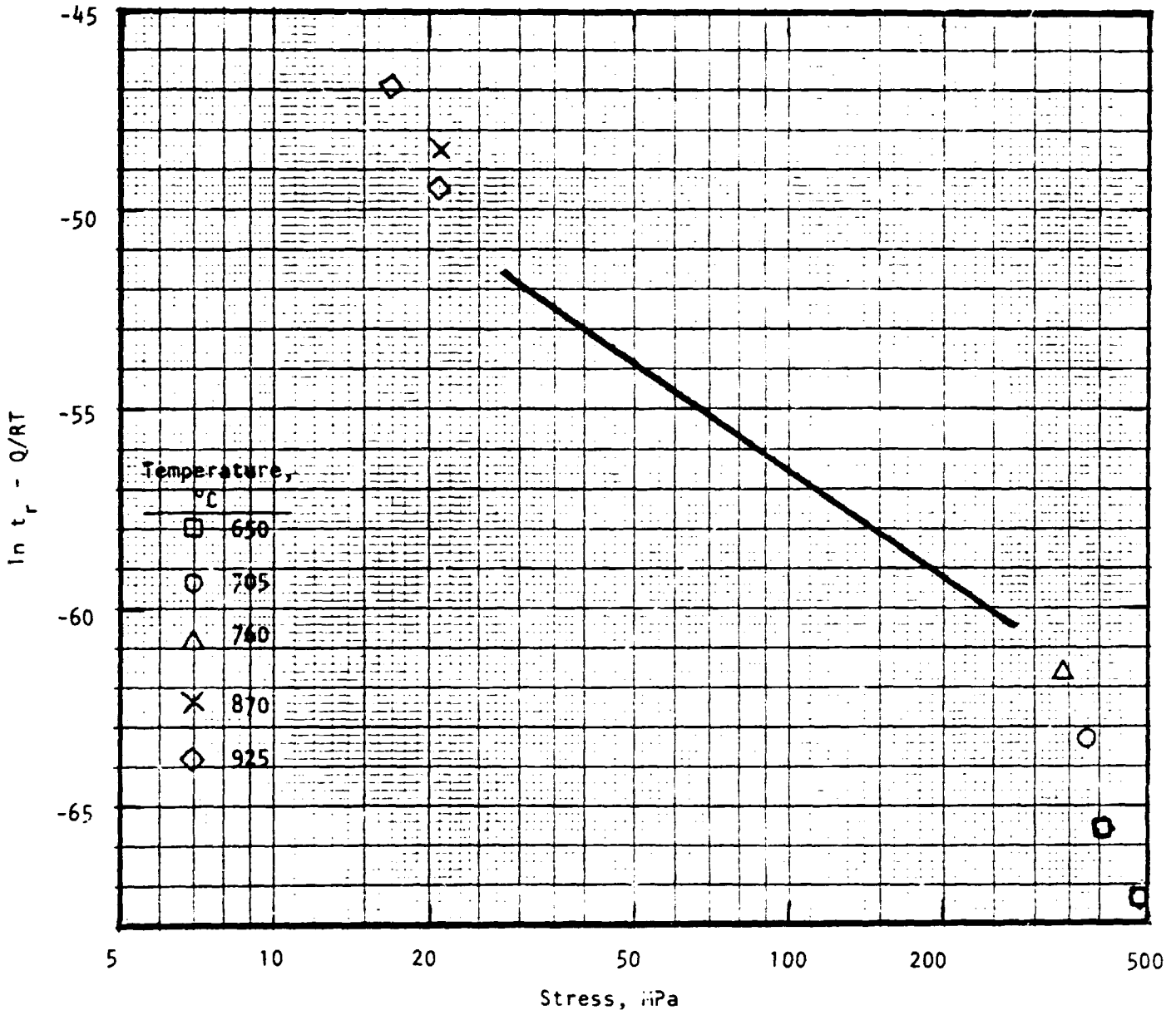


Figure C-2. Temperature-compensated rupture life vs. stress for A-286 tested in air (Case 2B, including Cases 2A and 2C data shown separately).

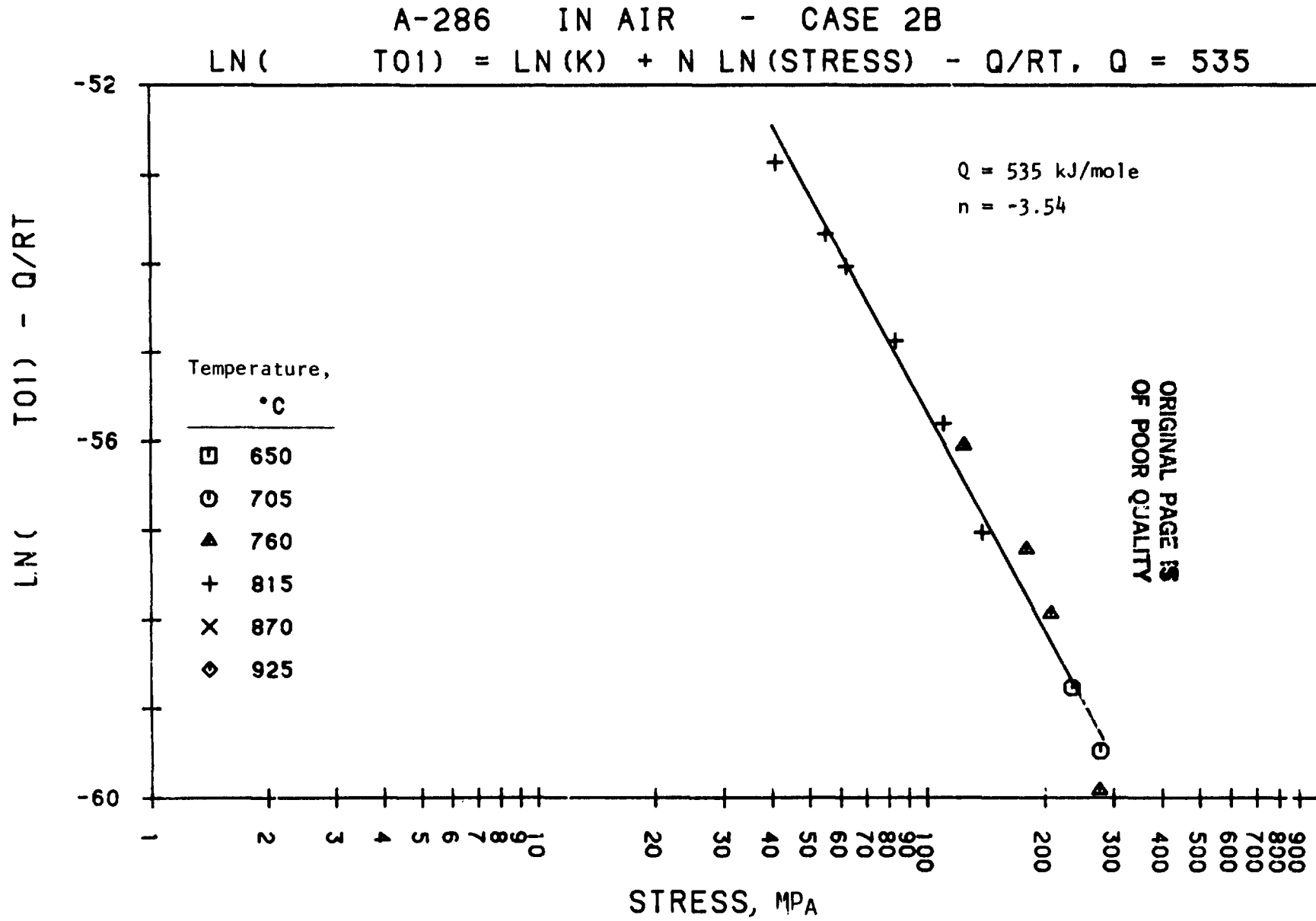


Figure C-3. Temperature-compensated time to 1% creep strain vs. stress for A-286 tested in air (Case 2B).

ORIGINAL PAGE IS
OF POOR QUALITY

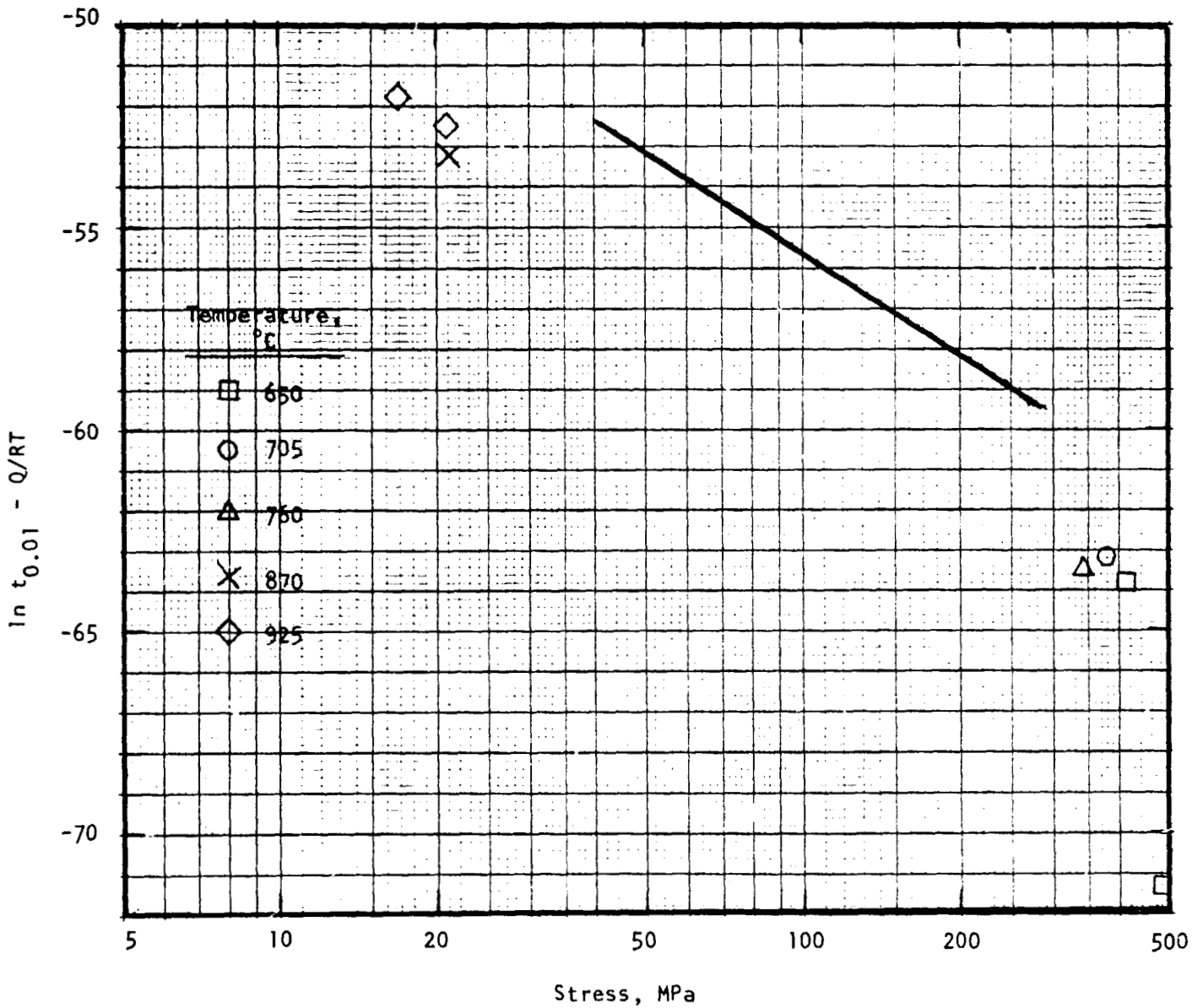


Figure C-4. Temperature-compensated time to 1% creep strain vs. stress for A-286 tested in air (Case 2B, including Cases 2A and 2C shown separately).

A-286 IN AIR - CASE 2B

$$\text{LN}(\text{CRPRAT}) = \text{LN}(K) + N \text{LN}(\text{STRESS}) + Q/RT, Q = 613$$

Q = 613 kJ/mole
n = 3.09

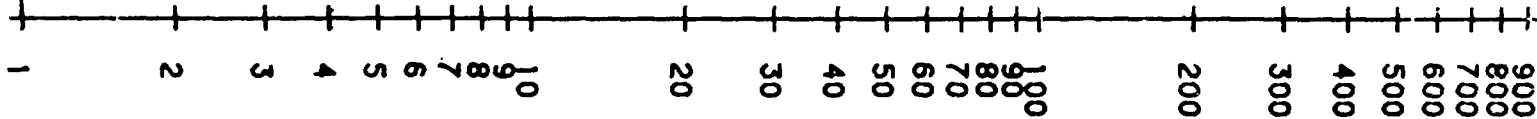
LN(CRPRAT) + Q/RT

51

Temperature,
°C

□	650
○	705
▲	760
+	815
X	870
◇	925

47



STRESS, MPa

Figure C-5. Temperature-compensated minimum creep rate vs. stress for A-286 tested in air (Case 2B).

ORIGINAL PAGE IS
OF POOR QUALITY

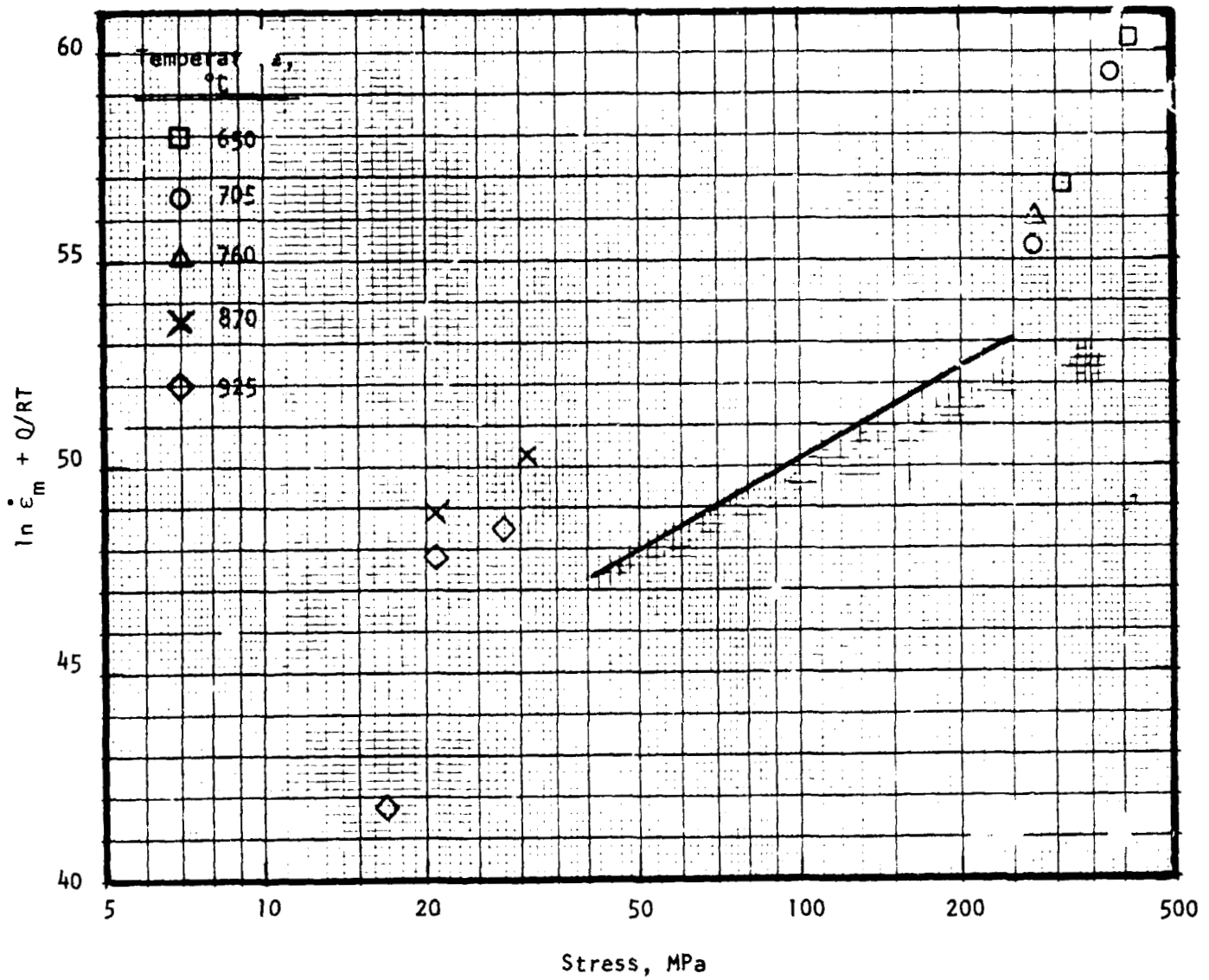


Figure C-6. Temperature-compensated minimum creep rate vs. stress for A-286 tested in air (Case 2B, including Cases 2A and 2C shown separately).

IN 800 IN AIR - CASE 2B
 $\ln(\text{TRUPT}) = \ln(K) + n \ln(\text{STRESS}) - Q/RT, Q = 406$

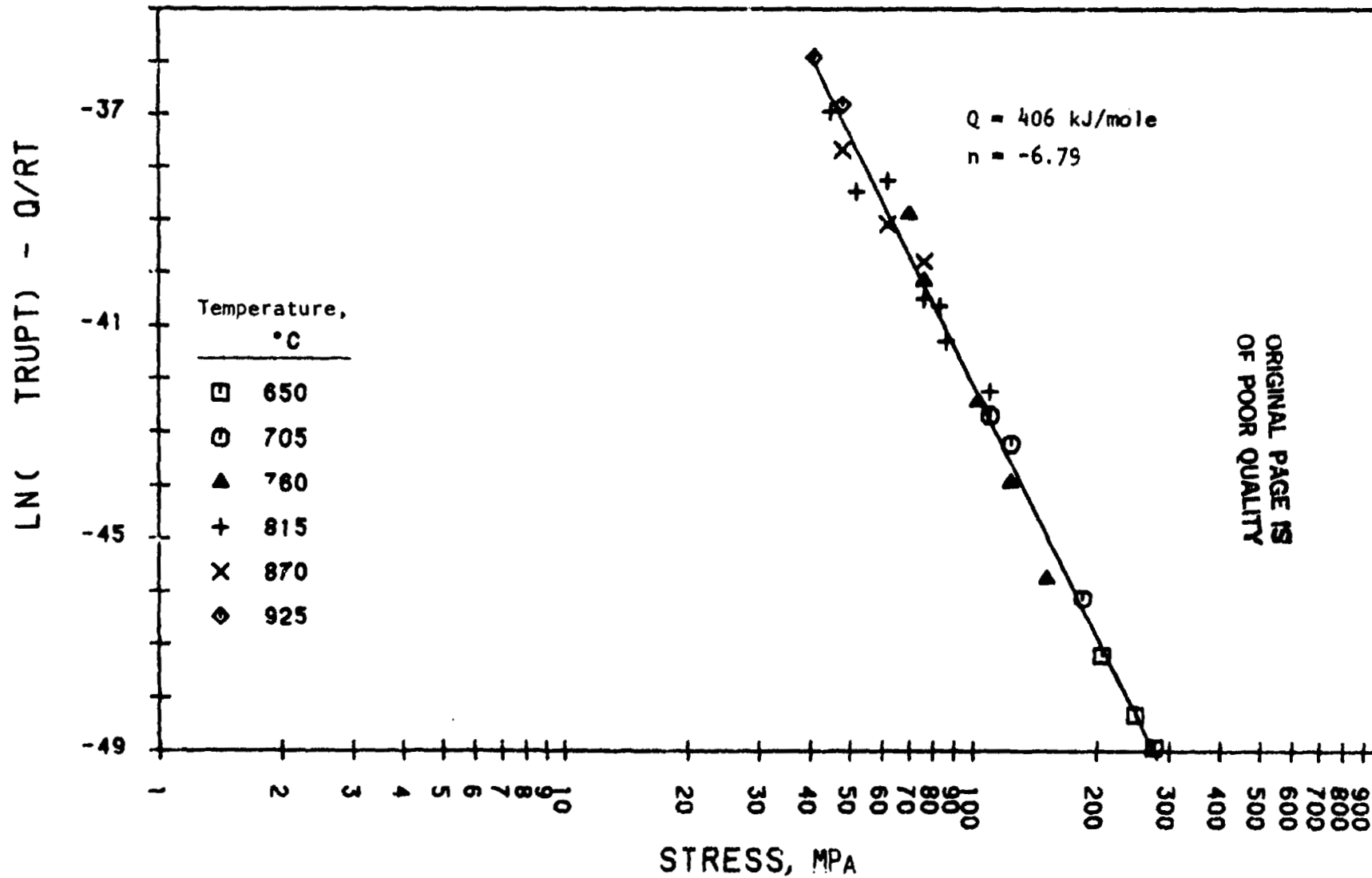


Figure C-7. Temperature-compensated rupture life vs. stress for IN 800H tested in air (Case 2B).

ORIGINAL PAGE IS
OF POOR QUALITY

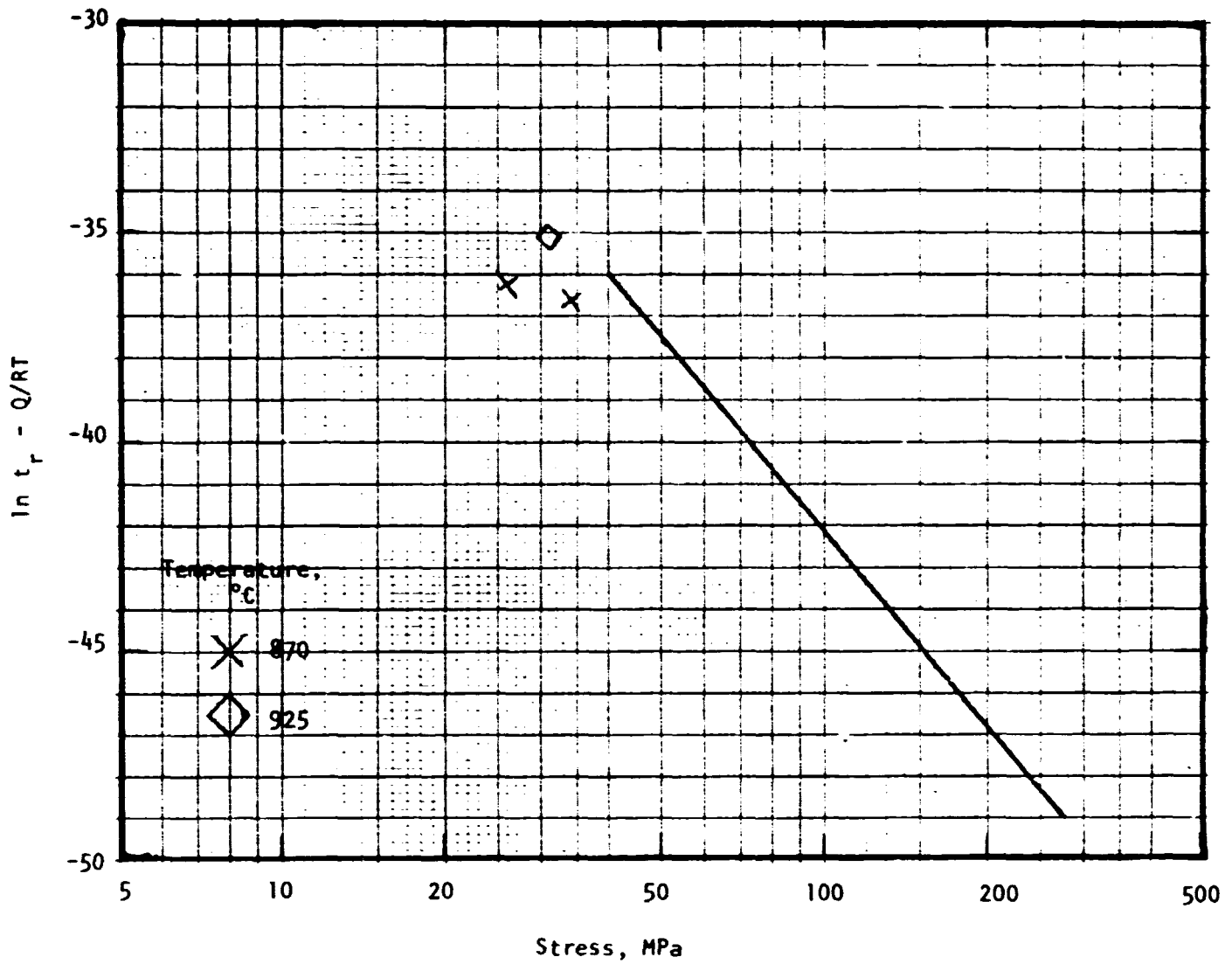


Figure C-8. Temperature-compensated rupture life vs. stress for IN 300H tested in air (Case 2B, including Cases 2A and 2C data shown separately).

IN 800 IN AIR - CASE 2B

$$\ln(T_01) = \ln(K) + n \ln(\text{STRESS}) - Q/RT, Q = 515$$

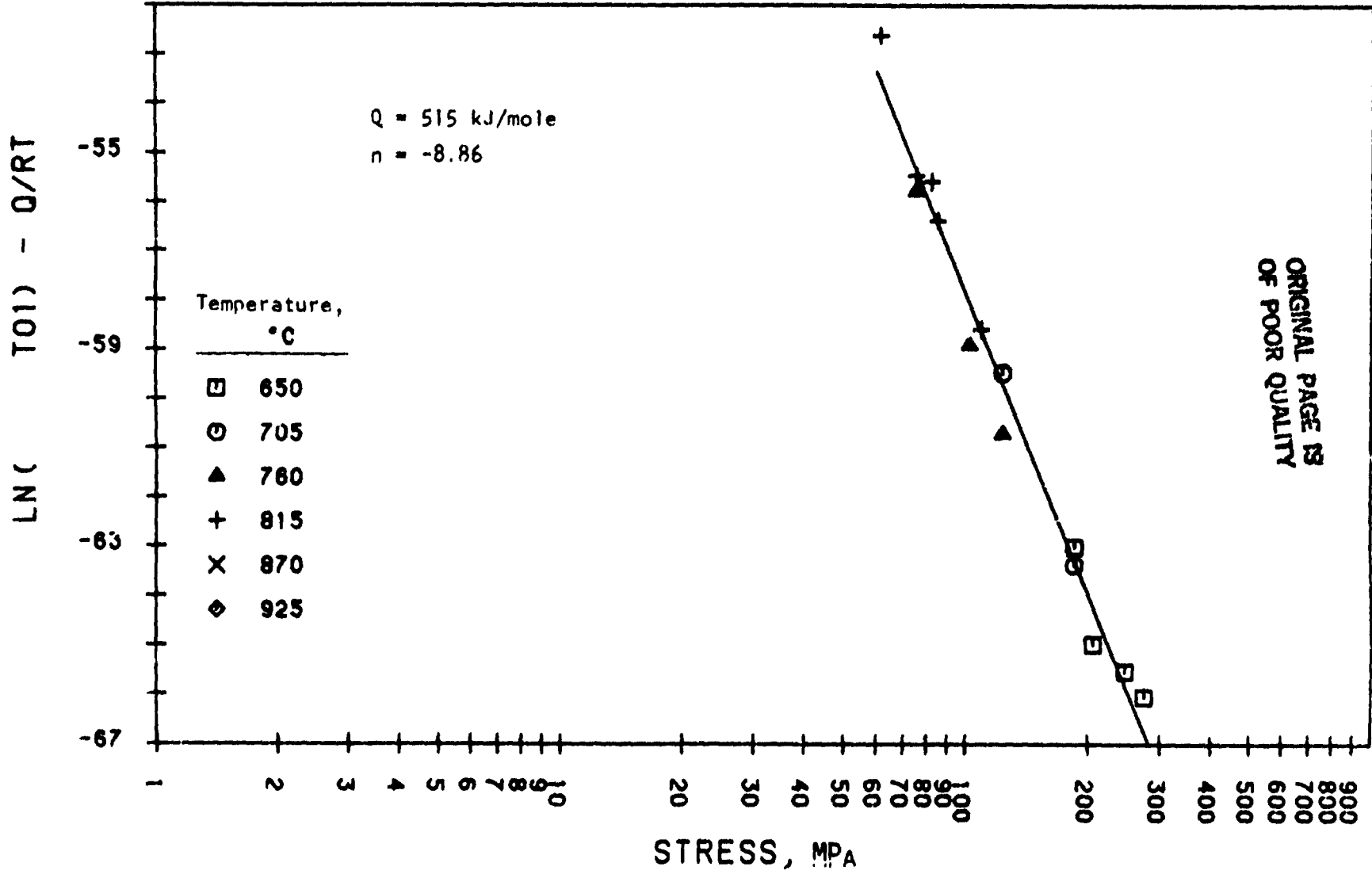


Figure C-9. Temperature-compensated time to 1% creep strain vs. stress for IN 800H tested in air (Case 2B).

ORIGINAL PAGE IS
OF POOR QUALITY

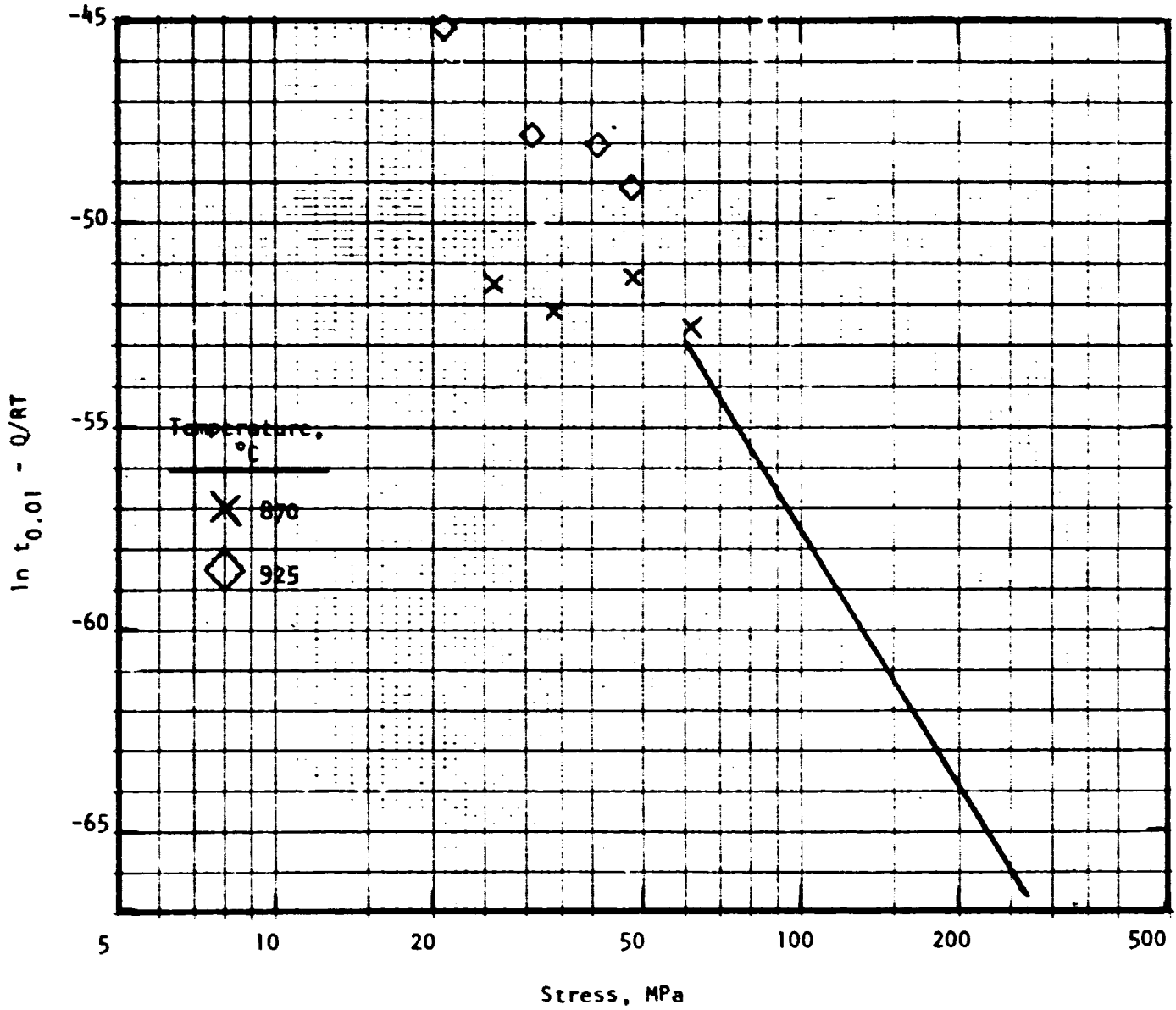


Figure C-10. Temperature-compensated time to 1% creep strain vs. stress for IN 800H tested in air (Case 2B, including Cases 2A and 2C shown separately).

IN 800 IN AIR - CASE 2B

$$\ln(\text{CRPRAT}) = \ln(K) + n \ln(\text{STRESS}) + Q/RT, \quad Q = 384$$

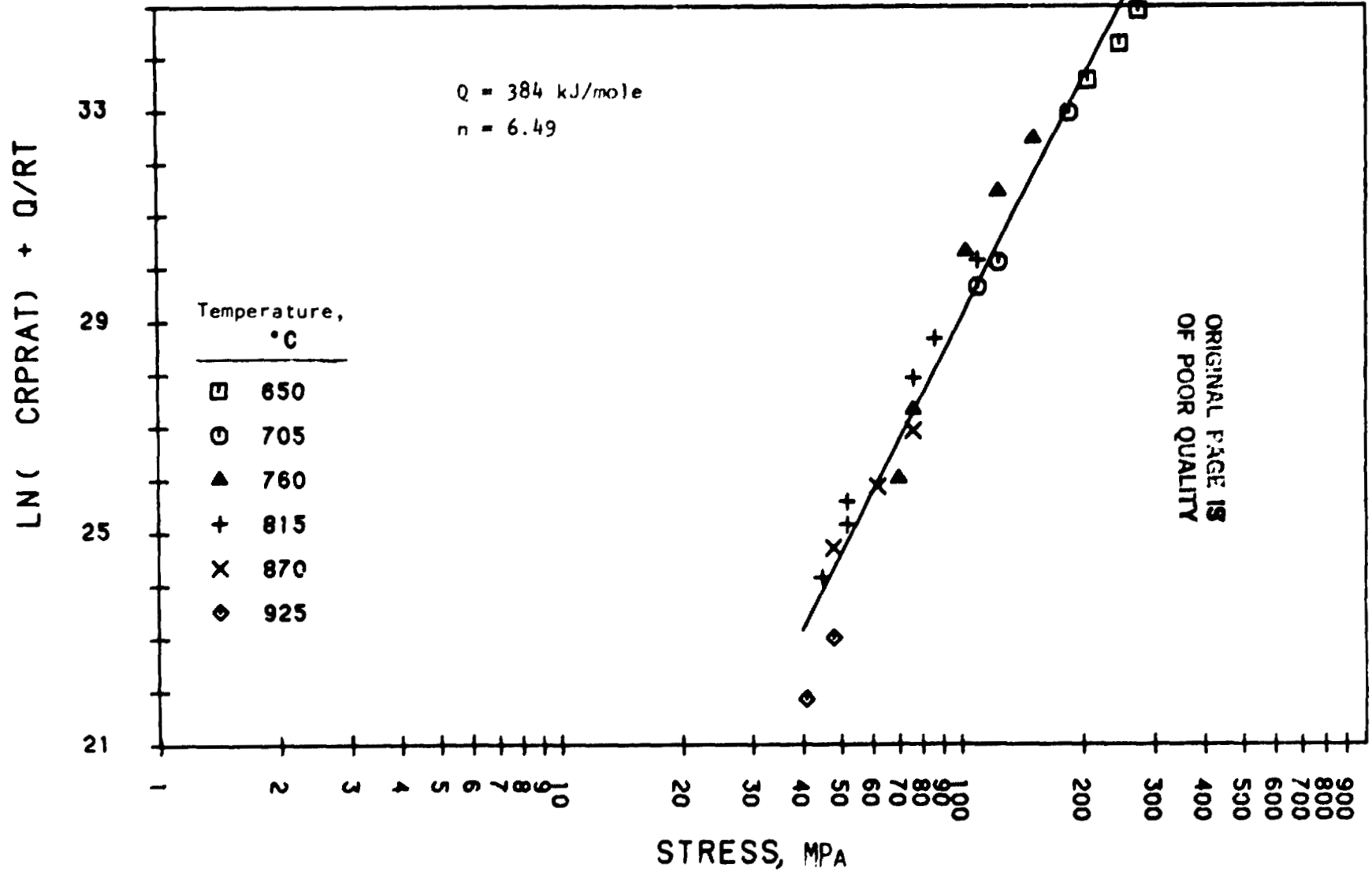


Figure C-11. Temperature-compensated minimum creep rate vs. stress for IN 800H tested in air (Case 2B).

ORIGINAL PAGE IS
OF POOR QUALITY

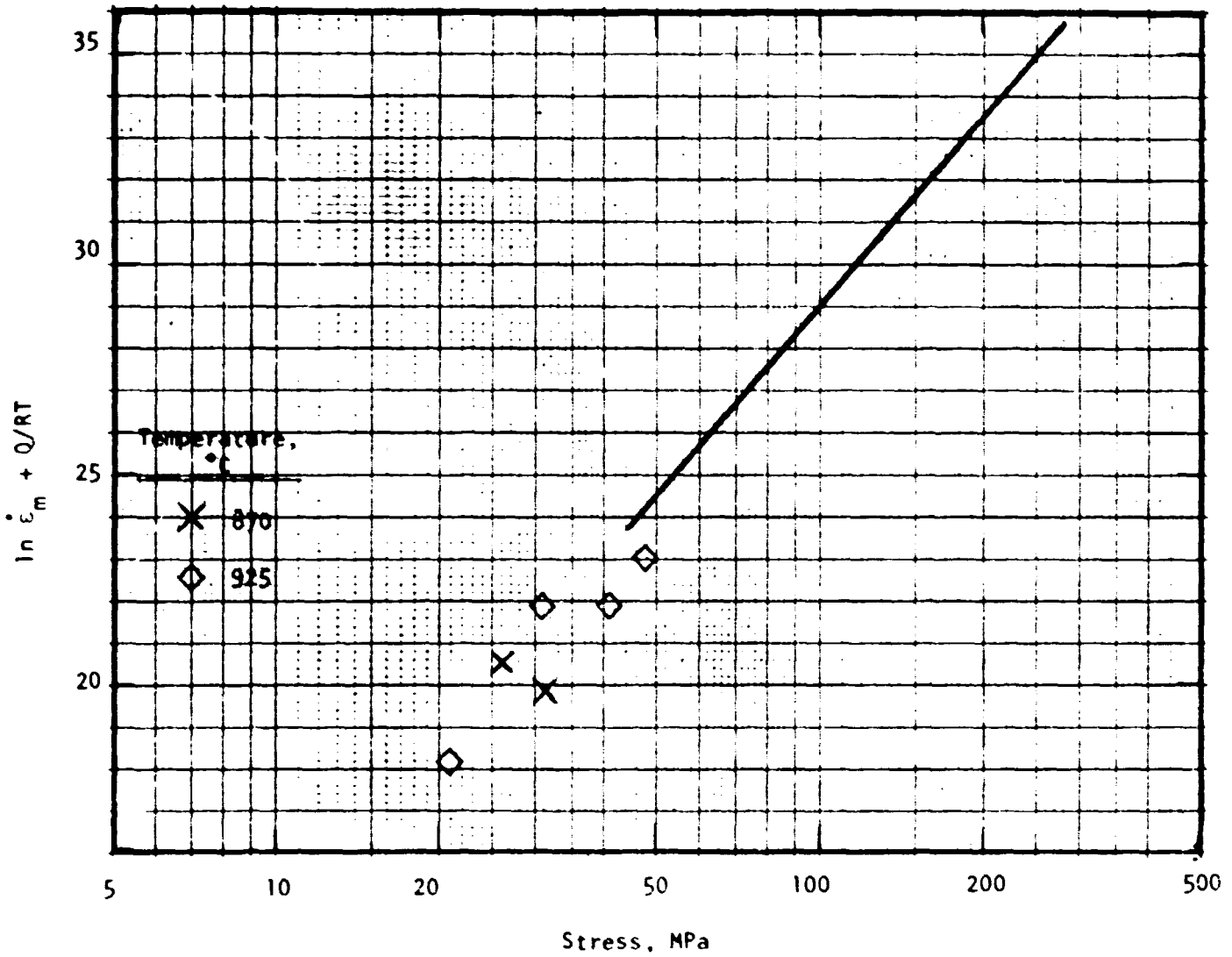


Figure C-12. Temperature-compensated minimum creep rate vs. stress for IN 800H tested in air (Case 2B, including Cases 2A and 2C shown separately).

N-155 IN AIR - CASE 2B
 $\text{LN}(\text{TRUPT}) = \text{LN}(K) + N \text{LN}(\text{STRESS}) - Q/RT, Q = 435$

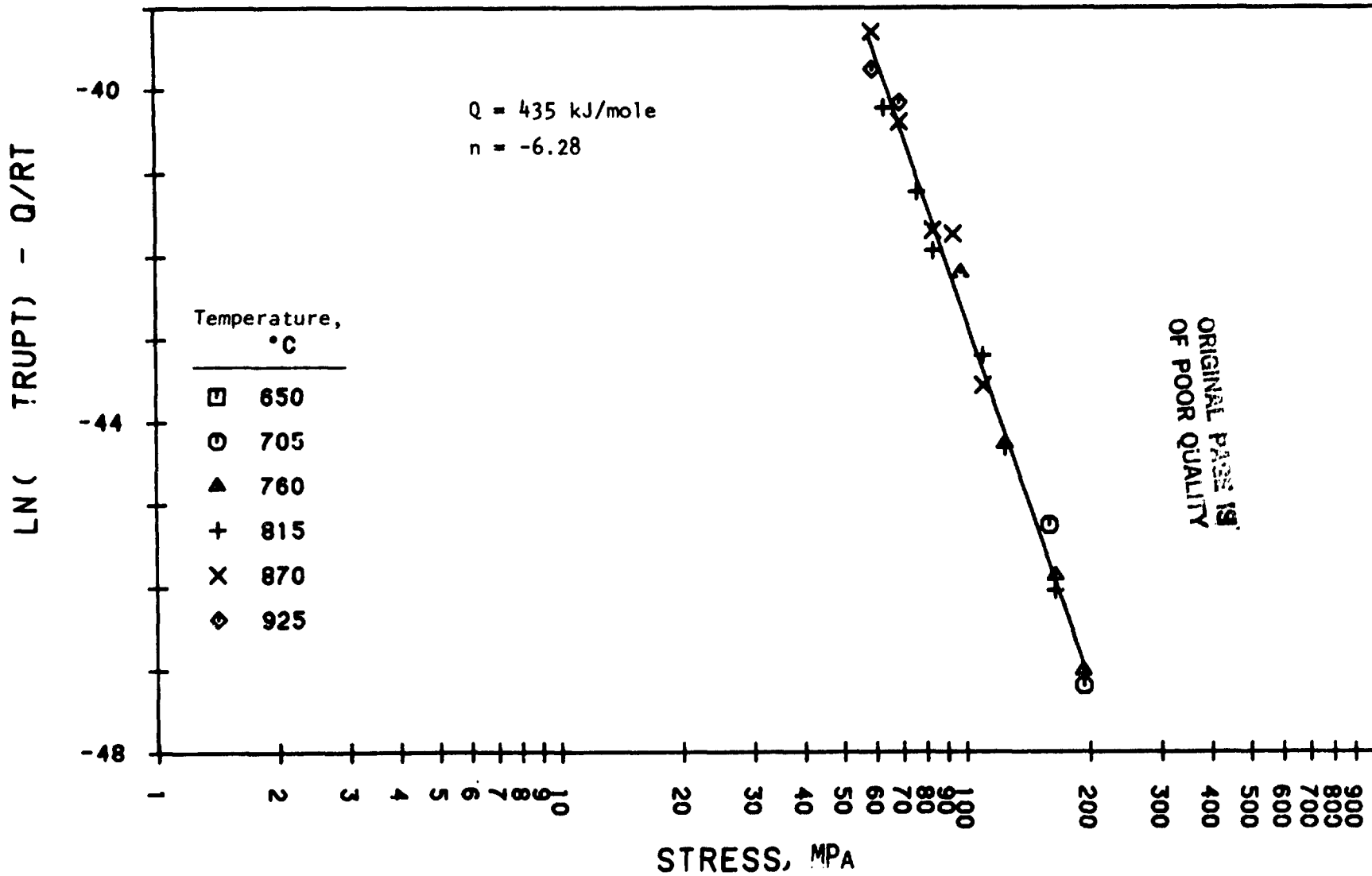


Figure C-13. Temperature-compensated rupture life vs. stress for N-155 tested in air (Case 2B).

ORIGINAL PAGE IS
OF POOR QUALITY

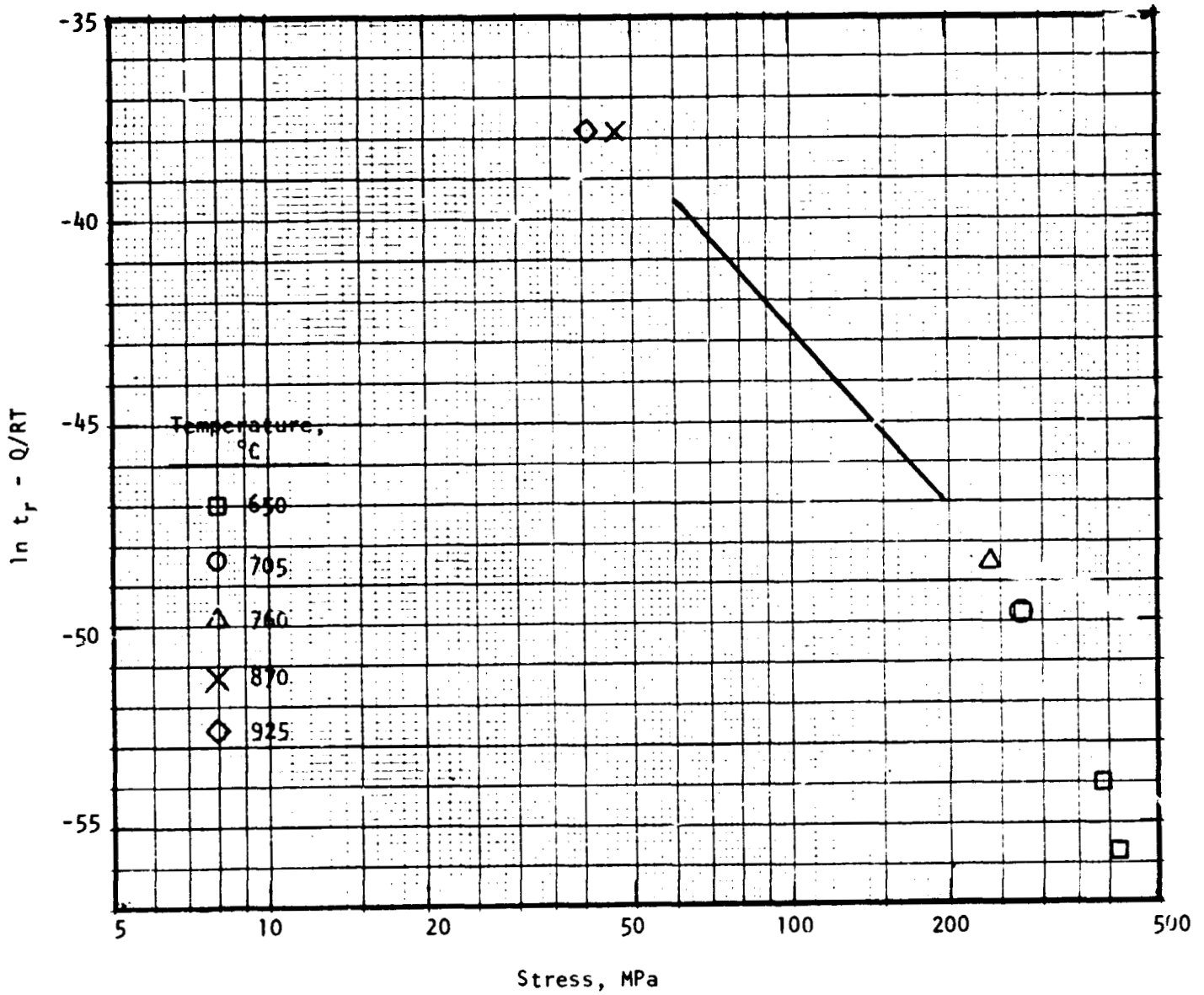


Figure C-14. Temperature-compensated rupture life vs. stress for N-155 tested in air (Case 2B, including Cases 2A and 2C data shown separately).

N-155 IN AIR - CASE 2B

$LN(T01) = LN(K) + N LN(STRESS) - Q/RT, Q = 467$

Q = 467 kJ/mole
n = -7.04

Temperature, °C	
□	650
○	705
▲	760
+	815
X	870
◇	925

ORIGINAL PAGE IS
OF POOR QUALITY

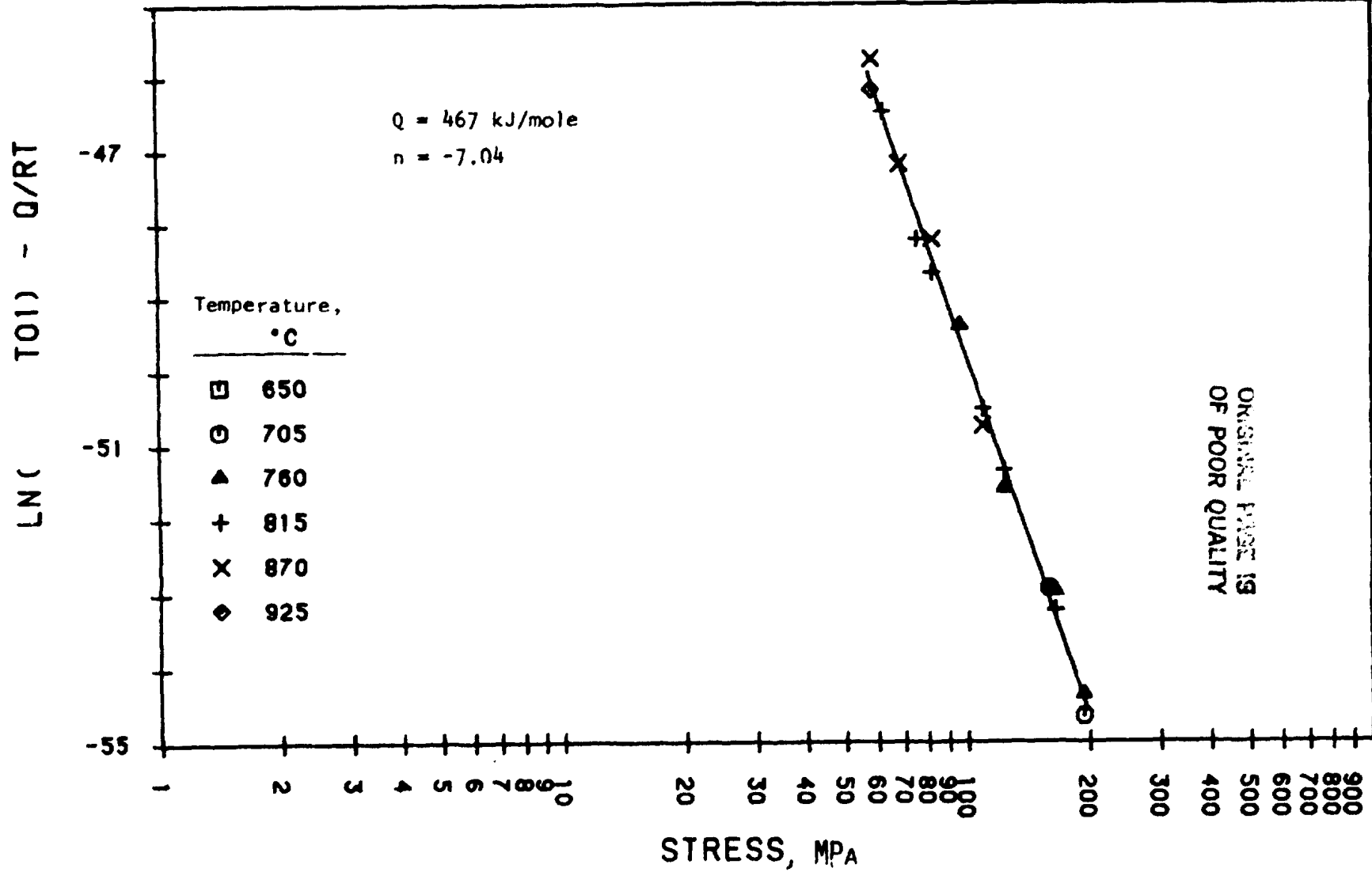


Figure C-15. Temperature-compensated time to 1% creep strain vs. stress for N-155 tested in air (Case 2B).

ORIGINAL PAGE IS
OF POOR QUALITY

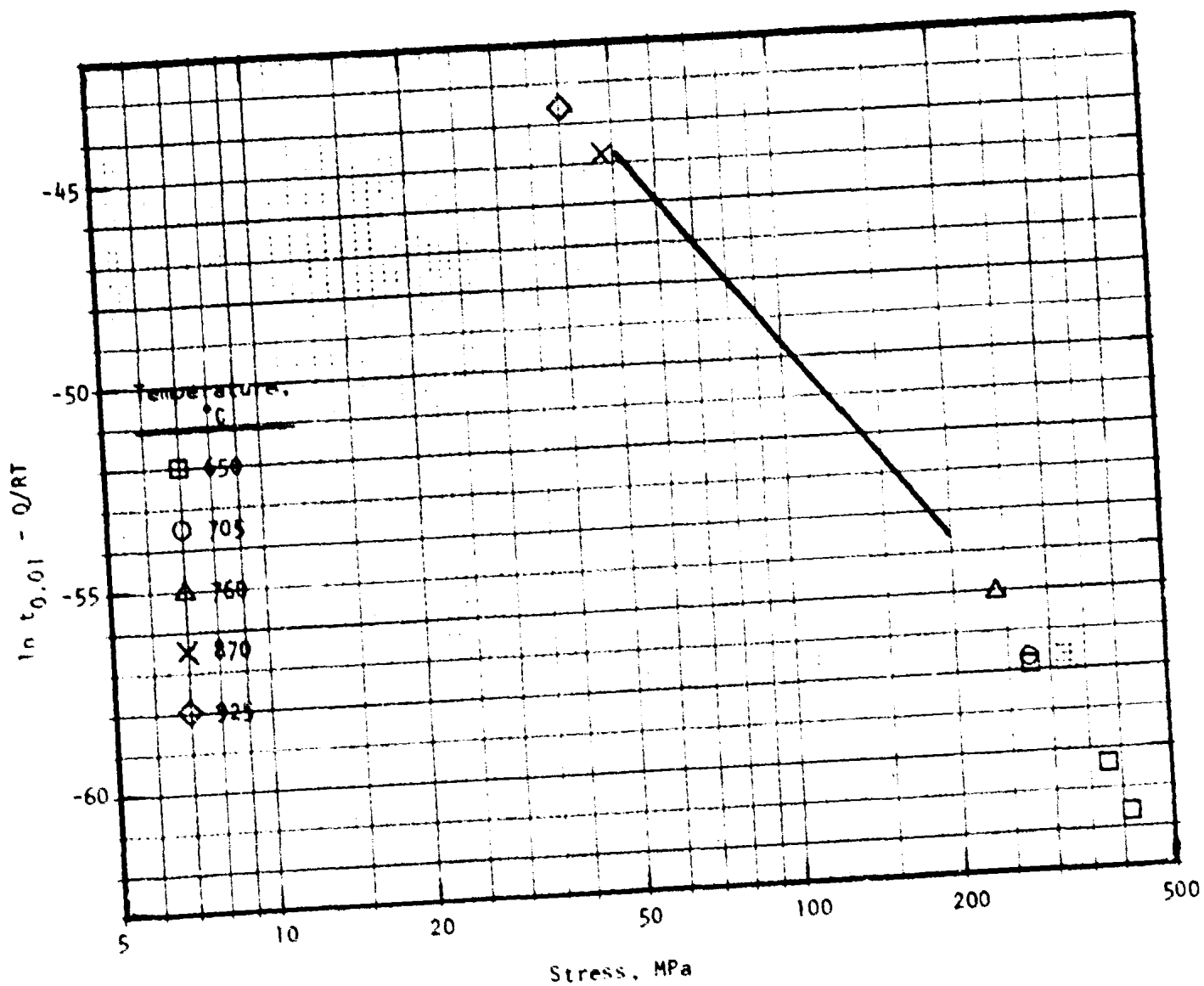


Figure C-16. Temperature-compensated time to 1% creep strain vs. stress for N-155 tested in air (case 2B, including cases 2A and 2C shown separately).

N-155 IN AIR - CASE 2B

$$\text{LN}(\text{CRPRAT}) = \text{LN}(K) + N \text{LN}(\text{STRESS}) + Q/RT, Q = 527$$

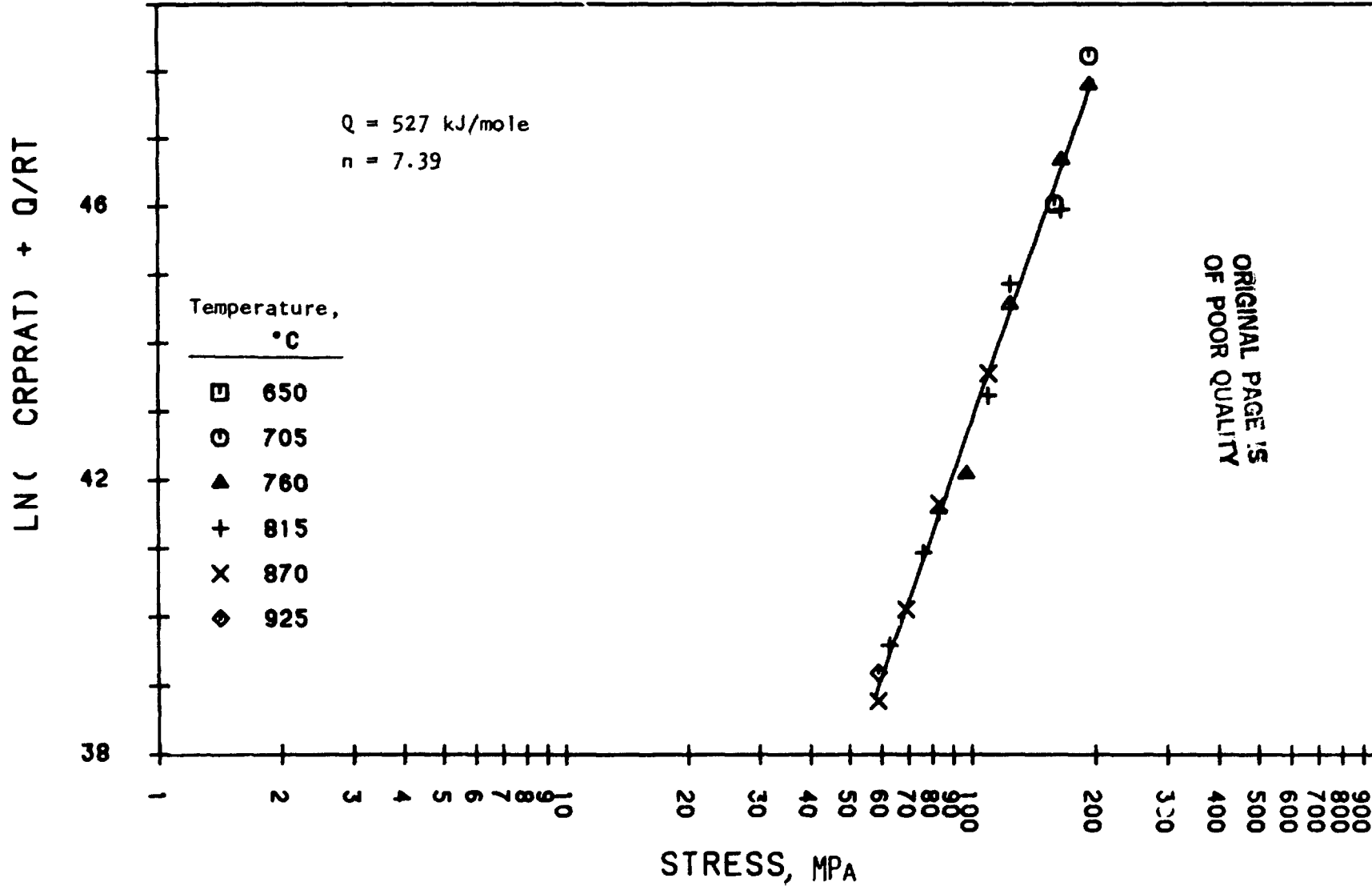


Figure C-17. Temperature-compensated minimum creep rate vs. stress for N-155 tested in air (Case 2B).

ORIGINAL PAGE IS
OF POOR QUALITY

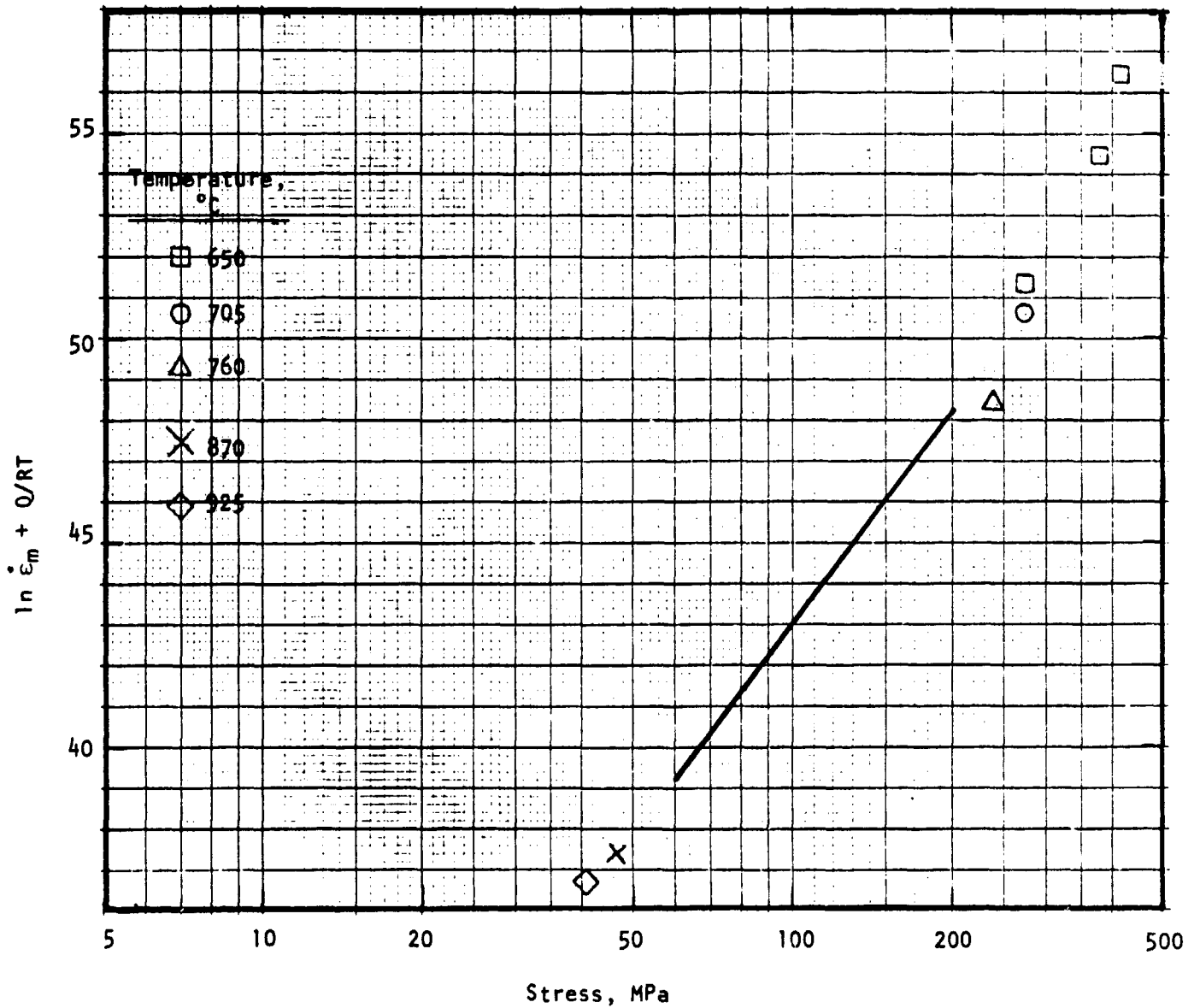


Figure C-18. Temperature-compensated minimum creep rate vs. stress for N-155 tested in air (Case 2B, including Cases 2A and 2C shown separately).

19-9DL IN AIR - CASE 2B
 $\ln(\text{TRUPT}) = \ln(K) + n \ln(\text{STRESS}) - Q/RT, Q = 461$

104

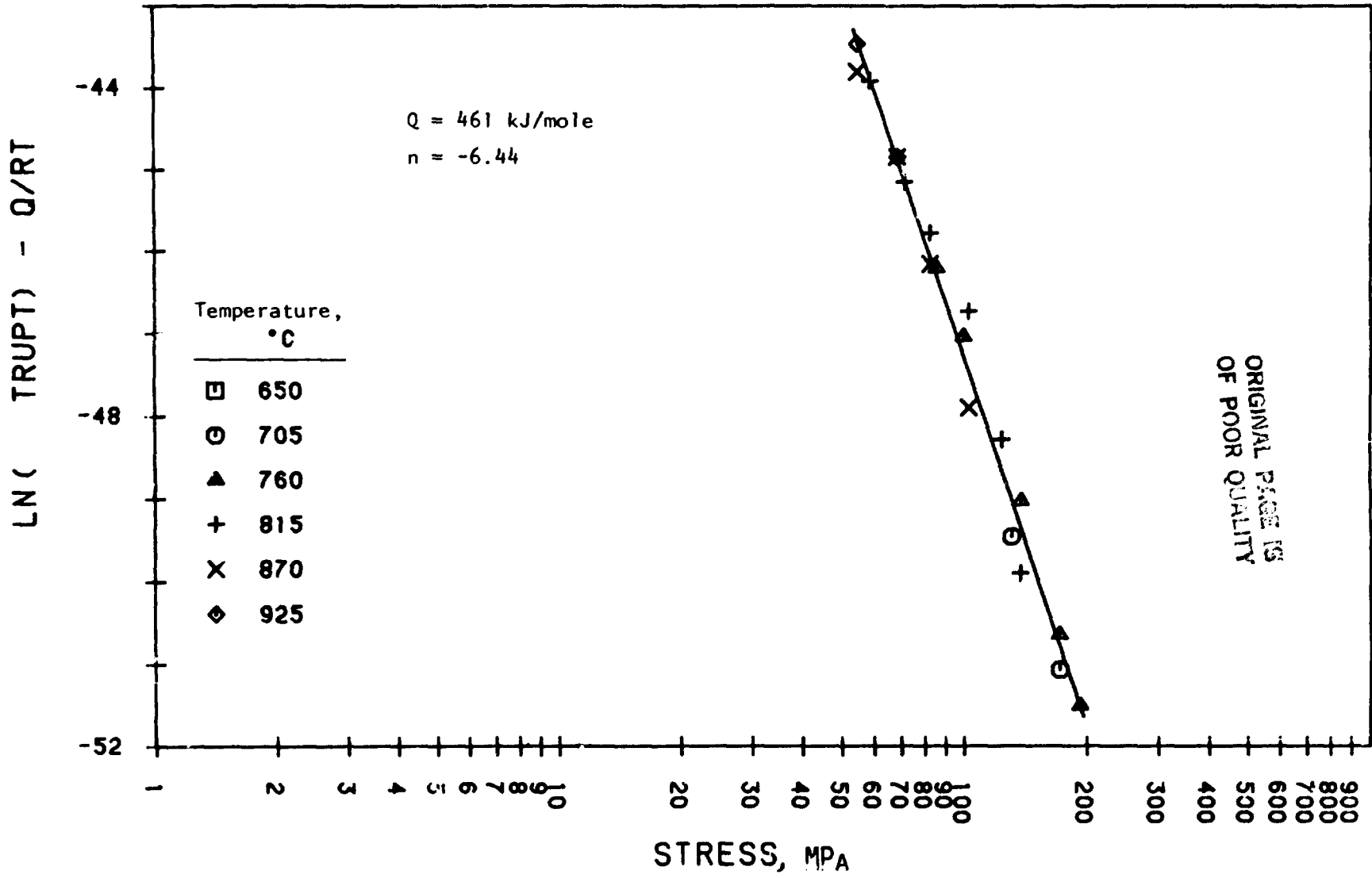


Figure C-19. Temperature-compensated rupture life vs. strain for 19-9DL tested in air (Case 2B).

ORIGINAL PAGE IS
OF POOR QUALITY

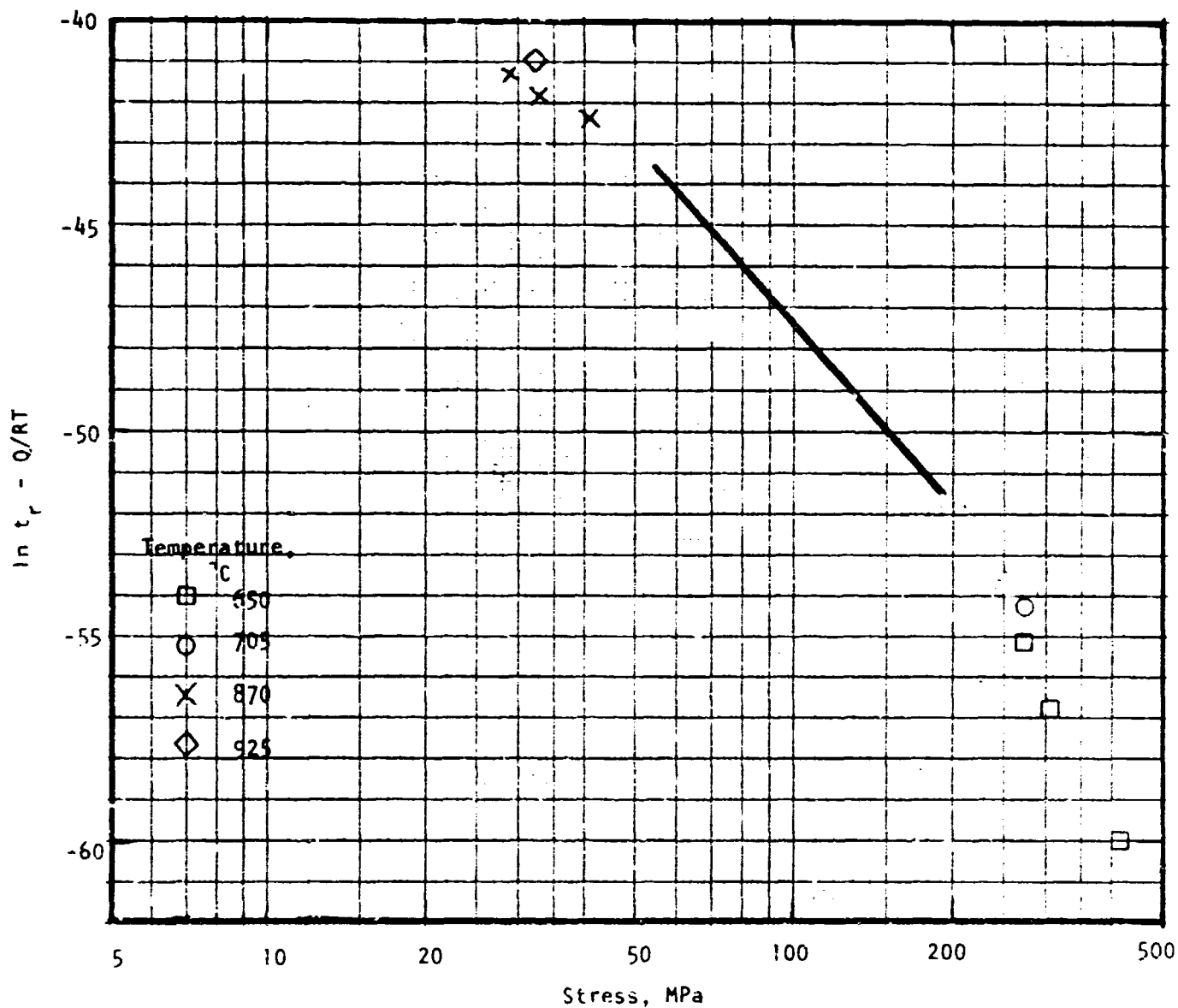


Figure C-20. Temperature-compensated rupture life vs. stress for 19-9DL tested in air (Case 2B, including Cases 2A and 2C data shown separately).

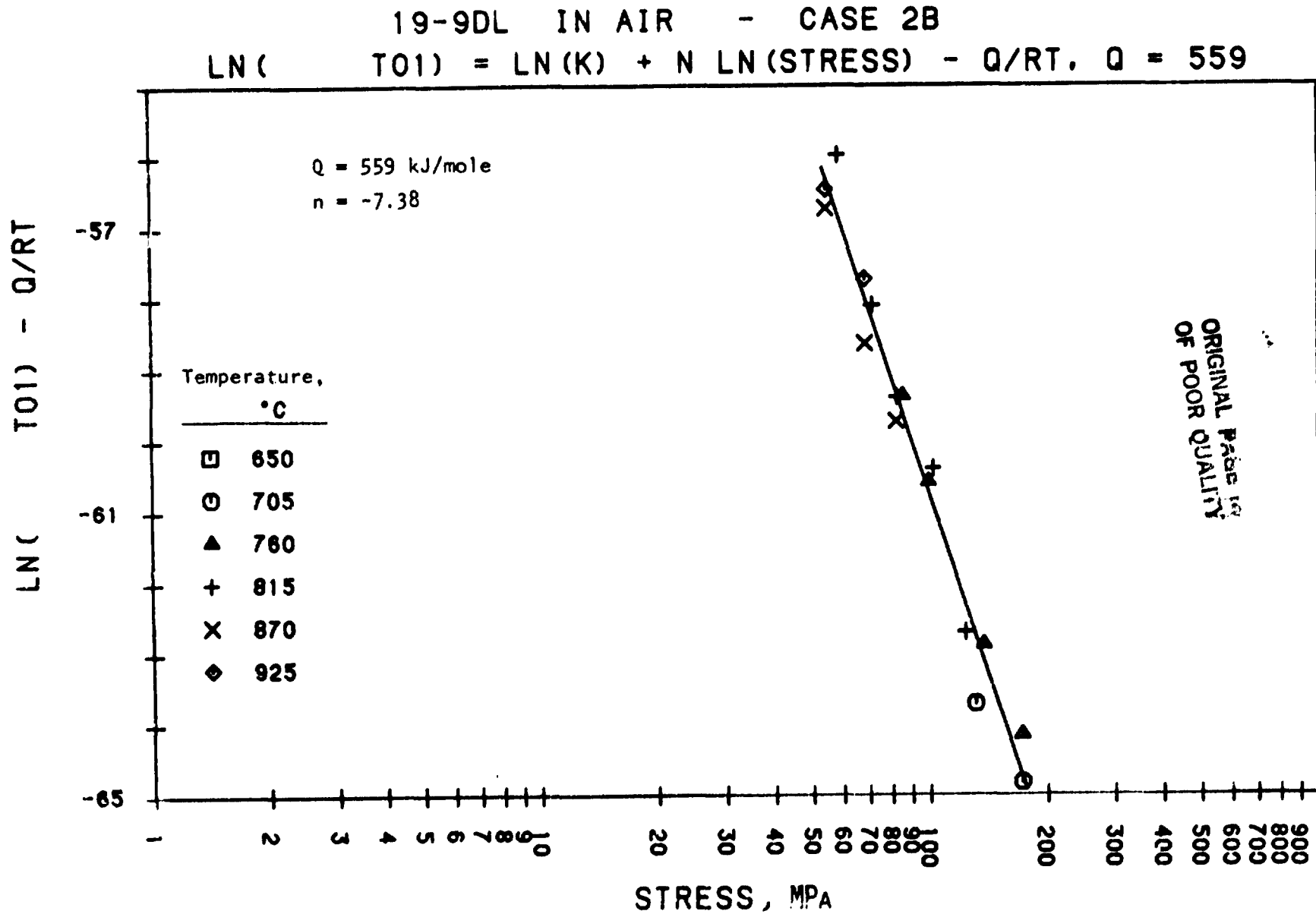


Figure C-21. Temperature-compensated time to 1% creep strain vs. stress for 19-9DL tested in air (Case 2B).

ORIGINAL PAGE IS
OF POOR QUALITY

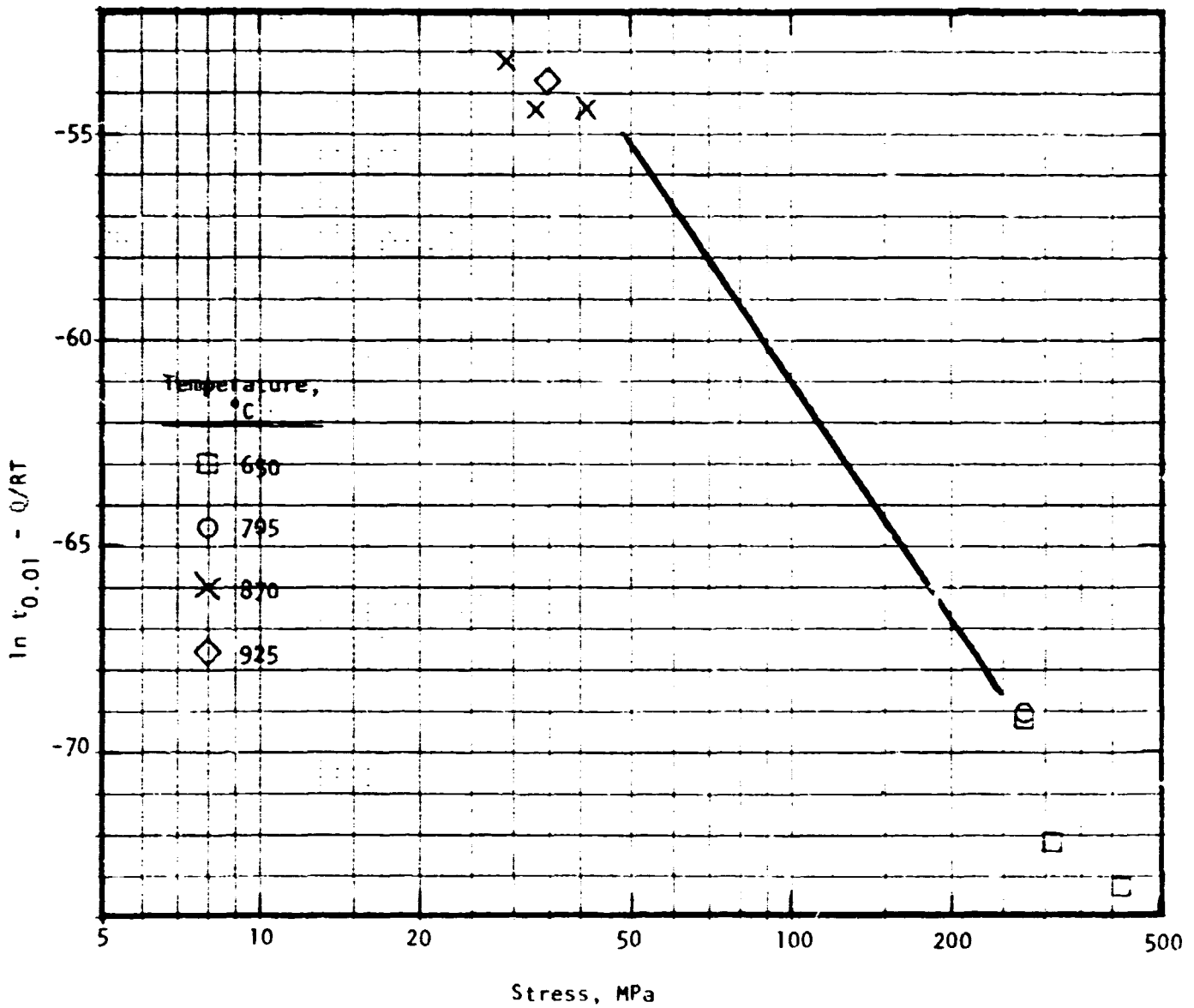


Figure C-22. Temperature-compensated time to 1% creep strain vs. stress for 18-90L tested in air (Case 2B, including Cases 2A and 2C shown separately).

19-9DL IN AIR - CASE 2B

$$\text{LN}(\text{CRPRAT}) = \text{LN}(K) + N \text{LN}(\text{STRESS}) + Q/RT, \quad Q = 573$$

108

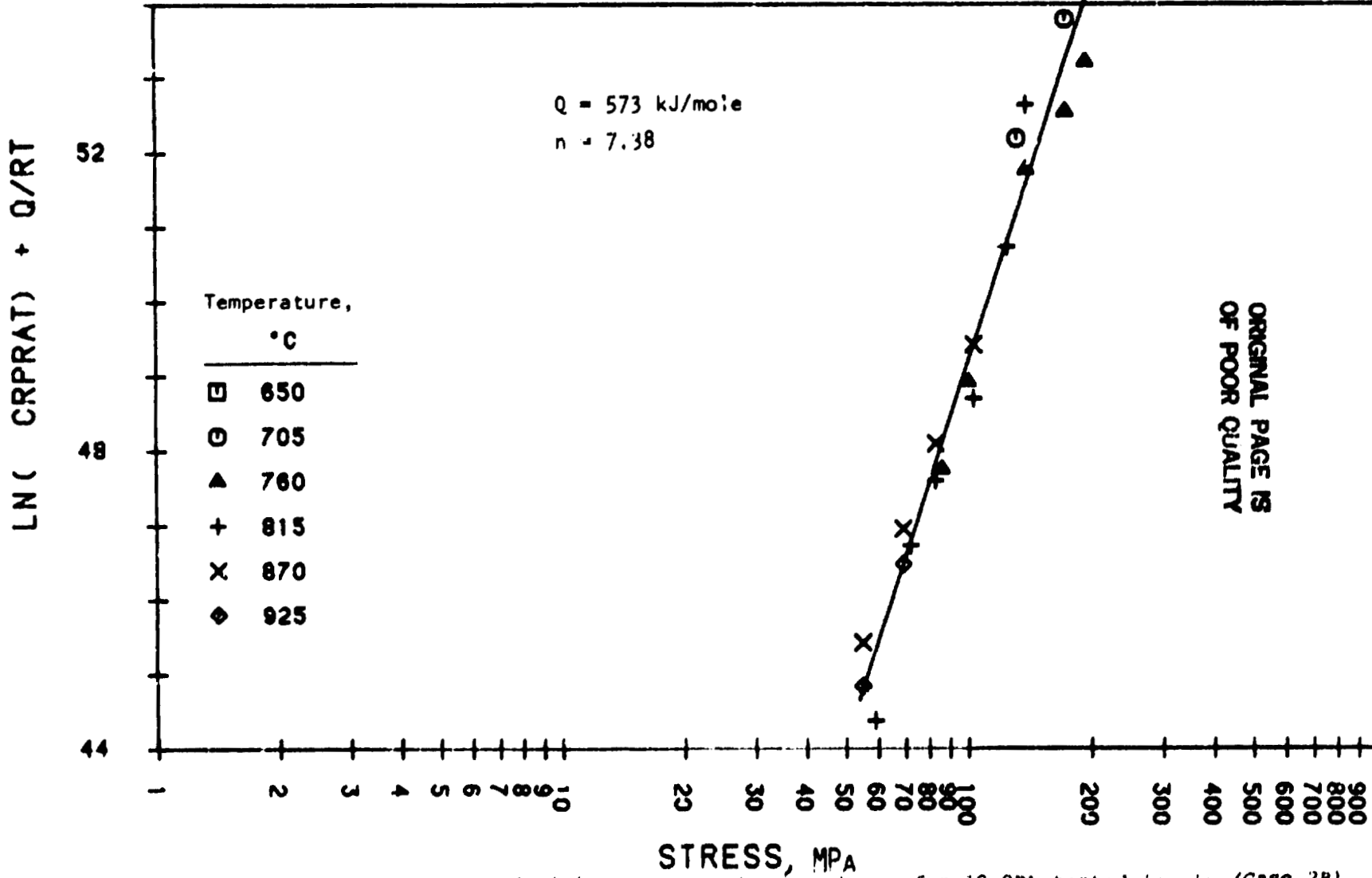


Figure C-23. Temperature-compensated minimum creep rate vs. stress for 19-9DL tested in air (Case 2B).

ORIGINAL PAGE IS
OF POOR QUALITY

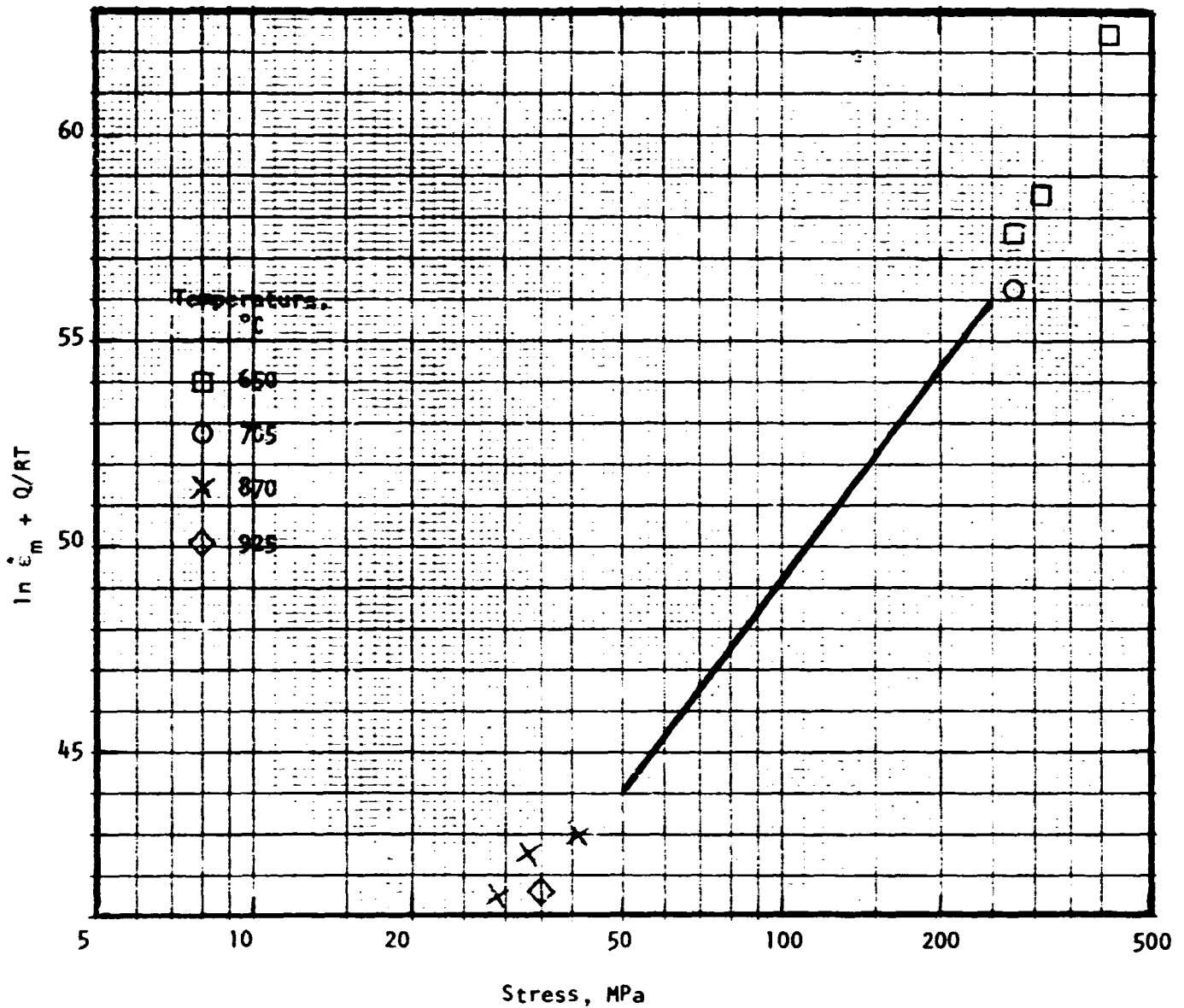


Figure C-24. Temperature-compensated minimum creep rate vs. stress for 19-9DL tested in air (Case 2B, including Cases 2A and 2C shown separately).

CRM-6D IN AIR - CASE 2B

$$\text{LN}(\text{TRUPT}) = \text{LN}(K) + N \text{LN}(\text{STRESS}) - Q/RT, Q = 461$$

Q = 461 kJ/mole
n = -9.12

LN(TRUPT) - Q/RT

Temperature, °C	
□	650
○	705
▲	760
+	815
X	870
◇	925

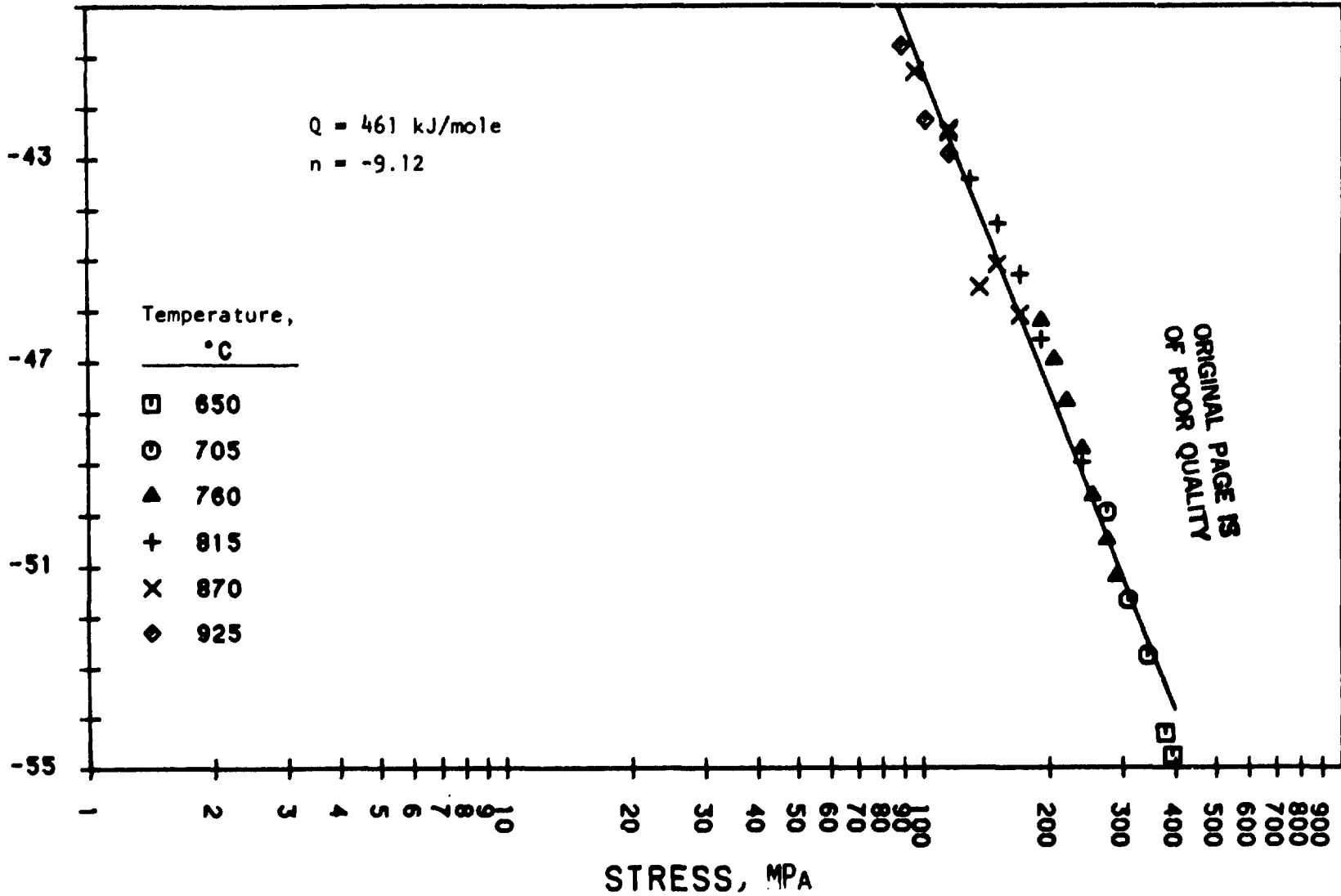


Figure C-25. Temperature-compensated rupture life vs. stress for CRM-6D tested in air (Case 2B).

ORIGINAL PAGE IS
OF POOR QUALITY

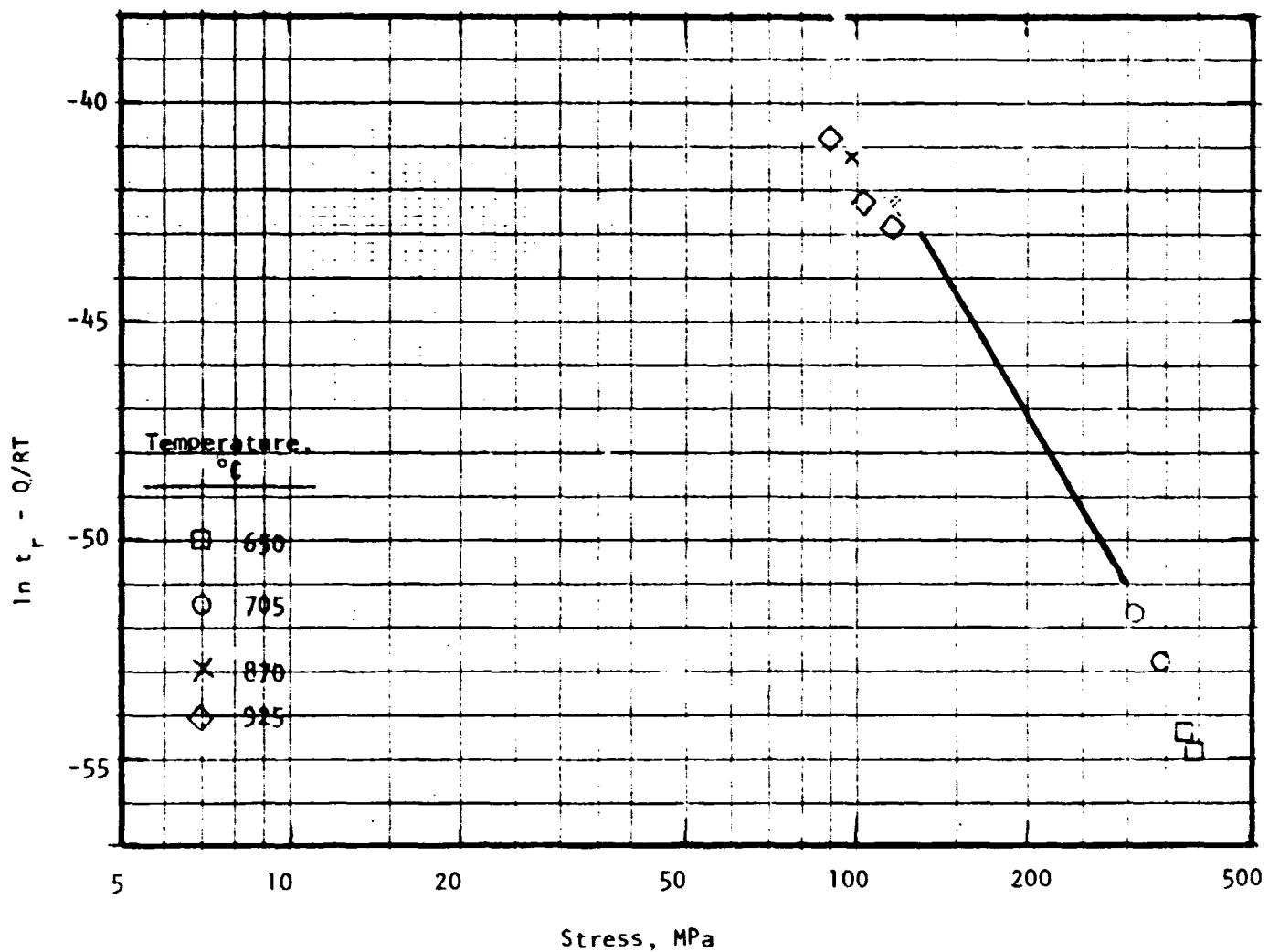
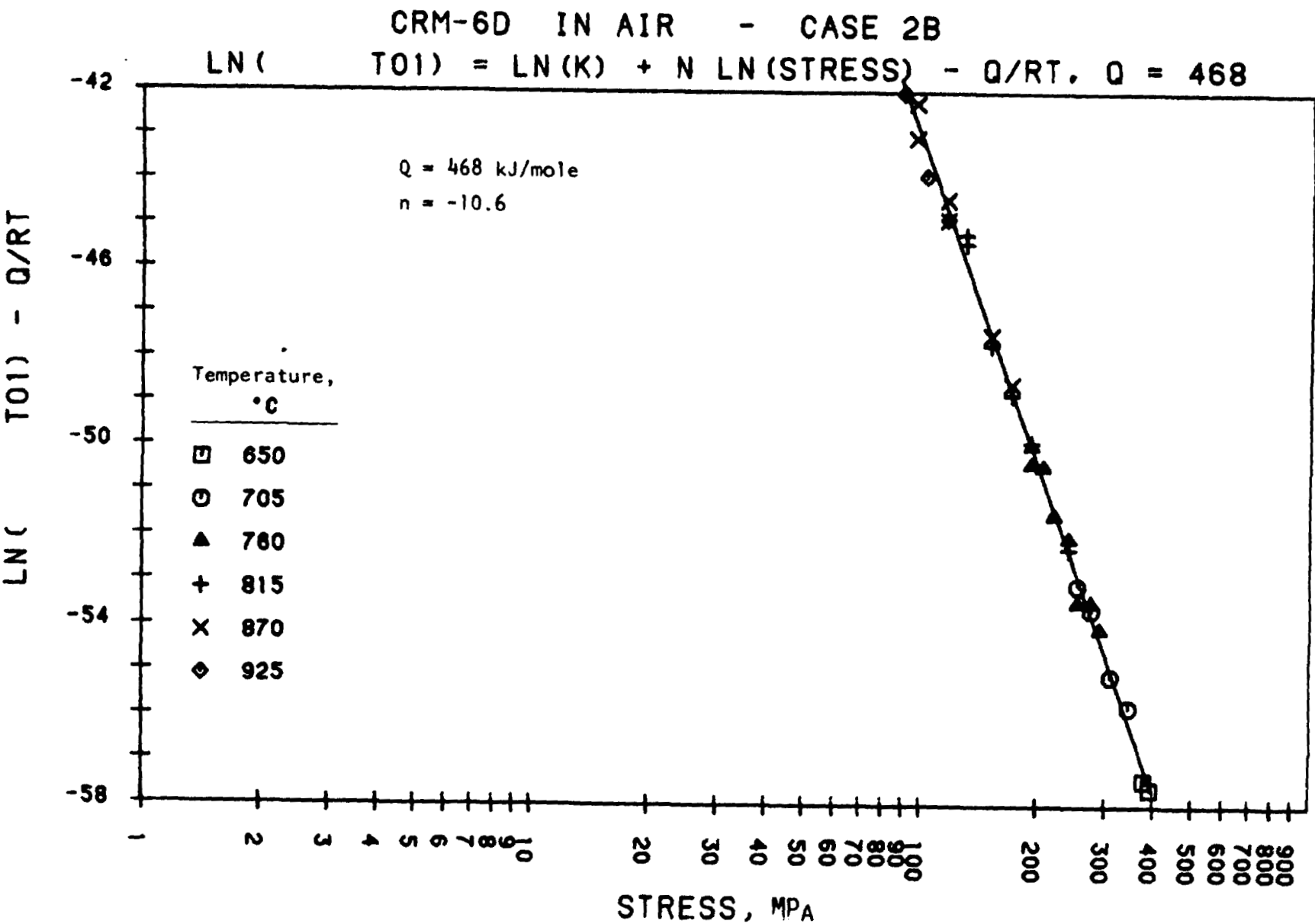


Figure C-26. Temperature-compensated rupture life vs. stress for CRM-6D tested in air (Case 2B, including Cases 2A and 2C data shown separately).



ORIGINAL PAGE IS
OF POOR QUALITY

Figure C-27. Temperature-compensated time to 1% creep strain vs. stress for CRM-6D tested in air (Case 2B).

ORIGINAL PAGE 19
OF POOR QUALITY

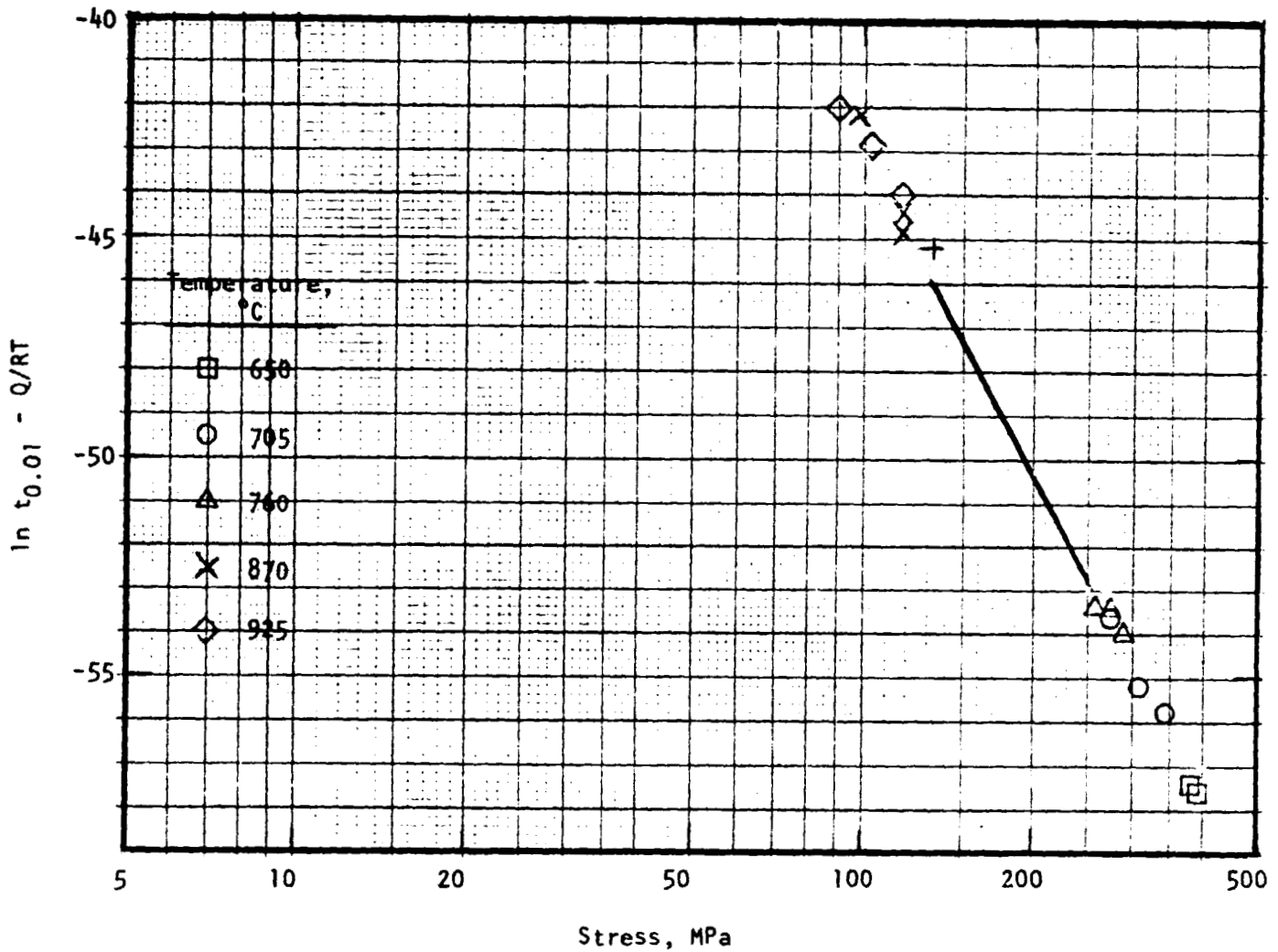


Figure C-28. Temperature-compensated time to 1% creep strain vs. stress for CRM-6D tested in air (Case 2B, including Cases 2A and 2C shown separately).

CRM-6D IN AIR - CASE 2B

$$\ln(\text{CRPRAT}) = \ln(K) + n \ln(\text{STRESS}) + Q/RT, \quad Q = 551$$

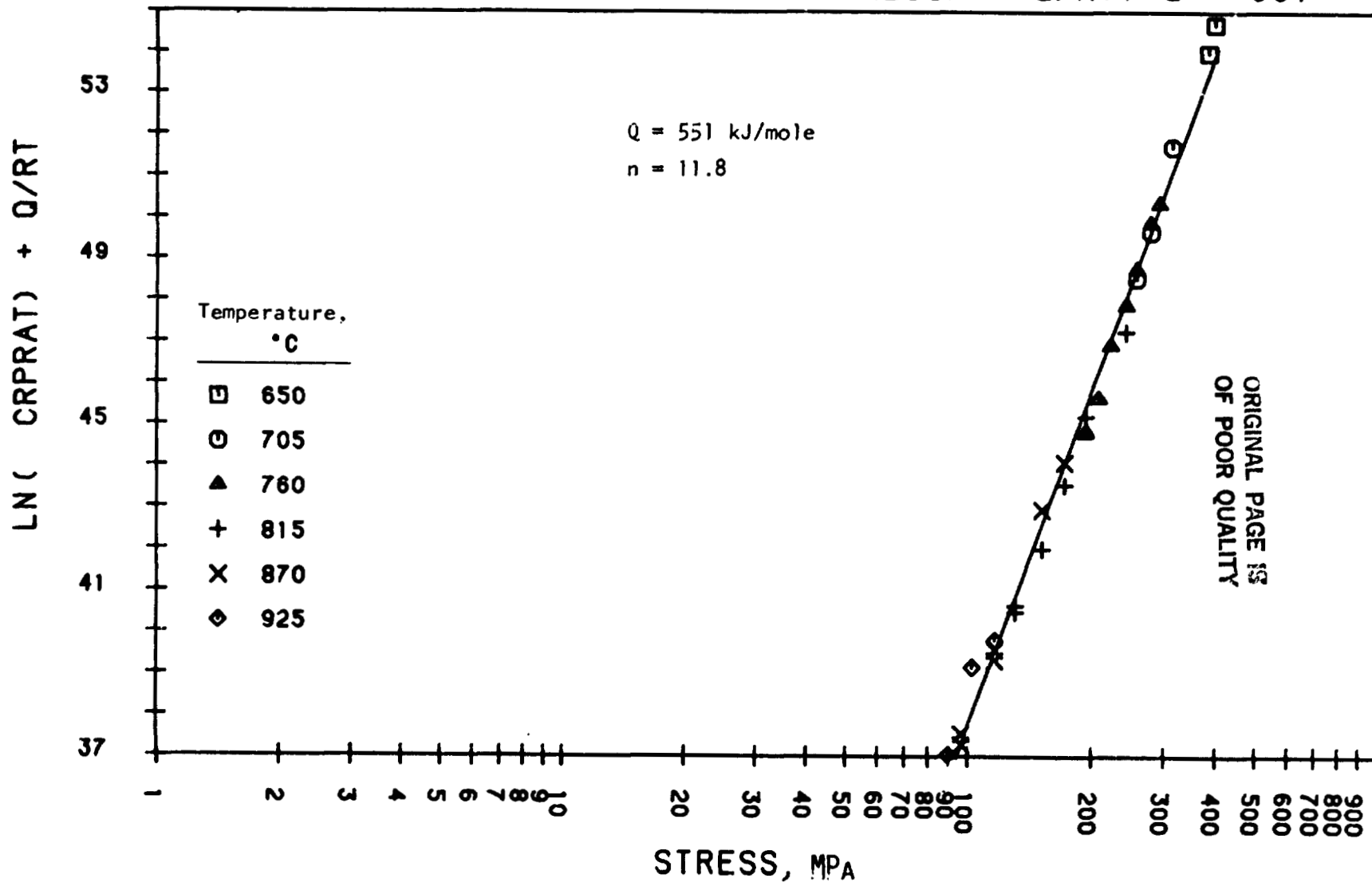


Figure C-29. Temperature-compensated minimum creep rate vs. stress for CRM-6D tested in air (Case 2B).

ORIGINAL PAGE IS
OF POOR QUALITY

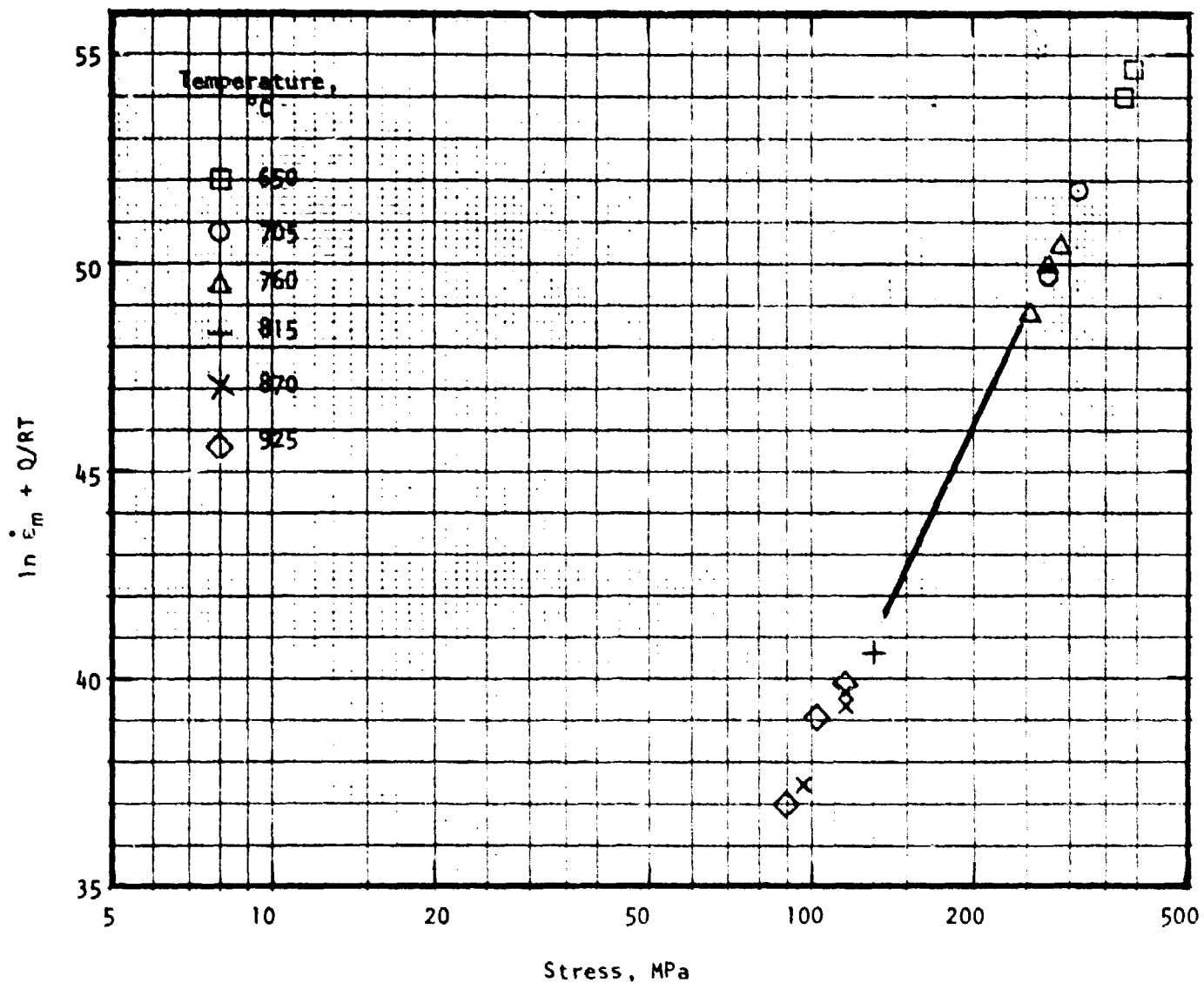


Figure C-30. Temperature-compensated minimum creep rate vs. stress for CRM-6D tested in air (Case 2B, including Cases 2A and 2C shown separately).

XF-818 IN AIR - CASE 2B

$$\ln(\text{TRUPT}) = \ln(K) + n \ln(\text{STRESS}) - Q/RT, \quad Q = 505$$

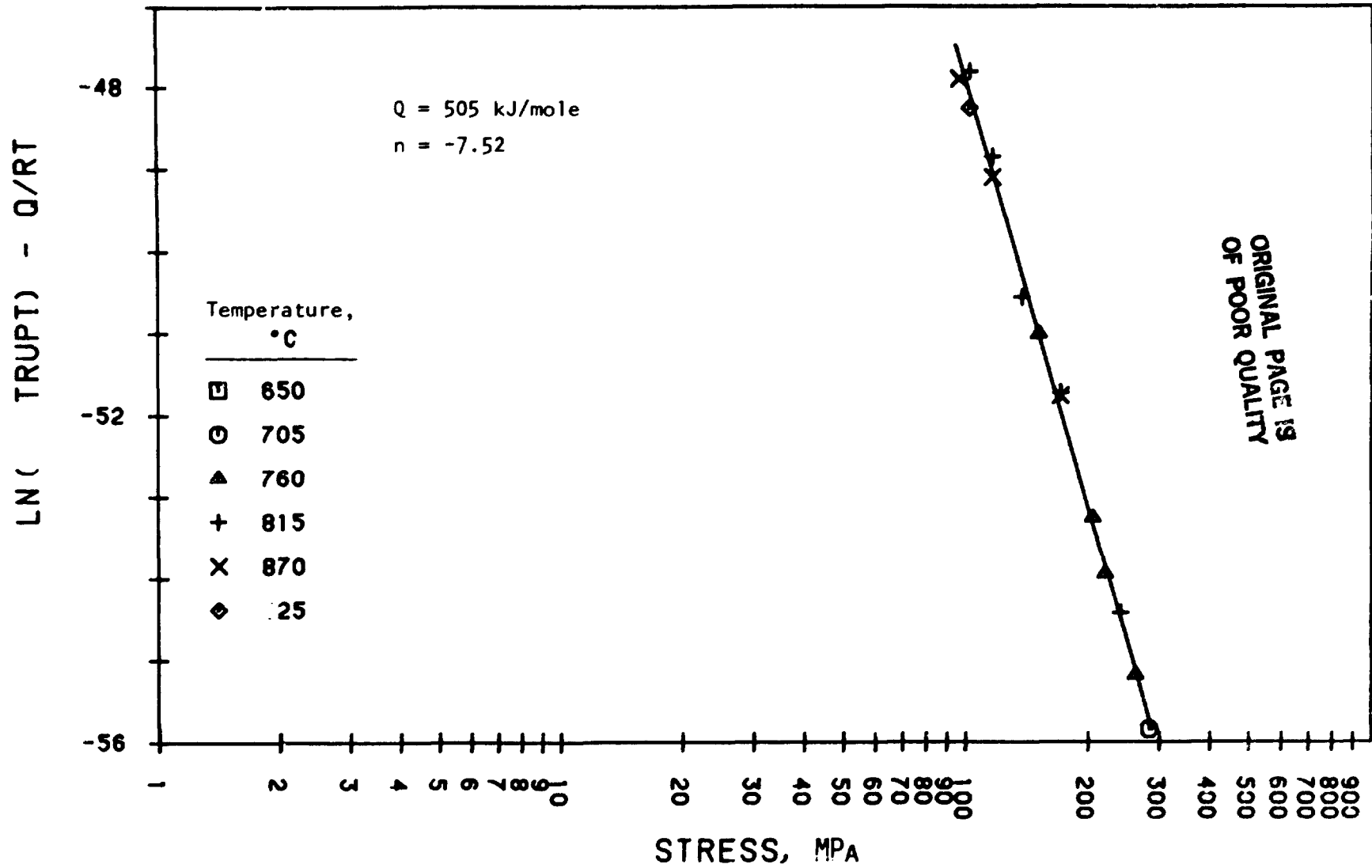


Figure C-31. Temperature-compensated rupture life vs. stress for XF-818 tested in air (Case 2B).

ORIGINAL PAGE IS
OF POOR QUALITY

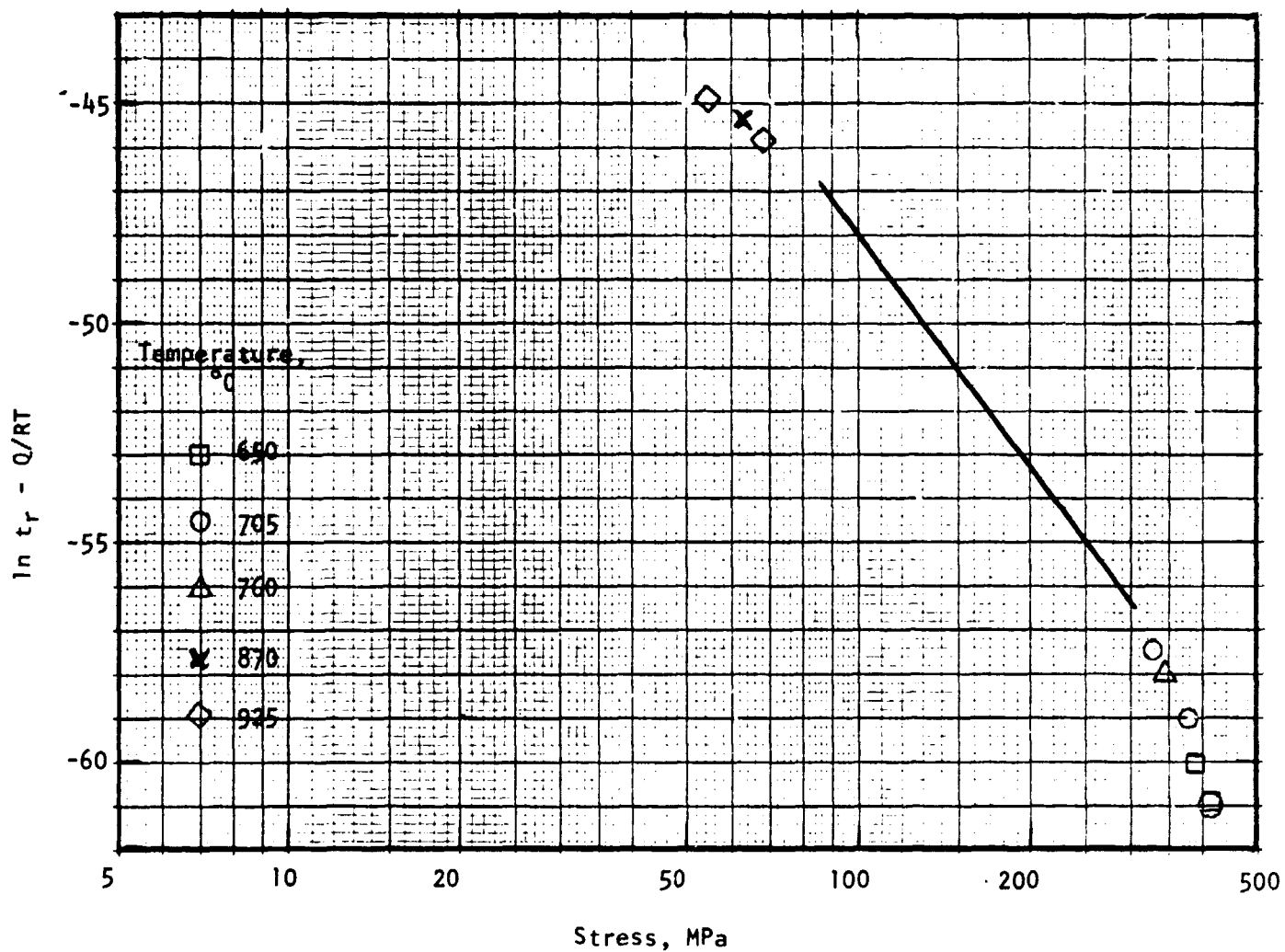
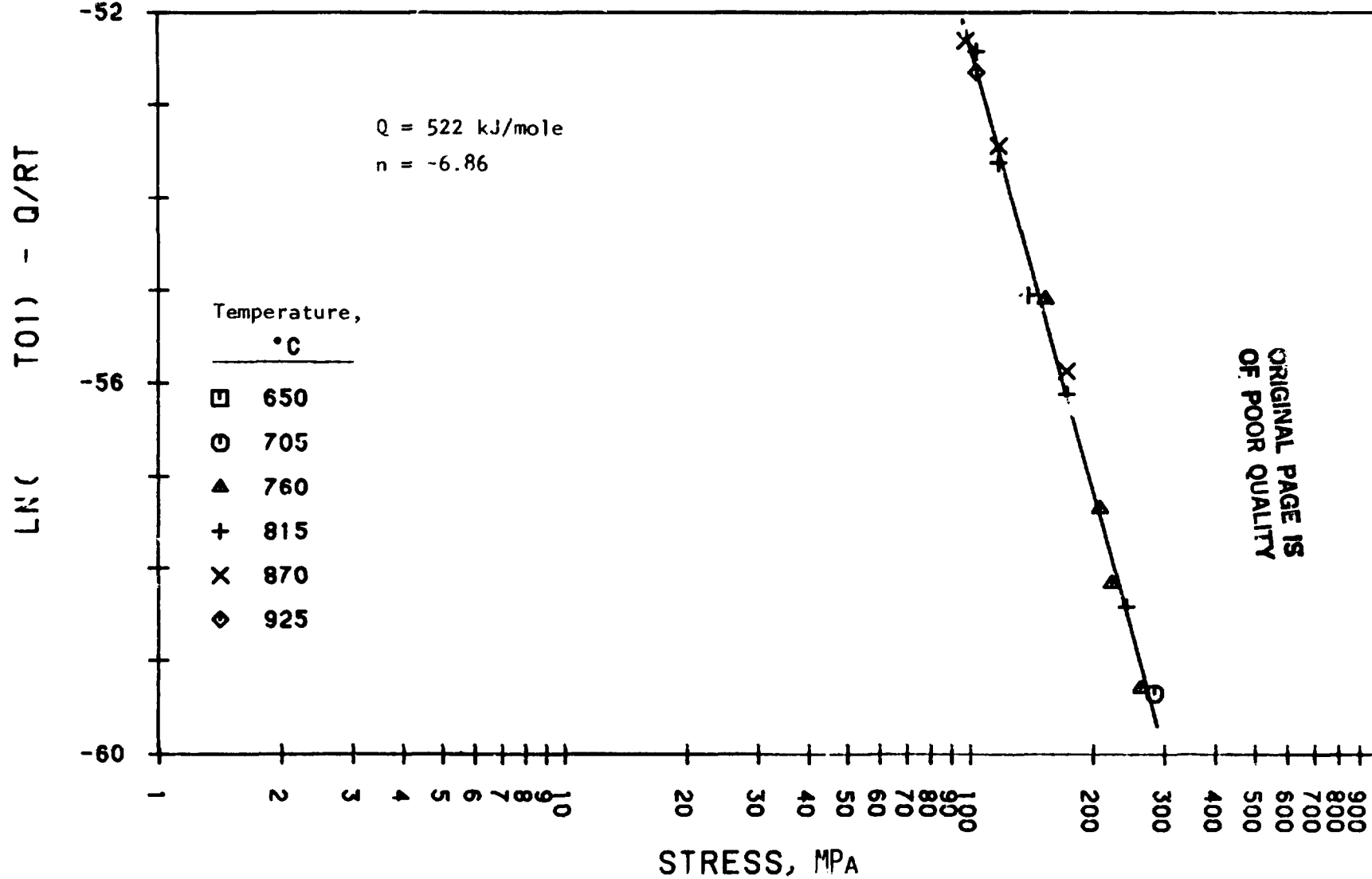


Figure C-32. Temperature-compensated rupture life vs. stress for XF-318 tested in air (Case 2B, including Cases 2A and 2C data shown separately).

XF-818 IN AIR - CASE 2B

$$\ln(t_{0.01}) = \ln(K) + n \ln(\text{STRESS}) - Q/RT, \quad Q = 522$$



ORIGINAL PAGE IS
OF POOR QUALITY

Figure C-33. Temperature-compensated time to 1% creep strain vs. stress for XF-818 tested in air (Case 2B).

ORIGINAL PAGE IS
OF POOR QUALITY

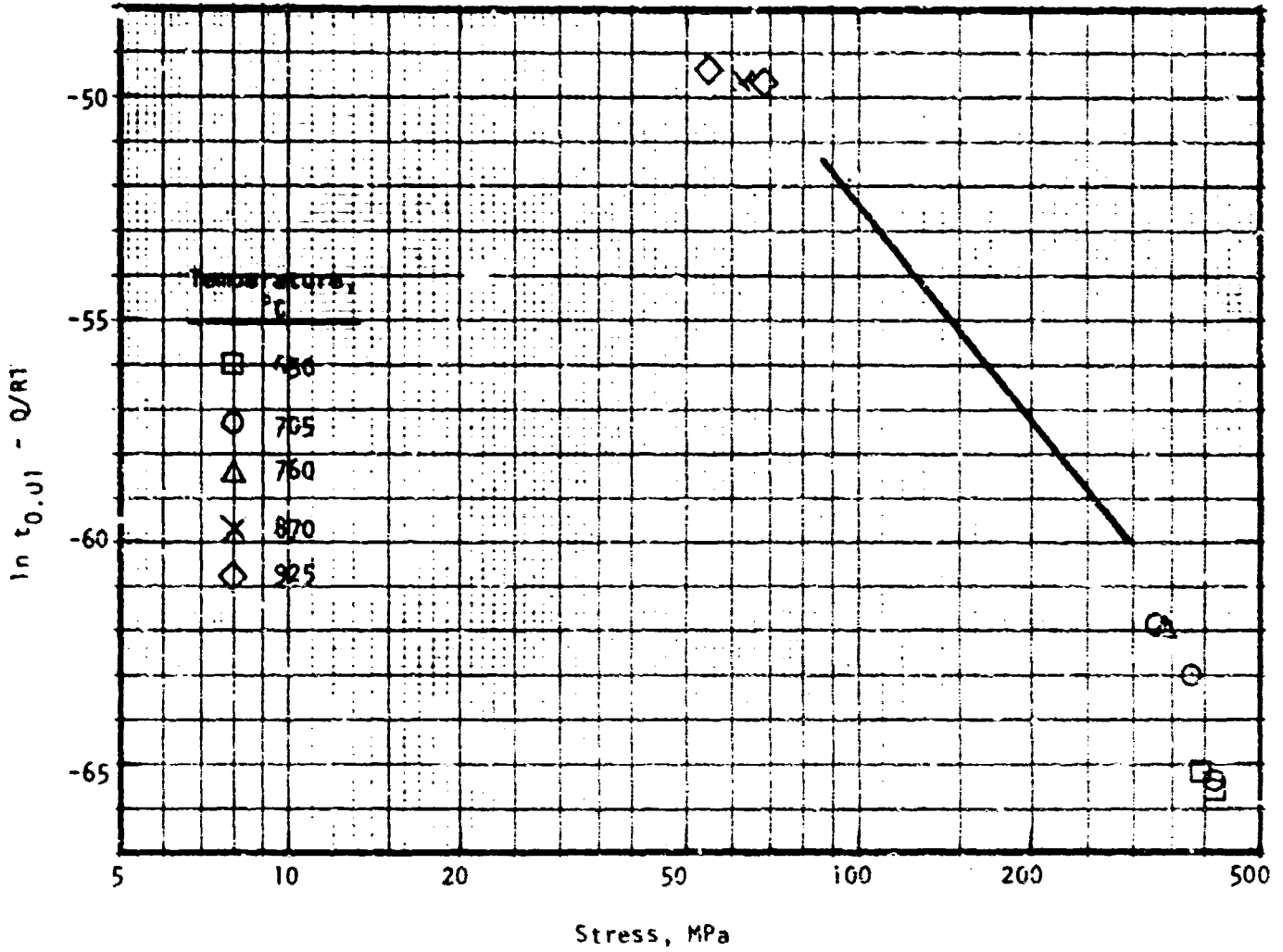


Figure C-14. Temperature-compensated time to 1% creep strain vs. stress for XF-819 tested in air (Case 2B, including Cases 2A and 2C shown separately).

XF-818 IN AIR - CASE 2B

$$\text{LN}(\text{CRPRAT}) = \text{LN}(K) + N \text{LN}(\text{STRESS}) + Q/RT, \quad Q = 545$$

Q = 545 kJ/mole
n = 7.47

LN (CRPRAT) + Q/RT

49
45
41

Temperature,	
°C	
□	650
○	705
▲	760
+	815
X	870
◇	925

1 2 3 4 5 6 7 8 9 10 20 30 40 50 60 70 80 90 100 200 300 400 500 600 700 800 900

STRESS, MPA

ORIGINAL PAGE IS
OF POOR QUALITY

Figure C-35. Temperature-compensated minimum creep rate vs. stress for XF-818 tested in air (Case 2B).

ORIGINAL PAGE IS
OF POOR QUALITY

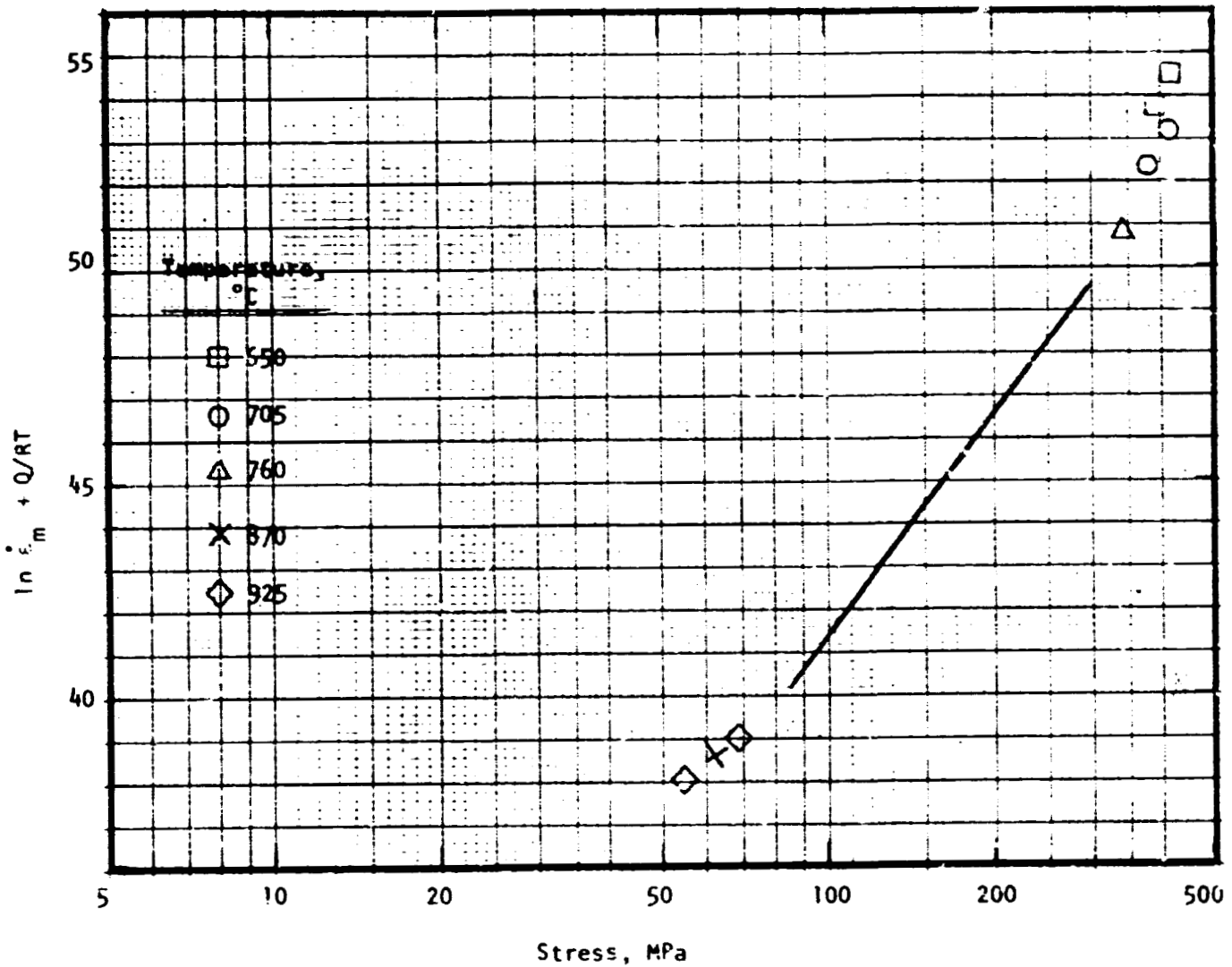


Figure C-36. Temperature-compensated minimum creep rate vs. stress for XF-818 tested in air (Case 2B, including Cases 2A and 2C shown separately).